Final Report

Application of the SEBAL Methodology for Estimating Evapotranspiration and Consumptive Use of Water Through Remote Sensing

Idaho Department of Water Resources
University of Idaho, Department of Biological and Agricultural Engineering

Submitted to

The Raytheon Systems Company
Earth Observation System Data and Information System Project

December 15, 2001

Anthony Morse
Idaho Department of Water Resources

Dr. Richard G. Allen
University of Idaho

Masahiro Tasumi
University of Idaho

William J. Kramber
Idaho Department of Water Resources

Ricardo Trezza
University of Idaho

Dr. James L. Wright
USDA-ARS

The principal report to Raytheon is summarized in this Part I component. Part II of the final report includes detail on refinements made to the SEBAL model during Phase II, detail on validation activities and results, and application to the Snake River Plain of Idaho for the year 2000. The Part II report contains results addressing specific SEBAL topics.

Part I

I. Executive Summary

This project had six objectives. The objectives and achievements of this project were as follows:

Objective 1: Refine the component sub-steps in SEBAL in order to make the SEBAL-derived ET consistent in accuracy among various land use classes and climates.

Achievement: The components examined and refined include an improvement in the soil heat flux estimation, the evaporative fraction, the vegetation index, emissivity, and net radiation.

Objective 2: Understand the inherent pixel-to-pixel variation in SEBAL ET using information from the fields surrounding the precision-weighing lysimeters.

Achievement:

Objective 3: Determine the best methods for extending the SEBAL ET derived at the time of the satellite overpass to the surrounding 24-hour period.

Achievement:: Hourly lysimeter summaries were retrieved for time periods surrounding the nineteen Landsat images. These summaries were used to provide measurements of ET fluxes concurrent with the satellite images as well as ET information for intervening days between images. Considerable time and effort was expended during the study to organize and perform quality control analyses on the extensive set of lysimeter measurements for the six years of images. The lysimeter data sets include the dates for satellite images as well as a majority of intervening dates between images.

The use of the crop coefficient proved to be widely successful in predicting ET for 24-hour periods from ET determined for the image time. The use of reference ET (ET_r) over a daily period represents well the variation in ET expected for each individual pixel. This has been a valuable affirmation from this Phase II study made possible with the lysimeter data sets.

Objective 4: Determine the best methods to extend the 24-hour SEBAL ET to longer periods of time, up to one month.

Achievement:: Results of extending SEBAL derived ET from image times and dates over time periods of as long as one month were shown to be successful using the crop coefficient approach as described in section 5. Comparisons of seasonal ET from SEBAL with that measured by lysimeter are given in Part II.

Objective 5: Determine the relationship between SEBAL ET and IDWR's ground-water pumpage data in order to estimate aquifer depletion from SEBAL ET.

Achievement:: The initial analysis of the relationship between pumpage and ET does not support the hypothesis that ET can be used to estimate pumpage. However, an examination of the two datasets reveals that SEBAL ET has patterns that are consistent with irrigation practices on the Eastern Snake River Plain, while the pumpage data do not. Close examination of a subset of the pumpage data confirms the presence of a number of errors in the data set. Definitive analysis awaits further, detailed examination and repair of the pumpage data.

Objective 6: Assess the utility of SEBAL-derived ET as input to the Eastern Snake River Plain ground water model to improve prediction accuracy for ground-water flow and sensitivity to human intervention.

Achievement:: The production of ET maps having 30 m resolution for the Eastern Snake River Plain Aquifer (ESPA) was highly successful. Sample results are included in Part II of this report. ET images were created for twelve dates during year 2000 and ET was integrated for the April – October period. These maps will be utilized by State of Idaho, University of Idaho, and US Bureau of Reclamation ground-water modelers to predict recharge of irrigation water to the ESPA.

II. Introduction

The Surface Energy Balance Algorithm for Land (SEBAL) is a satellite image-processing model for computing evapotranspiration maps for large areas. SEBAL is comprised of twenty-five computational steps that predict a complete radiation and energy balance for the earth's surface along with fluxes of sensible heat and evapotranspiration. SEBAL uses digital image data collected by Landsat or other remote-sensing satellites measuring visible, near-infrared and thermal infrared

radiation. Evapotranspiration (ET) is computed as a component of the energy balance on a pixel-by-pixel basis. A general schematic of the SEBAL process is illustrated in Figure 1. A detailed description of the model is provided in Bastiaanssen et al. (1998a), Bastiaanssen (2000). Phase I of this study, entitled "Application of the SEBAL Methodology for Estimating Consumptive Use of Water and Streamflow Depletion in the Bear River Basin of Idaho through Remote Sensing" (Morse et al., 2000), demonstrated the ability of SEBAL to create ET maps for large areas in the Bear River Basin of Idaho, Utah and Wyoming. The report is available at www.idwr.state.id.us/gisdata.

SEBAL is an emerging technology and has the potential to become widely adopted and used by the water resources communities, both nationally and globally. ET maps created using SEBAL will some day be routinely used as input to daily and monthly operational and planning models for dam operations, ground-water management, irrigation water supply planning, water rights regulation, and hydrologic studies. Because SEBAL is an emerging technology, it still has uncertainties that need to be eliminated or reduced if SEBAL is to become a widely operational model with widely used products. These uncertainties include 1) uncertainties in the best method for extrapolating the ET predicted at the time of the satellite overpass to longer periods of time; 2) uncertainties in the current method used in SEBAL to account for impacts of elevation on image-energy balance relationships. In addition, there is need to evolve how SEBAL can be integrated into IDWR business processes and in the processes of other water management entities, for example the federal Bureau of Reclamation, Bureau of Land Management, and Geological Survey agencies and agencies in other states, including local users, for example canal companies and cities.

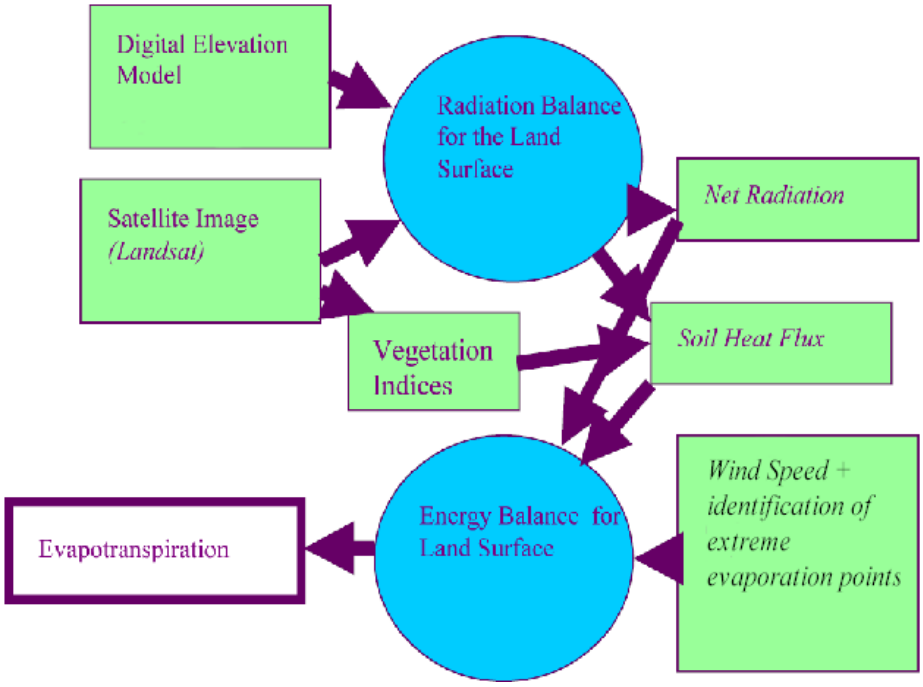

Figure 1. Schematic of the general computational process for determining evapotranspiration using SEBAL

For SEBAL to become operational, there needs to be demonstrated utility to business processes of IDWR (and other entities), particularly in regard to water rights management and ground-water modeling and planning. The question to be asked by water rights management is in how the utility of SEBAL measurements is affected by 1) pixel size and 2) repeat cycle. For ground-water modeling, the question is in regard to how aggregated ET for irrigation projects compares with recorded irrigation diversions. ET predictions, coupled with diversion records and estimates of ground-water pumpage, may allow the evaluation of 1) the relative efficiency of projects (i.e., fraction of diverted water that is evaporated); 2) the distribution in space and time of incidental recharge to ground-water systems, which is a residual of diverted water; 3) the change in time of year and between years for these various performance indicators; and 4) impacts of timing of return flows from irrigation projects on downstream ground-water and river discharges.

Phase 1 of the SEBAL project demonstrated the potential utility of SEBAL to compute ET in Idaho. Phase 1 was modestly funded in terms of both dollars and data, and the conclusions were appropriately limited. Phase 2 of the SEBAL project is a more extensive investigation designed to examine the validity of SEBAL on the Eastern Snake River Plain. The project was better-funded and had approximately 20 times more data for analysis than did Phase I.

The validation of SEBAL on the Snake River Plain has centered on the use of two precision weighing lysimeter systems for evapotranspiration measurement that were in place at Kimberly, Idaho from 1968 to 1991. The lysimeter system was

installed and operated by Dr. James Wright of the USDA-ARS (Wright, 1982, 1996) and measured ET fluxes continuously. ET data are available for a wide range of weather conditions, surface covers, and crop types. In addition, measurements of net radiation, soil heat flux and plant canopy parameters were routinely made at or near the lysimeter site.

The lysimeter data sets at Kimberly are extremely valuable in that they represent absolute, continuous measurements of ET fluxes spread over a long period of time. They provide valuable information to verify procedures used to extrapolate SEBAL and other remote sensing algorithms over various time scales and for various types and categories of land cover. The lysimeter data sets and associated micrometeorological data for Kimberly represent typical climatic conditions, yet also include years that had weather anomalies. Therefore the data sets are valuable for testing remote sensing estimates of ET under dry and wet conditions.

Nineteen Landsat 5 satellite image dates were selected for Kimberly, Idaho, covering a six year period between 1986 and 1991. These dates coincide with cloud-free conditions at Kimberly when high quality lysimeter and corresponding micrometeorological data were available. The dates represent a balanced combination of various cropping growing stages and times of the year. More clear images and lysimeter data were available during the growing season than during the wintertime.

The lysimeter data for intervening periods between image dates were used to assess the impact of various methods for extending ET maps from a single day to longer time periods. They have also been used to assess the variability in the "crop coefficient" (K_c) over the course of a day and for a 24-hour period. The success of SEBAL is partially predicated on the assumption that K_c for a 24-hour period can be predicted from the K_c for an instantaneous satellite image.

K_c is defined as the ratio of ET derived from SEBAL or ET measured by lysimeter to the "reference" evapotranspiration (ET_r). ET_r is calculated from local weather measurements and represents the evapotranspiration from a well-watered, fully vegetated crop, in this case, full-cover alfalfa 0.5 m in height. ET_r was calculated from weather measured near the lysimeter that included solar radiation, wind speed, air temperature and vapor pressure. Lysimeter data analysis showed the use of $K_c = ET / ET_r$ to be preferable to the evaporative fraction (EF) parameter used during previous applications of SEBAL, due to its consistency during daytime hours and agreement between hourly K_c at the satellite overpass time and daily average K_c. EF is defined as the ratio of ET to $R_n - G$. ET_r is a preferred basis because it includes effects of changes in wind speed and vapor pressure deficit during the course of a day in addition to R_n and G. ET_r was calculated using the recently standardized ASCE Penman-Monteith equation (Jensen et al., 1990; ASCE, 2000). The predication that K_c at the satellite overpass time is equivalent to K_c for the day was extensively tested for Kimberly.

III. Objectives

Phase II has six objectives. These objectives and a summary of accomplishments are as follow:

Objective 1: Refine the component sub-steps in SEBAL in order to make the SEBAL-derived ET consistent in accuracy among various land use classes and climates.

A number of tasks during the Phase II study were directed at improvement of components within SEBAL to better predict ET for environments found in the western United States. These included the prediction of net radiation and soil heat flux components, improvement in identification and assessment of the energy balance for "indicator" pixels (i.e., the so-called "hot" pixel and "cold" pixel of SEBAL), determination of mean wind speeds in mountain areas, prediction of aerodynamic roughness for various vegetation covers, and development of the K_c approach for extending ET between images. Some of these results are discussed under Part 5: Product Development.

Objective 2: Understand the inherent pixel-to-pixel variation in SEBAL ET using information from the fields surrounding the precision-weighing lysimeters.

The lysimeter measurements at Kimberly afforded a valuable opportunity for assessing pixel-to-pixel variation in ET from SEBAL relative to lysimeter measurements. Much of the data from the lysimeter systems had been processed previously by Wright to daily totals of ET, and in most instances were available as totals for hourly or shorter periods. Considerable effort was expended during this study in retrieving or reconstructing hourly ET and associated micrometeorological data from paper printouts, ink charts, ASCII text files or spreadsheet files and reorganizing and storing the data in modern spreadsheet formats. During the data analysis, substantial error checking and correction of spurious data were made. The ET data are supported by measurements of solar radiation, humidity, air temperature, wind speed, soil moisture, soil temperature, vegetation height and leaf area, and in many cases by measurements of net radiation and sensible heat flux to the ground. These supporting data were also subjected to a detailed quality assessment analysis.

Summaries of results are shown in section 5: Product Development and in Appendix I of Part II of this report. Comparisons between SEBAL and lysimeter are considered to be very good. In addition to evaluation of SEBAL ET near lysimeters, variation among pixels was discovered within some large center-pivot irrigated fields, but not in others, illustrating the ability of SEBAL to identify problems in crop water consumption, and consequently crop yield, within a field due to poor uniformity of

water or fertilizer application, or due to impacts of poor crop stand or disease pressures. Close-ups of SEBAL ET images for clusters of fields showing various uniformities are included in Part II of this report.

Objective 3: Determine the best methods for extending the SEBAL ET derived at the time of the satellite overpass to the surrounding 24-hour period.

Hourly lysimeter summaries were retrieved for time periods surrounding the nineteen Landsat images. These summaries were used to provide measurements of ET fluxes concurrent with the satellite images as well as ET information for intervening days between images. Considerable time and effort was expended during the study to organize and perform quality control analyses on the extensive set of lysimeter measurements for the six years of images. The lysimeter data sets include the dates for satellite images as well as a majority of intervening dates between images.

As described in part 5 below, the use of the crop coefficient proved to be widely successful in predicting ET for 24-hour periods from ET determined for the image time. The use of reference ET (ET_r) over a daily period represents well the variation in ET expected for each individual pixel. This has been a valuable affirmation from this Phase II study made possible with the lysimeter data sets.

Objective 4: Determine the best methods to extend the 24-hour SEBAL ET to longer periods of time, up to one month.

Results of extending SEBAL derived ET from image times and dates over time periods of as long as one month were shown to be successful using the crop coefficient approach as described in section 5. Comparisons of seasonal ET from SEBAL with that measured by lysimeter are given in section 5.

Objective 5: Determine the relationship between SEBAL ET and IDWR's ground-water pumpage data in order to estimate aquifer depletion from SEBAL ET.

The initial analysis of the relationship between pumpage and ET does not support the hypothesis that ET can be used to estimate pumpage. However, an examination of the two datasets reveals that SEBAL ET has patterns that are consistent with irrigation practices on the Eastern Snake River Plain, while the pumpage data do not. Close examination of a subset of the pumpage data confirms the presence of a number of errors in the data set. Definitive analysis awaits further, detailed examination and repair of the pumpage data.

Objective 6: Assess the utility of SEBAL-derived ET as input to the Eastern Snake River Plain ground water model to improve prediction accuracy for ground-water flow and sensitivity to human intervention.

The production of ET maps having 30 m resolution for the Eastern Snake River Plain Aquifer (ESPA) was highly successful. Sample results are included in Part 5 following and in Part II of this report. ET images were created for twelve dates during year 2000 and ET was integrated for the April – October period. These maps will be utilized by State of Idaho, University of Idaho, and US Bureau of Reclamation ground-water modelers to predict recharge of irrigation water to the ESPA.

IV. User Community

The immediate user community for Synergy products is IDWR and its associated, local water organizations. IDWR is the state agency responsible for water management in Idaho. Several IDWR business processes can benefit directly from Synergy products. These business processes include 1) modeling the Eastern Snake River Plain aquifer, 2) participation in the Bear River Commission, and 3) monitoring ground water pumpage with the Water Management Information system. The associated water organizations include the Idaho Ground Water Users Association and six Ground Water Measurement Districts. These organizations have applications that need both Synergy data products and the information derived from them.

The most immediate need for Synergy products is for ET data. ET is used now in ground water modeling of the Eastern Snake River Plain Aquifer, and in allocating irrigation water in the Bear River Basin.

IDWR has begun re-calibrating the Eastern Snake River Plain ground water model that is used to simulate ground-water levels and movement. The model is also used to predict interactions of the aquifer system with stream-flows of the Snake River. The Snake River Plain aquifer system is very large, spanning more than 14,000 square miles (an area larger than the states of Massachusetts, Connecticut, and Rhode Island combined), with over 3,000 square miles of irrigated farmland. The re-calibrated model will be used in support of conjunctive management of ground and surface water. One of the major goals during the re-calibration is to obtain better estimates of aquifer recharge as input to the model.

Recharge from both irrigated and non-irrigated lands is a major component in developing the long-term water balance for the model, and is the amount of water remaining after ET is subtracted from the amount of water diverted from surface-water sources plus precipitation. An improved ET estimate (spatially, temporally and in total magnitude) will significantly reduce the uncertainty involved in computing the net recharge input term for the model. An accurate recharge term is a critical part of model re-calibration. SEBAL allows IDWR to compute the agricultural ET component of the model in an efficient and inexpensive way, and to compute the wildland ET component for the first time.

In 1958 the Bear River Compact was developed to establish how the three states of Idaho, Utah and Wyoming would equitably distribute and use water from the Bear River. Eighteen years later, interested parties entered into six years of negotiation to resolve concerns about the original compact, and in February 1980 the Amended Bear River Compact was signed into federal law. The Bear River Commission is the administrative authority that oversees and enforces the compact.

The compact assigns a depletion (i.e. ET) allotment to each state and directs the commission to develop and implement "approved procedures" to account for and calculate the amount of water depleted. The role of IDWR is to compute depletion for the Idaho part of the Basin to support Idaho's position in negotiations with the other two states. IDWR will continue to refine and apply SEBAL in the Bear River basin to assist in administration of the Bear River Compact.

In the Bear River basin, improvement in accuracy of predicting past, present and future ET in the basin will facilitate better water management and equity among the parties to the Bear River compact. In addition, as other needs and interests in stream flow of the Bear River increase over time, for example for water quality enhancement, recreation, fisheries, wildlife and endangered species, members of the Bear River compact will require ever-increasing information on disposition, fluxes, and hydrology of the water resources of the basin. The results of Phase II will be compiled with the results of Phase I and presented to The Bear River Basin Technical Advisory Committee (TAC). The TAC has requested additional SEBAL-lysimeter comparisons be done for their evaluation of SEBAL as an operational technology.

Managing water rights and irrigation on the Snake River Plain and tributary basins presents a particular challenge to IDWR. Water for irrigation comes from both surface and ground sources. For various historical reasons, the use of surface water has been directly measured and regulated by IDWR while the use of ground water has not. This situation began to change in 1995 when the Water Measurement Information system (WMIS) Program was established within IDWR to measure ground-water use.

IDWR has dedicated considerable resources to water measurement, including three full-time positions to monitor some 5,000 points of diversion, mostly wells. As useful as these data are, they do not provide all the information necessary for effective management of the resource. Information regarding the ET or consumed fraction of diversions is needed. SEBAL can be used in conjunction with Water Measurement data in an efficient program to help manage water development, use and stewardship. SEBAL covers large areas inexpensively and efficiently, thereby extending Water Measurement Data in both time and space, and the Water Measurement data, in turn, can be used to validate or calibrate the SEBAL results.

This combined program offers many advantages over present methods. First, it offers the ability to monitor whether or not water has actually stopped being used for irrigation after a water shut-off order has been issued. Second, it can discover if more water has been used than is authorized. Third, it can quantify and be used as proof of beneficial use of a right. Fourth, it can be used as an unbiased, quantitative record of historic use. Fifth, the consumed fraction and return of non-evapotranspired water to the resource can be quantified. Sixth, estimations of yield and productivity can be made to assess benefits of water development and potential tradeoffs in water management.

There are other potential users of Synergy data associated with the WMIS program. These include the U.S. Bureau of Reclamation, U.S. Geological Survey, and

Idaho National Environmental Engineering Laboratory. Ground-water recharge maps computed using SEBAL ET maps will be used by USBR and USGS in ground-water models housed within their facilities and well as in river operations models. We anticipate that these federal entities will ultimately make their own applications of SEBAL for specific years and areas of interest. Interest in the SEBAL product has been high and has included rangeland ecologists, wetlands biologists and fire control professionals. The INEEL has requested ET maps from the Phase II application for portions of the INEEL reservation lying on the Snake Plain aquifer system. In addition, INEEL plans to use ET maps for the Big Lost River Drainage as part of a large hydrologic basin-scale field laboratory to be established within the region.

V. Product Development

From the perspective of IDWR, the three most important products are 1) the refinement of the SEBAL model, 2) the analysis of the relationship between lysimeter ET and SEBAL ET, and 3) the analysis of the relationship between ground water pumpage and SEBAL ET. From the Idaho user community in general, the most important product generated by the Synergy Project is the large number of geo-coded and terrain-corrected Landsat TM scenes purchased for the project.

VI. Infomart Development

The infomart has two components. The first component is the availability of ET images for download from the State of Idaho ftp site, and the serving of ET images by means of an interactive web-server. The second component is the availability of some 94 terrain-corrected Landsat TM digital data-sets for Idaho applications.

Making ET images available is useful, both for historical time periods and for near-real time applications. A major utility of ET data stems from making the data available as soon as possible after an overpass. This information is of substantial use in crop and water use monitoring and in identification of areas needing human intervention. A library of historic ET data will be useful to a range of researchers in areas of hydrology, water resources management, flood control, hydrogeology, rangeland ecology, forest management, fire control, and wild-life resources. INSIDE Idaho at the University of Idaho has begun a data-exchange web site to make available Idaho Landsat scenes to researchers and others needing historic Landsat data. The infomart has already filled two such data requests from University of Idaho researchers.

The infomart web address for data-sharing of Landsat 7 TM data is http://inside.uidaho.edu/geodata/Landsat7ETM/Landsat7ETMFindData.htm. The address for Landsat 5 TM data is http://inside.uidaho.edu/geodata/Landsat5TM/Landsat5TMFindData.htm. The SEBAL data generated by this project are available through an ArcIMS application at http://www.idwr.state.id.us/gisdata/mapserver.htm.

VII. Experience of the User Community

Data Use

The primary immediate user of the Informat data, IDWR, has used ET in its business processes for over twenty years. ET has been a critical component of the Eastern Snake River Plain hydrologic model, which IDWR has run since 1980. ET is the basis on which waters of the Bear River Basin have been apportioned among Wyoming, Idaho, and Utah. IDWR has had a long-standing need for ET, which has meant that there has been no need to develop a market for the data with IDWR. The primary requirement of the Synergy Project has been to demonstrate to IDWR's satisfaction that IDWR can generate SEBAL-derived ET data quicker and cheaper than by previous methods, and with at least an equal accuracy.

User Interactions

IDWR, as users of the data, feel the need to be able to generate the SEBAL ET themselves. Project personnel have structured the Synergy Project to transfer the SEBAL technology to IDWR. The technology transfer has been in the form of 1) generation of a final report that included a step-by-step manual on running SEBAL, 2) SEBAL training conducted at IDWR, and 3) SEBAL processing done at IDWR.

IDWR personnel used the SEBAL manual to process one of the Landsat scenes that had been processed by UI personnel. The goal of this duplication was to understand the degree to which the manual provided directions clearly enough to produce correctly-processed SEBAL data. A comparison of the scenes showed about a 98% agreement, which was considered to be excellent.

Under the umbrella of the Synergy project, two SEBAL training sessions were held at IDWR done by UI personnel and by the project consultant, Wim Bastiaanssen, who developed SEBAL. These training sessions covered a total of eight days, and covered the theory of SEBAL, the components of SEBAL, how to implement SEBAL, and sensor calibration.

All SEBAL processing for the first phase of the project was done at IDWR, which allowed IDWR personnel to directly participate in the process.

Impact

The impact from the SEBAL work is still evolving because IDWR and other potential users have not had a chance to evaluate the final results of application and to consider the implications. Nevertheless, there have been significant impacts.

IDWR found the results of Phase I sufficiently compelling to request funding from the Idaho Legislature to include SEBAL as the ET source for the recalibration of the Eastern Snake River Plain aquifer model. The value to this IDWR business process is in being able to generate ET on a 30-meter-cell basis rather than on a full-county basis. The model uses 5 km grid cells, and aggregating ET up to a 5 km cell is preferable to trying to disaggregate from a county-sized cell. In addition, the funding by the Idaho Legislature is supporting a University of Idaho graduate student in Hydrology to use SEBAL-derived ET maps to develop methods for adjusting tables previously used by the Idaho water community to predict consumptive use for specific types of crops. This work represents one of many anticipated projects that will occur due to the availability of ET images via Infomart.

Since 1996, IDWR has led a $2.5 million, multi-agency (state and federal) project to study the water resources of the Lower Boise Valley. This area is receiving significant attention because of rapid population growth in the valley.

One of the main aspects of the study is the creation of a ground water model. The U.S. Bureau of Reclamation has spent the last three years studying irrigation diversions from the Boise River and irrigation return flow into the river in order to better quantify the water balance for the model. The third main component of the water balance is ET. The Bureau of Reclamation and IDWR have recently agreed to cooperate on a project to compute the ET portion of the water balance using SEBAL. The bureau's contribution to the project will be $40,000

IDWR has begun the process to make SEBAL an operational technology. IDWR has drafted the "Outline for Creation of Water Districts and Administration of Rights to the Use of Ground Water From the Eastern Snake Plain Aquifer in IDWR Administrative Basins 35, 36, 41, and 43", which is dated Dec. 10, 2001. Attachment B to that outline is a set of instructions to district watermasters. In Section 1-j of those instructions, watermasters are directed to.., " Monitor water use in the district in accordance with the approved annual work plan, including obtaining and reporting the data necessary for SEBAL computations."

These standards will be finalized and adopted as a formal Rule of the Department of Water Resources. The approach that IDWR will take is to do the SEBAL processing itself and then transfer information on ET to the Water Districts. The goal of using SEBAL-derived ET is to become more efficient in monitoring ground-water pumping.

The desirability of becoming more efficient in monitoring ground water pumping is cost-related. The potential cost savings are significant.

Cost Savings

SEBAL ET data are clearly less expensive to generate than are standard ET data. There are several ways to use the SEBAL-derived figures. ET is a component of ground-water models; it can be used to estimate depletion from aquifers; and it can used as a tool in managing water rights. It is possible to compare the costs for deriving ET from the traditional means and from SEBAL, but it is difficult to quantify the benefits.

Since IDWR is still in the process of processing the SEBAL data, a quantitative cost-benefit analysis is premature. Nevertheless, it is possible to do a cost comparison based on some available figures, a comparison that will give a sense of whether or not the project is on the right track. A couple of assumptions on the costs are necessary, but the costs are conservative for monitoring and reasonable for remote sensing since IDWR has some experience with both monitoring and remote sensing.

The costs for monitoring water use are approximately $ 500,000 per year. This is a reasonable cost: in state FY 2000, IDWR spent approximately $150,000 on this program. The associated Water Measurement Districts spent about the same amount, and other regulated water users spent many times this amount.

The costs for remote sensing are approximately $30,000. This cost includes costs for 15 TM scenes, which represent 5 dates for the whole eastern Snake Plain ($15,000 for the data). The processing requires about 3 days per scene (45 days * 8 hours = 360 hours * $30.00 per hour = $10,800). The total for remote sensing is $25,800. Adding 15% for set-up and time for aggregation of ET results in a GIS structure results in a total remote sensing cost of $29,670 which can be rounded to $30,000.

Using these figures, the remote sensing/measurement cost ratio is $30,000/$500,000 = .06. The remote sensing costs about 6% of the measurement costs, but the measurement costs are for a subset of the total number of wells, all of which are not measured in a single year. In contrast, SEBAL data cover the entire Snake River Plain and all places of use (i.e., all irrigated areas) and associated wells.

The next logical question is this: How much of a reduction in accuracy can one tolerate in order to save $470,000 a year and obtain estimates of pumpage for all wells, not only a subset of them? In Phase 1, the Bear River Basin, the difference between SEBAL and the lysimeter, total, for the growing season was 4%. For the Phase 2 comparison with precision weighing lysimeters at Kimberly, differences were less than 2%. These comparisons represent a small sample, but are probably typical. Error as high as 10 to 20%, if distributed randomly, could probably be tolerated by IDWR and by the water user communities.

These figures are somewhat deceptive in that the use of SEBAL ET will not replace the existing measurement program, per se. Pumpage data that can be related to individual water rights will be needed to regress against the SEBAL ET data for the same water rights to establish the relationship between volume pumped and volume of ET. That relationship can then be applied to all other non-monitored water rights and their associated wells to estimate both aquifer depletion and water use by individual water rights. However, the costs for extending knowledge of water pumpage to the rest of the irrigated areas in southern Idaho will be only 6% of costs for extending a water measurement program to the entire ESPA area.

User Willingness to Operate the System

Of the potential users, the Idaho Department of Water Resources is able and willing to operate the system. IDWR has the hardware, software, experienced personnel, and the mission to do SEBAL processing for itself as well as for other potential users in Idaho. More importantly, IDWR has business processes in place now that either use ET or can use ET as a surrogate for other, more expensively-collected data.

The commitment of IDWR is demonstrated by actions taken by the Department. The first action is the dedication of $54,000 of Idaho General-Fund monies toward the evaluation and implementation of SEBAL. The second action is the provision in the draft Water District standards for the information gathering that will support SEBAL analysis. The third action is the joint decision by IDWR and the U.S. Bureau of Reclamation to use SEBAL to generate the ET component of the Lower Boise Valley ground water model. The U.S. Bureau of Reclamation's commitment is $40,000 specifically to SEBAL ET.

VIII. Infomart Synergy

IDWR's first experience with Infomart synergy came in using Infomart data to help quell a water management conflict over development of ground water from an aquifer shared by two states. The flow of Locomotive Springs, a fresh water spring on the north shore of the Great Salt Lake in Utah, is less than that measured 20 to 50 years ago. The springs support fish and wildlife habitat important to the local area. Water management officials in Utah and local officials in Utah were concerned that the decline in spring flow was occurring because of continued extensive ground water irrigation in the Curlew Valley of Idaho. New irrigation development has been stopped in Utah and in a portion of Idaho for the last 25 years, but the Utah officials believed that development had continued unabated in Idaho, perhaps even in the closed portion. The issue received high-level attention, with the Governors of both states having been notified of the matter. Officials from the Idaho Department of Water Resources (IDWR) used Infomart products to demonstrate effectively and conclusively that there had been very little irrigation development in the Idaho part of the Curlew Valley, and therefore the observed reduction in spring flows were not resulting from recent actions in Idaho.

IDWR was able to generate the remote sensing/GIS products in part because of the establishment of an Infomart built on the support from Synergy. The image-maps that were the Synergy Data products were the Landsat FCC presentation clipped to USGS 1:100,000-scale quadrangle boundaries. These Infomart products (for example Figure 21) were used in an onsite review of the matter by the Director of IDWR to demonstrate conclusively to those in attendance (including the Utah State Engineer, the Director of Utah Department of Water Resource and local officials) that there had been very little new irrigation development over the last 15 years in Idaho. With this misunderstanding set aside, the officials were able to move on to explore ways to determine the actual cause of the reduced spring flow with the intent of finding workable solutions.

There is very large potential and value for coupling SEBAL ET processing and resultant maps with Synergy Informart partners in North Dakota (A Crop and Range Alert System in the Upper Midwest) and in Missouri (Forestry and Forest Stewardship Applications by MoRAP/ICREST and Disease Management Infomart by IntRePID). Provision of crop water use and ET information with various vegetation and disease indices provides substantial value-added information and assists both consultants and users with additional information for interpretation and in identification of causes and effects.

.

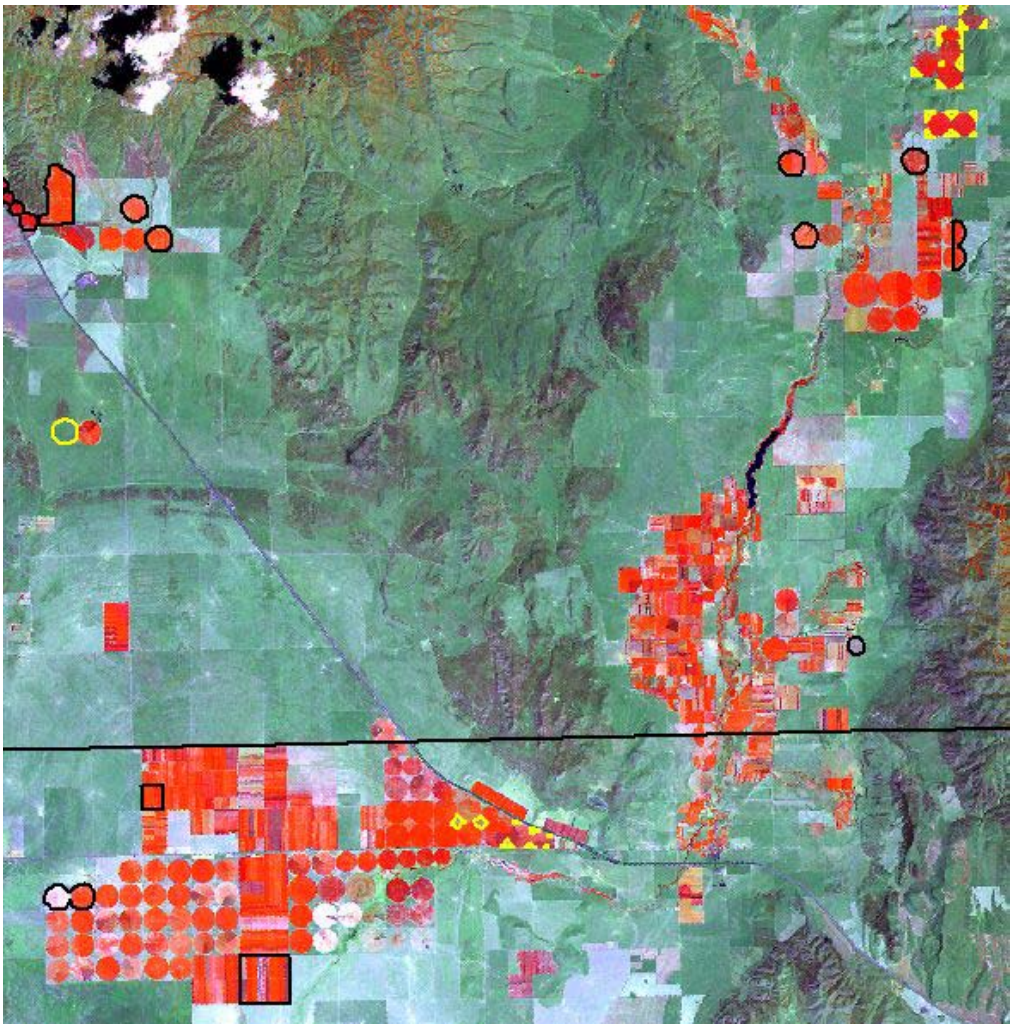

Figure 21. IDWR personnel used two Landsat images from each of two years: Landsat MSS from 1986 and Landsat TM from 2000. The 2000 images are part of the set purchased by the Synergy project. The image shows the Idaho-Utah border in black, and black polygons

IX. Sustainability

A. Vision

The products and services of the Infomart as developed under the Synergy umbrella will be sustained as end-user products and services when they are useful to the end user. The largest potential end user of products and services generated by the Idaho Synergy project is the Idaho Department of Water Resources (IDWR). In order for IDWR to sustain the Synergy Infomart, IDWR must 1) demonstrate the utility of Infomart products to the Idaho water-user community; 2) quantify the costs of generating evapotranspiration (ET) information from SEBAL, and define the processing steps well enough so that costs can be reliably predicted; and 3) educate the Idaho water-user community about the availability and utility of Infomart data.

IDWR has the opportunity to serve its own needs as well as the needs of other potential users. Within IDWR, ET data has demonstrated uses in three broad applications. The first application is the water measurement program within the Water Distribution Section. The second application is in administration of the Bear River Compact. The third application is in the use of ET as input to the Eastern Snake River Plain ground-water model. The latter two applications use ET now, albeit ET computed in a more laborious way. Although ET is not presently used in the water measurement program, the high correlation between ET and ground water pumpage coupled with the efficiency of SEBAL makes SEBAL-derived ET an extremely attractive alternative to direct measurement of pumpage volume.

Other potential Infomart customers include the Idaho and U.S. Departments of Agriculture, the U.S. Bureau of Reclamation, U.S. Geological Survey, USDA Natural Resources Conservation Service, Idaho National Environmental and Engineering Laboratory, Idaho canal companies, irrigation districts, and water measurement districts, and the Idaho Ground Water Users Association. In addition, the latter entities have counterparts in most states who are potential customers.

B. Description of Products and Services

The Idaho Informant generates both products and services. The products generated by the Informart are, first, the seven-band, terrain-corrected Landsat TM scenes processed to yield ET; and second, the SEBAL-derived ET images. The Infomart services will be related to ET: a summary of ET by time period by area, for example, the amount of water consumptively used by irrigated agriculture in the Twin Falls North Side irrigation District during the period 15 July, 2000 to 30 August, 2000.

The Water Distribution Section of IDWR works actively with ground water measurement districts to monitor ground water pumping. If SEBAL is a viable alternative

to the much more expensive method now used to estimate pumpage, it will be implemented in the Water Distribution Section as the first operational use. The Water Measurement Districts, with which the Water Distribution Section work, are made up of irrigators. It is anticipated that the cost savings from using SEBAL rather that the present system of estimation, will convince the irrigators or the utility of SEBAL. It is the irrigators themselves who will promote SEBAL as a cost-savings technology.

Other useful products that can be derived during the SEBAL process include estimates of crop yield. These estimates have not been made during the Phase I and II studies, but can be incorporated as a routine part of SEBAL. This is being done by Bastiaanssen (1999) in applications of SEBAL in some other areas.

C. Identify Demand on an On-going Basis

The means for evaluating customer satisfaction is straight-forward: IDWR is a state agency, and if SEBAL-derived ET meets its needs, IDWR will dedicate funding to continue using SEBAL. The measure of customer satisfaction in this case will be binary: either IDWR is satisfied and budgets funds to continue using SEBAL, or IDWR is not satisfied and does not.

Evaluation of satisfaction on the part of other customers, such as Irrigation Districts or Water Users Associations will most likely come in the form of requests from those organizations to IDWR for SEBAL products and support.

The current user community for ET images is the Idaho Department of Water Resources. IDWR is responsible for the management of water resources within the state of Idaho, and has three on-going business processes that need accurate and timely ET data. These business processes are 1) the Water Measurement Program, 2) the management of water rights in the Bear River Basin, and 3) operation of the Eastern Snake River Plain aquifer model.

The size of the user community has the potential to grow considerably. Various Ground Water Measurement Districts in Idaho spend between $100,000 and $200,000 annually in measuring the pumpage from ground-water wells. The potential for cost savings using SEBAL makes these organizations likely candidates for SEBAL-derived ET data. Their participation will be dependent on 1) the perceived accuracy and reliability of the SEBAL ET, 2) the cost of the ET data to those organizations, and 3) the ability of the organizations to interpret and apply the data.

D. Partners

IDWR is the key player at this point in the project. At least for the next one to two years, it will be necessary to have IDWR provide the SEBAL processing and helping

potential partners interpret the results. The exception to this scenario will come about if Federal water-management agencies, such as the Bureau of Reclamation, see a need for SEBAL-derived ET and begin doing their own SEBAL processing. In any event, IDWR will be at the center of the effort to build a network of partners to expand the use of Infomart data in Idaho.

The other users of Infomart data, specifically the SEBAL data, include irrigation districts, canal companies, water users associations, and their attorneys. It is possible that Federal agencies and private-sector firms will be interested in applying SEBAL, as well.
IDWR will play a leadership role in helping these organizations learn to use SEBAL data by doing the data processing, education, training, and application development.

IDWR already has in place operational relationships with these potential partners, which will greatly help in technology and information transfer. IDWR is the state agency responsible for water management and for natural resources GIS in Idaho. In that capacity, IDWR will be willing to contribute its remote sensing and GIS expertise

What is your strategy to build this network of partners?

The strategy for introducing water measurement districts and ground water users is to educate these groups about 1) the accuracy of SEBAL as measured by the correlation of SEBAL ET with ground water pumpage, and 2) the requirements for implementation. This work will be done in conjunction with the Water Distribution Section of IDWR.

E. Milestones/Benchmarks

Dec. 15, 2001 End of SEBAL Phase 2
Dec. 15, 2001 – Mar. 1, 2002 Evaluation of SEBAL results by IDWR Water Management personnel and ongoing analysis and evaluation by the Univ. Idaho.

F. Cost/Budget to Implement

Estimate the resources you may require to implement your plan.

per single, terrain-corrected, Landsat TM scene

$1,000	for Data:
$1,000	in personnel time to process
$2,000	

The Snake River Plain is covered by six Landsat scenes. Assuming five scenes per growing season, the total cost to compute ET for most of Idaho's irrigated land is approximately $30,000.

There will be no income stream from this data processing. IDWR is an Idaho State agency, and is prohibited by law from charging a fee for data. Nevertheless, it is anticipated that cost-sharing arrangements can be made with other government agencies and with non-governmental organizations.

Differentiate between R & D and operational aspects.

The work being carried out under Phases 1 and 2 of this project is clearly research. Because the results of Phase 2 confirm those of Phase 1 and show a strong correlation between SEBAL ET and both the lysimeter ET and the pumpage data, then it is highly probable that SEBAL will be accepted as an operational tool.

G. Issues

The only potential barrier to using SEBAL at IDWR is in the perceived quality of the ET estimate. If the ET results from SEBAL are seen as being as good, or almost as good, as the results from previous methods of ET generation, then the overwhelming cost advantage of SEBAL will in all likelihood cause SEBAL to become operational.

The potential barriers to implementing SEBAL as an operational technology in secondary users, such as irrigation districts and water users associations, are 1) budgetary, 2) institutional, and 3) operational.

Operational barriers are more likely to be found in the secondary users. All of these secondary users have chronic budgetary issues to contend with. However, if SEBAL ET is widely perceived as a useful tool, it is likely that IDWR will foot most of the bill.

Institutional issues will manifest themselves in the form of a need to build comfort levels with SEBAL. This will be done by training on how SEBAL works, on interpreting the results from SEBAL, and in integrating SEBAL results with other data to generate information that is useful to the organization.

The operational issues will be centered on the need for augmentation of hardware and software in order to use the data, and on training.

X. Lessons Learned

1. Always order Landsat data in Fast Format, never in Geotiff. Fast Format has all the metadata in a header file, which is missing in the geotiff. With geotiff, you have to go to the web, and neither the data nor USGS assistance personnel are reliable.

2. These projects would be better structured as 3-year projects, not as 3 one-year projects. As 3 one-year projects, there are 3 separate start-up phases that severely eat into the project time-lines. It is very difficult to structure a multi-year project in a way that shows definitive results and benefits after just one year.

XI. Phase III Potential

Potential work for Phase III is centered on education and outreach to 1) the irrigation/water-use community; 2) the remote sensing community, especially to the private sector to develop SEBAL-derived ET as a standard product; and 3) to state and federal government agencies with responsibilities in water-management.

The outreach to the irrigation and water-use community is designed to educate Idaho water users on the potential uses and benefits of SEBAL with the goal of including the water users in future SEBAL projects for the purpose of cost-sharing and better resource management.

The outreach to the remote sensing community is designed to educate private sector firms about the potential for SEBAL as the basis of a value-added product for Landsat TM data.

The outreach to state and federal agencies is designed to educate resource management agencies about the potential application of SEBAL to appropriate issues. Examples of these issues at the federal level is the need by the US Bureau of Reclamation for timely and consistent ET estimates for irrigated agriculture for the Colorado River Basin. ET estimates now are compiled from a variety of sources using inconsistent techniques. At the state level, the State of Oklahoma keeps statistics on ground water pumpage, but the statistics are reported by the individual well owners on no more than 80% of the irrigation wells in the state, and without any verification. In both of these circumstances, SEBAL offers an efficient, timely, and inexpensive alternative to present data collection.

It is anticipated that Phase III will include funding for continued refinement and development of SEBAL by the University of Idaho. Areas benefiting from refinement include the prediction of ET in mountainous terrain. This is an area of uncertainty using the current SEBAL methodology. Reliable prediction of ET in mountains would open up the use of SEBAL by the U.S. Forest Service in prediction of fire potential, in prediction of disease pressures and impacts, and in conducting hydrology studies. Federal and state wildlife and fisheries agencies would utilize ET maps for assessing impacts of hydrologic characteristics of a basin on biological resources. Specific areas of refinement include prediction of wind speed (i.e., air movement) in mountainous terrain, lapse correction of surface temperature when used to predict surface--air temperature differences, and incorporation of procedures for predicting heat budgets for snow.

Part II Results

Refinement of the SEBAL model

The following are summaries for various components the SEBAL that have received extensive attention and modification during the Phase II study to improve the operational accuracy of SEBAL for application in the Western U.S.

Improvement of Soil Heat Flux Estimation

In SEBAL, ET is computed as the residual of the energy balance: $ET = R_n - G - H$ where G is soil heat flux and H is sensible heat to the air. A considerable amount of effort was applied to developing an improved method for predicting the amount of energy absorbed by G. The refinement in G was considered to be a critical part of the 2001 SEBAL application. Measurement data for G are uncommon, however, a substantial amount of data were available from Dr. J.L. Wright, USDA-ARS, Kimberly, Idaho that had been collected by the USDA-ARS during the 1970's. These data were supplemented by data collected by the University of Idaho during a 1999 field campaign near Kimberly.

Details of development of equations for G for various types of vegetation and bare soil, and testing of results are described in Appendix 2 of Part II of this report.

Evaluation of Evaporative Fraction and need to use a crop coefficient

In the SEBAL-2001 application, ET for 24-hour periods was computed using the ratio of ET from the satellite image to reference evapotranspiration (ET_r) rather than using the evaporative fraction (EF) that has been used in past applications. The move to using K_c was due to the consistency found for $K_c = ET/ET_r$ during daytime periods as compared to the evaporative fraction (EF) ($EF = ET / (R_n - G)$). Figures 2 and 3 show EF for measured ET from the Kimberly grassed lysimeter (lysimeter 1) for two days in May, 1989. An upward trend in EF with time of day is evident, especially for May 29. More importantly, the 24-hour EF is 63% higher than the EF at 1100 for May 29 and 46% greater for May 30. These differences would potentially cause underestimation of 24-hour ET of as much as 30% if based on EF. EF_{24} was computed as $EF_{24} = ET_{24}/(R_n-G)_{24}$.

Crop coefficients, K_c are shown for the same two days in Figures 4 and 5. Here, the K_c remained relatively stable during the day and the 24-hour K_c, computed as $K_{c\ 24} = ET_{24}/ET_{r\ 24}$ was 8% higher than the 1100 K_c for May 29 and only 1% greater for May 30. The result of similarity in $K_{c\ inst.}$ and $K_{c\text{-}24\ hour}$ is high accuracy in computed 24-hour ET.

Appendix 5 of Part II includes additional figures that show hourly K_c vs. time of day for satellite image dates during 1989. These figures include 24-hour K_c and show close agreement between $K_{c\ 24}$ and the K_c at the time of satellite images (approx. 1050 MST), similar to Figures 4 and 5 shown here. These results provide good support for using K_c rather than EF.

Vegetation Index

A Soil Adjusted Vegetation Index (SAVI) was found to be more consistent in identifying bare soil from image to image than the normalized difference vegetation index (NDVI) previously used in SEBAL. The SAVI index was applied using parameter L = 0.1. The development is described in Appendix 6 of Part II. SAVI was used to predict leaf area index (LAI), and LAI was in turn used in prediction of emissivity, G and aerodynamic roughness, z_{om}.

Emissivity

Emissivity values were optimized during the Phase II study for use with Landsat TM Band 6 to calculate surface temperature. A lower limit for emissivity was set at 0.965 for all surfaces and maximum at 0.98, based on field measurements of emissivity for soils, vegetation, water and exposed rock conducted during the study. For most land classes, emissivity is predicted in SEBAL-2001 as emissivity = 0.965+0.005*LAI. Emissivity for water is fixed at 0.985. Field measurements of emissivity used a fine-wire thermocouple coupled with an infrared thermometer.

Net Radiation

The equation used in SEBAL to predict instantaneous R_n was modified for southern Idaho conditions using incoming long wave radiation measurements collected during the 1999 University of Idaho “RAPID” campaign (Allen, deBruin, Hartogensis, Kramer, Wright cooperators). In application of SEBAL-2001, incoming long wave radiation was predicted for all pixels using air temperature predicted for the “cold” pixel in an image based on surface temperature. The value for air temperature was considered to represent the general temperature of the lower portion of the atmospheric air mass, and was lapse corrected before application to each pixel.

.
.

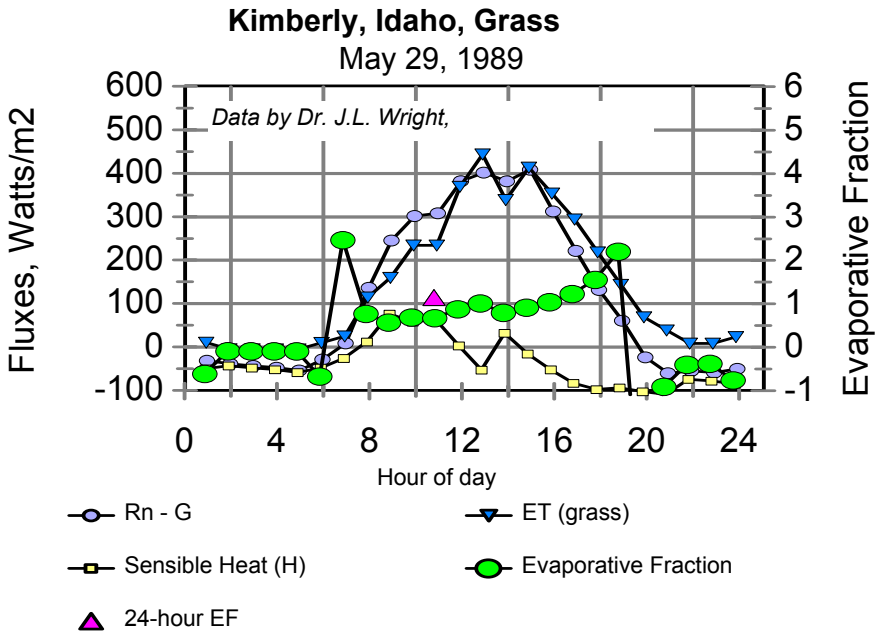

Figure 2. Hourly available energy (R_n - G), measured ET and sensible heat flux for May 29, 1989 and evaporative fraction calculated hourly and for the 24-hour period at Kimberly, Idaho.

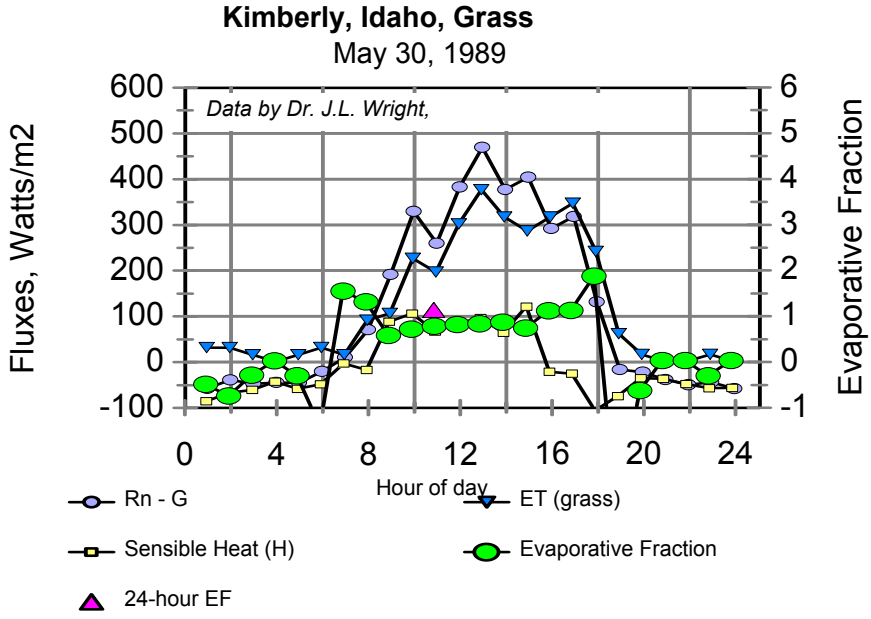

Figure 3. Hourly available energy (R_n - G), measured ET and sensible heat flux for May 30, 1989 and evaporative fraction calculated hourly and for the 24-hour period at Kimberly, Idaho

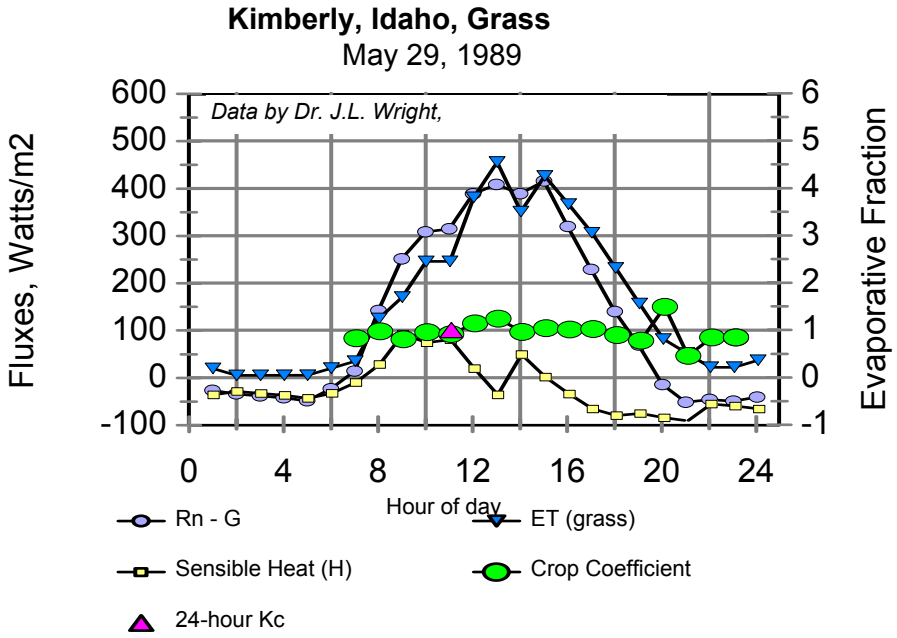

Figure 4. Hourly available energy (R_n - G), measured ET and sensible heat flux for May 29, 1989 and crop coefficient calculated hourly and for the 24-hour period at Kimberly, Idaho

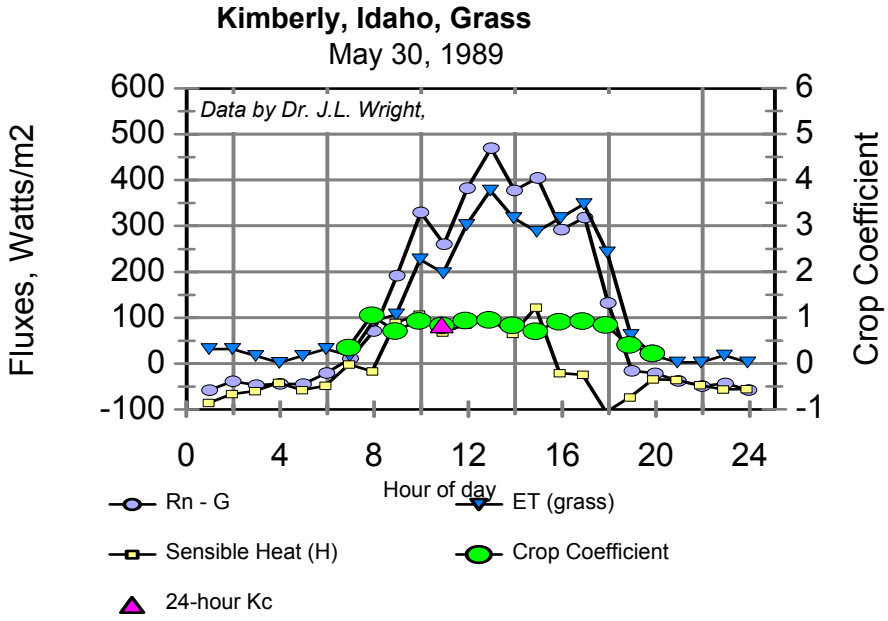

Figure 5. Hourly available energy (Rn - G), measured ET and sensible heat flux for May 30, 1989 and crop coefficient calculated hourly and for the 24-hour period at Kimberly, Idaho

Aerodynamic Roughness

The z_{om} parameterization method in SEBAL was modified so that z_{om} for nonagricultural areas was predicted using a developed land-use map rather than from NDVI data as was done previously. z_{om} for nonagricultual pixels were assigned specific values. z_{om} for agricultural areas was computed as a function of crop height, where z_{om} = 0.123 H. Crop height, H, was in turn computed as a function of LAI, where H = 0.1 LAI, so that z_{om} = 0.0123*LAI, for z_{om} and H in m. LAI was based on the $SAVI_{L=0.1}$ index.

Wind speed in mountainous areas

When SEBAL is applied to mountainous areas, ET is often overpredicted, even after lapse-correction of surface temperature and correction of solar radiation for effects of slope and aspect. The cause of the overprediction of ET was determined to be caused by an underprediction of sensible heat transfer (H) in mountainous areas. The two basic reasons that sensible heat is underestimated in mountainous regions when traditional wind speed and roughness algorithms are applied are:

a) SEBAL does not implicitly account for the impact of terrain roughness in mountains on “effective” aerodynamic roughness. Slopes, ridge lines and abrupt changes in mountain topography as well as frequency of rock outcroppings and other land form aberrations tend to increase the transfer of momentum from the air mass to earth. This increased transfer increases H transfer, as well. The impact is an increase in a “geometrical” z_{om} for mountain areas.

b) Higher winds are expected in mountainous areas due to the occurrence of a general venturi effect as atmospheric streamlines converge over ridgelines and changes in terrain. In addition, mountain areas, being at higher elevations than surrounding regional terrain, protrude into higher velocity regions of the atmosphere. Both of these factors tend to cause higher wind velocities in mountainous terrain than is measured in valley floors or open plain areas.

Appendix 8 of Part II describes general correction algorithms that were developed to account for terrain roughness and wind aerodynamics in mountainous terrain. These algorithms are considered to be a “first cut,” and future field work in mountain areas to measure aerodynamic roughness and relative wind speeds is recommended.

Pixel-to-Pixel Variation in SEBAL ET

Two precision lysimeters were operated at Kimberly during the 1986-1991 period by Dr. J.L. Wright of the USDA-ARS Irrigation and Soils Research Laboratory near Kimberly, Idaho. Dr. Wright was a collaborator during this study. The physical size of each lysimeter was about 2 m x 2 m horizontally and 1.8 m deep. Each lysimeter "tank" was mounted on a precision counter-weighted cantilevered balance so that electronic load cells could be used to measure change in tank mass caused by evapotranspiration. The load cell signals were recorded onto paper charts as continuous traces. The resolution of the weighing lysimeters was less than 0.05 mm, or about 1% of 24-hour ET, on average, and less than 10% of mid-day ET (Wright, 1996). Accuracy of hourly ET measurements was improved by applying visually-based smoothing to data, aided by use of computed hourly ET_r as a guide, along with ET measured by the other lysimeter.

The lysimeter fields were approximately 2.6 ha in area (6.4 acres) each and had dimensions and context as shown in Fig. 6. An aerial photograph showing the two lysimeter fields is in Fig. 7.

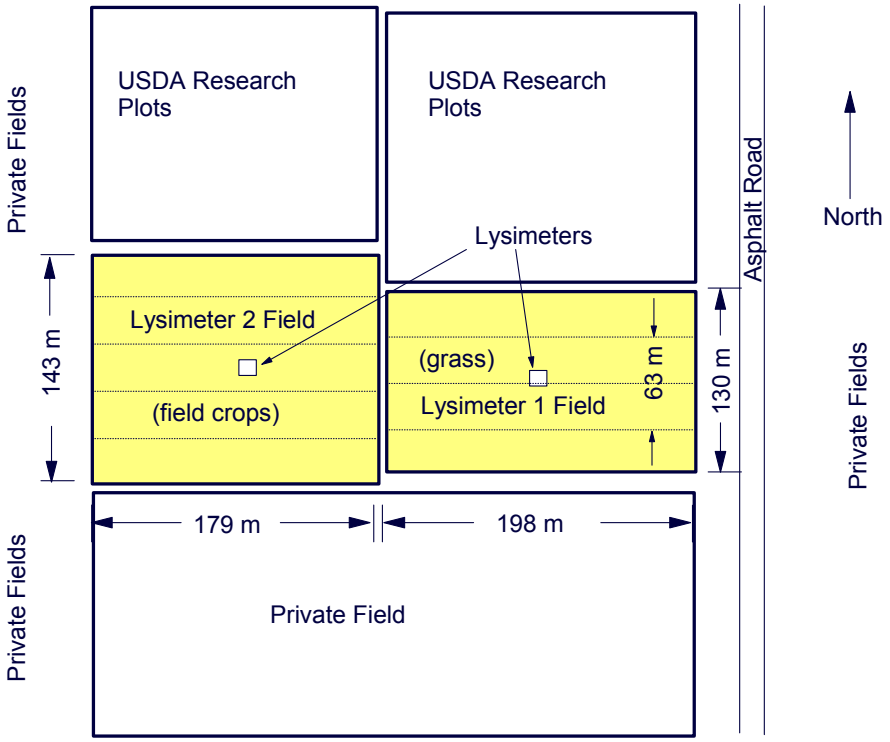

Figure 6. Plan view of Kimberly lysimeters and surroundings

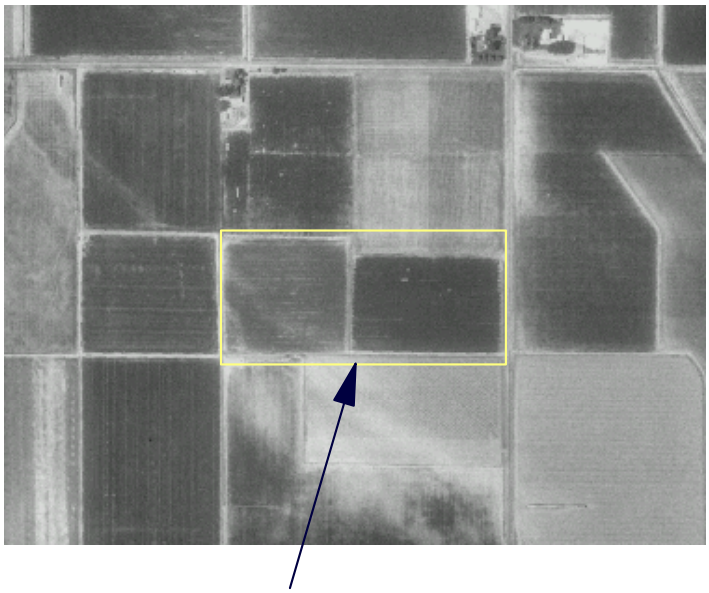

Figure 7. Aerial view of two lysimeter fields at Kimberly and surrounding fields.

The Kimberly lysimeters were planted to the same crop as the overlying field. The lysimeter fields were of sufficient size to provide good fetch for lysimeter measurement of crop ET. However, the field sizes were small enough, relative to the size of thematic mapper (TM) pixels (30 m), and especially the Band 6 thermal pixel (120 m) of Landsat 5, to present challenges in obtaining a large sample of ET pixels whose attributes corresponded to only the lysimeter crop. In fact, several image dates had band 6 pixels oriented so that no single band 6 pixel (120 m x 120 m) had a majority position on a lysimeter field. This challenge was especially difficult for Lysimeter 1, since the northern ¼ of and southern ¼ of lysimeter 1 field were sometimes planted to crops other than grass. As a consequence, as shown in Figure 6, the useful dimensions of grass in lysimeter field 1 were 190 m east-west and 63 m north-south. Emphasis during the comparison study was therefore concentrated on lysimeter 2 which was planted to field crops of sugar beets, potatoes, spring wheat, peas, and alfalfa during the study period, and was therefore, of more interest than lysimeter 1 to validation of SEBAL.

Despite problems caused by incongruencies in band 6 pixels relative to the actual lysimeter fields, comparisons between ET from SEBAL and lysimeter measurements were considered to be quite good. Details of overlays of pixels onto the lysimeter fields and selection of representative pixels for comparison with lysimeter are

given in Appendix I of Part II. Comparisons between SEBAL and lysimeters are summarized in a following section.

Figure 8 shows false color composites (bands 2, 3, and 4) of close-ups of the two lysimeter fields for two dates representing two of the nineteen TM images obtained from 1986 - 1991. The 30 m pixels are identifiable and provide an indication of the challenge of obtaining representative samples from the lysimeter fields. The band 6 (thermal) pixels, being 120 m in height and width, encompass sixteen 30-m pixels (4 x 4). The more red colors represent higher levels of vegetation.

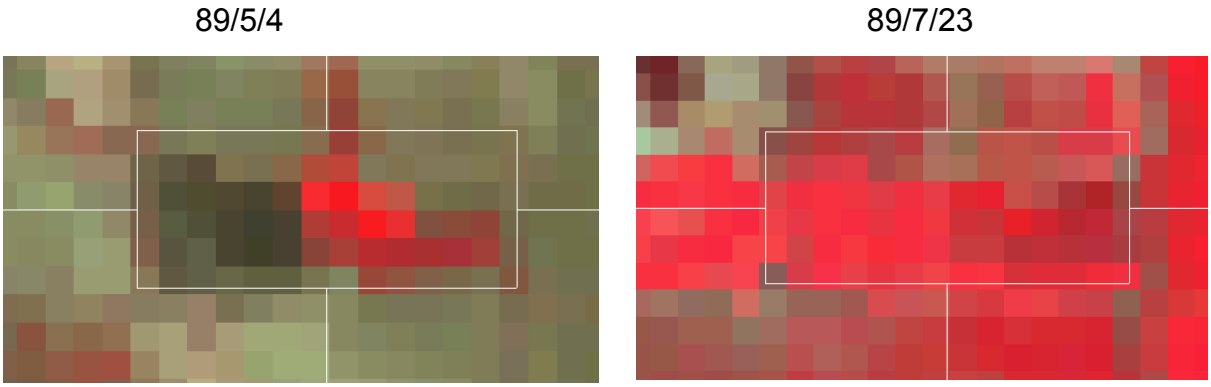

Figure 8. False color composites (TM bands 2,3,4) showing the side-by-side lysimeter fields at Kimberly for May 4 (left image) and July 23 (right image), 1989.

Comparison with Lysimeter-measured ET and Extrapolation of ET over a Growing Season

The following Table 1 summarizes error between SEBAL and lysimeter measurements of ET during 1989. Absolute error averaged 30% for the eight days. However, when the April 18 date was omitted, the average absolute error for a given image date was only 14%. The April 18 date was before planting of the sugar beets and represented a period of drying of bare soil following precipitation. Spatial variation in surface condition of the field surrounding lysimeter 2 during this period may have been large and may not have matched conditions within the lysimeter. The standard deviation of errors between SEBAL and lysimeter for the seven dates from May – September was 13%. In comparison, a commonly quoted standard error for ET prediction equations that are based on weather data, for example based on a Penman or Penman-Monteith-type of ET equation, is about 10% for daily estimates. SEBAL is able to obtain close to this level of accuracy, but for more than 30 million pixels at a time.

Table 1. Percent Error Between SEBAL and Lysimeter 2 (Sugar Beets) near Kimberly, Idaho, for the dates of satellite images for 1989.

	Lysimeter mm d^{-1}	SEBAL mm d^{-1}	Error %	Comments
4/18/89	0.73	1.74	139	Before planting and during a period of drydown following precipitation. Bare soil surface condition may have been spatially variable
5/4/89	6.61	5.09	-23	Field (seen by SEBAL) was irrigated two days before the image, whereas the lysimeter was irrigated only one day before. The –23% error reflects this difference in surface wetness
5/20/89	1.37	1.34	-2	mostly a bare, drying surface
6/5/89	1.73	1.78	3	“”
6/21/89	2.39	2.54	6	partially developing canopy
7/7/89	7.96	5.89	-26	thermal (band 6) pixels were substantially blurred by adjacent fields
7/23/89	7.64	7.17	-6	full ground cover by canopy
9/25/89	5.51	7.40	34	very high winds, wind and ET_r data were missing and synthesized

Data in Table 1 are illustrated graphically in Figure 9, where ET is expressed in the form of a crop coefficient ($K_c = ET / ET_r$) where ET_r is predicted from ground-based weather data using a Penman-Monteith ET equation. K_c was used to normalize results for differences in climatic demand (i.e. ET_r). The round symbols and horizontal line segments in Figure 9 represent K_c that was “measured” by lysimeter on the satellite image date. These values are those directly compared with SEBAL predictions in Table 1. The triangular symbols in Figure 9 represent the K_c predicted by SEBAL for the image date.

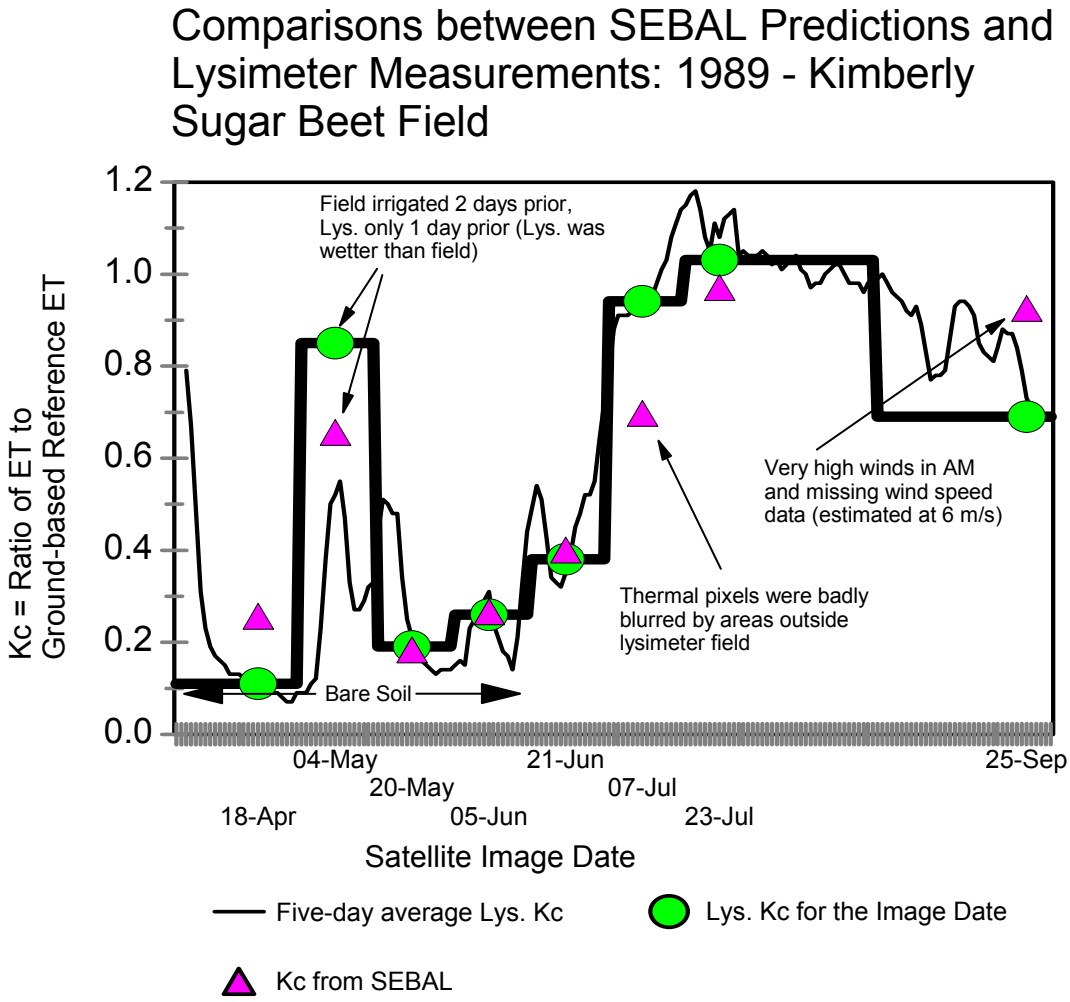

Figure 9. Comparison of final results by SEBAL with Measurements by Lysimeter (results are shown in the form of the crop coefficient, where K_c = ET / reference ET). The "thin" line represents the five-day average K_c for lysimeter and the thick line represent the assumption used in SEBAL to extrapolate between images.

Table 2 summarizes the extrapolation of ET by SEBAL over the season long period (April 1 – Sept. 30). The periods represented by each image date were 16 days in length, centered on the satellite image date, with the exception of April 18, which represented April 1 – April 25 and the July 23 image, representing July 16 to August 24 and the Sept. 25 image, representing Aug. 25 through Sept. 30.

Table 2. Summary and computation of ET during periods represented by each satellite image and sums for the April 11 – September 30, 1989 period for Lysimeter 2 (Sugar Beets).

Image Date	Lysimeter ET mm d^{-1}	SEBAL ET mm d^{-1}	ET_r on date, mm	ET_r for period, mm	Lysimeter ET summed daily for period, mm	Lysimeter ET for period, based on image date, only, mm	SEBAL ET for period, mm
(1)	(2)	(3)	(4)	(5)	(6)	(7)	(8)
4/18/89	0.73	1.74	6.78	147	28	16	38
5/4/89	6.61	5.09	7.76	94	30	80	62
5/20/89	1.37	1.34	7.27	90	22	17	17
6/5/89	1.73	1.78	6.68	118	24	30	31
6/21/89	2.39	2.54	6.33	127	62	48	51
7/7/89	7.96	5.89	8.44	120	116	113	84
7/23/89	7.64	7.17	7.38	253	266	262	246
9/25/89	5.51	7.40	8.00	201	171	138	186
4/1 – 9/30					**718[a]**	**705[b]**	**714[c]**
Percent Error					**--------**	**-1.8%**	**-0.6 %**

[a] The sum of daily measurements of ET by lysimeter computed as the sum of ET from all 183 days between April 1 and Sept. 30.
[b] The sum of ET computed for each lysimeter period, where the ET of each period was computed by multiplying the summed ET_r during the period by the ratio of ET measured by lysimeter on the image date to ET_r on the image date (i.e., using a K_c that was computed from the lysimeter on the date of each image).
[c] The sum of ET predicted by SEBAL for the lysimeter 2 field, computed by multiplying the summed ET_r during the period by the ratio of ET computed on the image date by SEBAL to ET_r on the image date (i.e., using a K_c that was computed by SEBAL on the date of each image).

The relative error for individual periods is the same as shown in Table 1 for individual image dates. What is surprising, given the error for any particular image period, is the close agreement for seasonal ET predicted for the April 1 – September 30 period. The difference between the SEBAL estimate (714 mm) and the lysimeter measurement (718 mm) was less than 1% for the sugar beet crop. It appears that much of the error occurring on an individual date is randomly distributed, and a substantial portion of this randomness cancels when summed over a long time period.

SEBAL-derived ET for the Eastern Snake Plain Aquifer System

SEBAL was successfully applied to 12 image dates for year 2000 for a land area containing six Landsat TM images. This area contains the Eastern Snake Plain ground-water aquifer (ESPA) that is of substantial importance to the economy of southern Idaho. The outline of the ESPA is shown in Figure 10. A land classification for the

Landsat images (paths 39 and 40 and rows 29, 30 and 31) is shown in Figure 11. The 3-row paths extend from Utah and Nevada to the south, through Southern Idaho, and into Montana to the north.

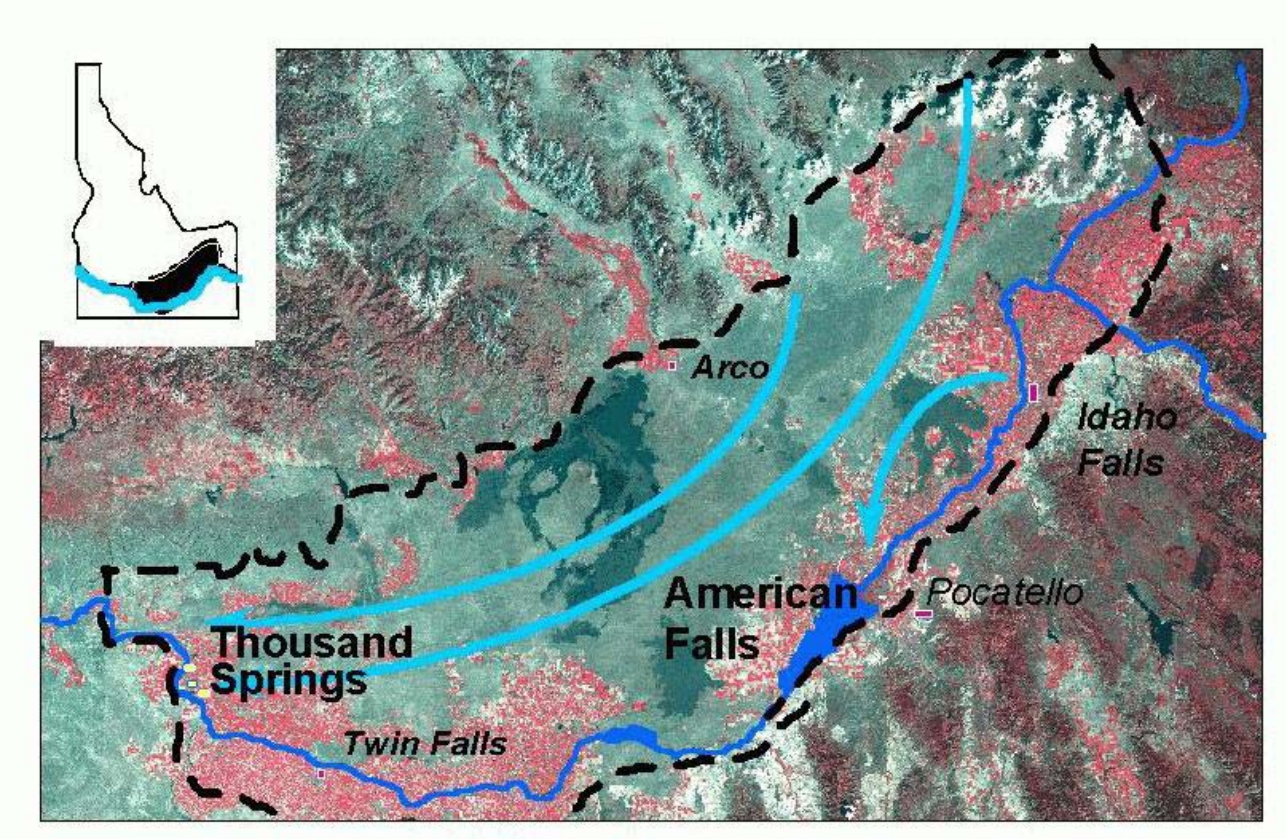

Figure 10. Outline of the Eastern Snake Plain Aquifer system (dashed line) with irrigated areas identified as red via bands 2, 3, and 4 of a TM image. The large, dark area in the center of the ESPA contains the Craters of the Moon National Monument. The irrigated strip north of the monument is in the Big Lost River basin.

Images were purchased from both Landsat 5 and Landsat 7 archives to increase the number of images available for the Southern Idaho area. Often, images were available where the dates for adjacent paths were separated by only one day. This was made possible by obtaining Landsat 5 images for one path and Landsat 7 images for the adjacent path. We found Landsat 5 images to be of immense value in providing ET for similar periods between paths.

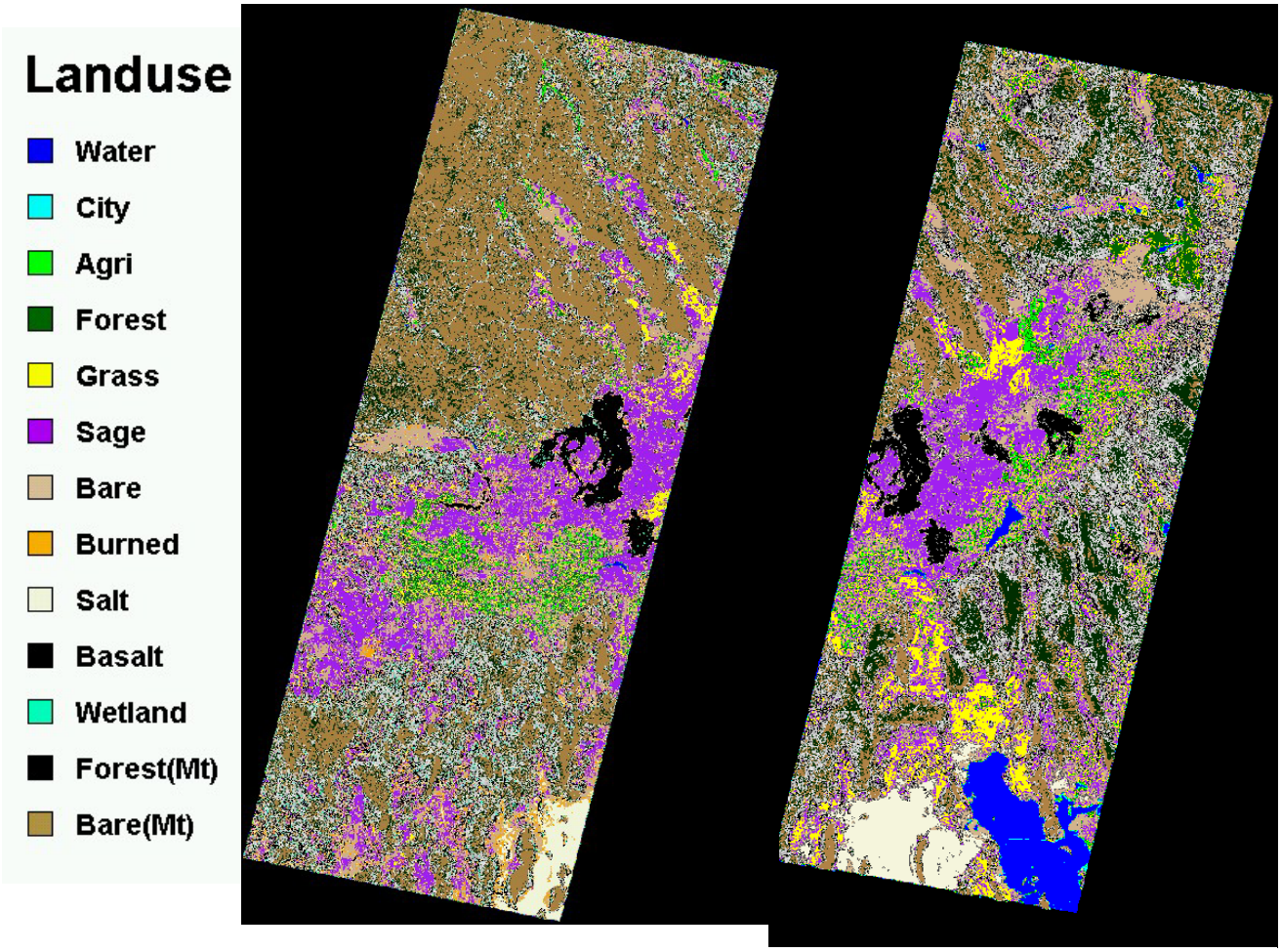

Figure 11. Land use classification for paths 40 (left) and 39 (right) for rows 29, 30 and 31, representing NE Nevada (lower left), NW Utah (lower right), ESPA (center), and mountain areas of south-central Idaho and SW Montana (upper parts of images). The Great Salt Lake is shown in the lower right corner.

The following sets of images from the 2000 application to the ESPA help to illustrate the spatial distribution of evapotranspiration over time and space.

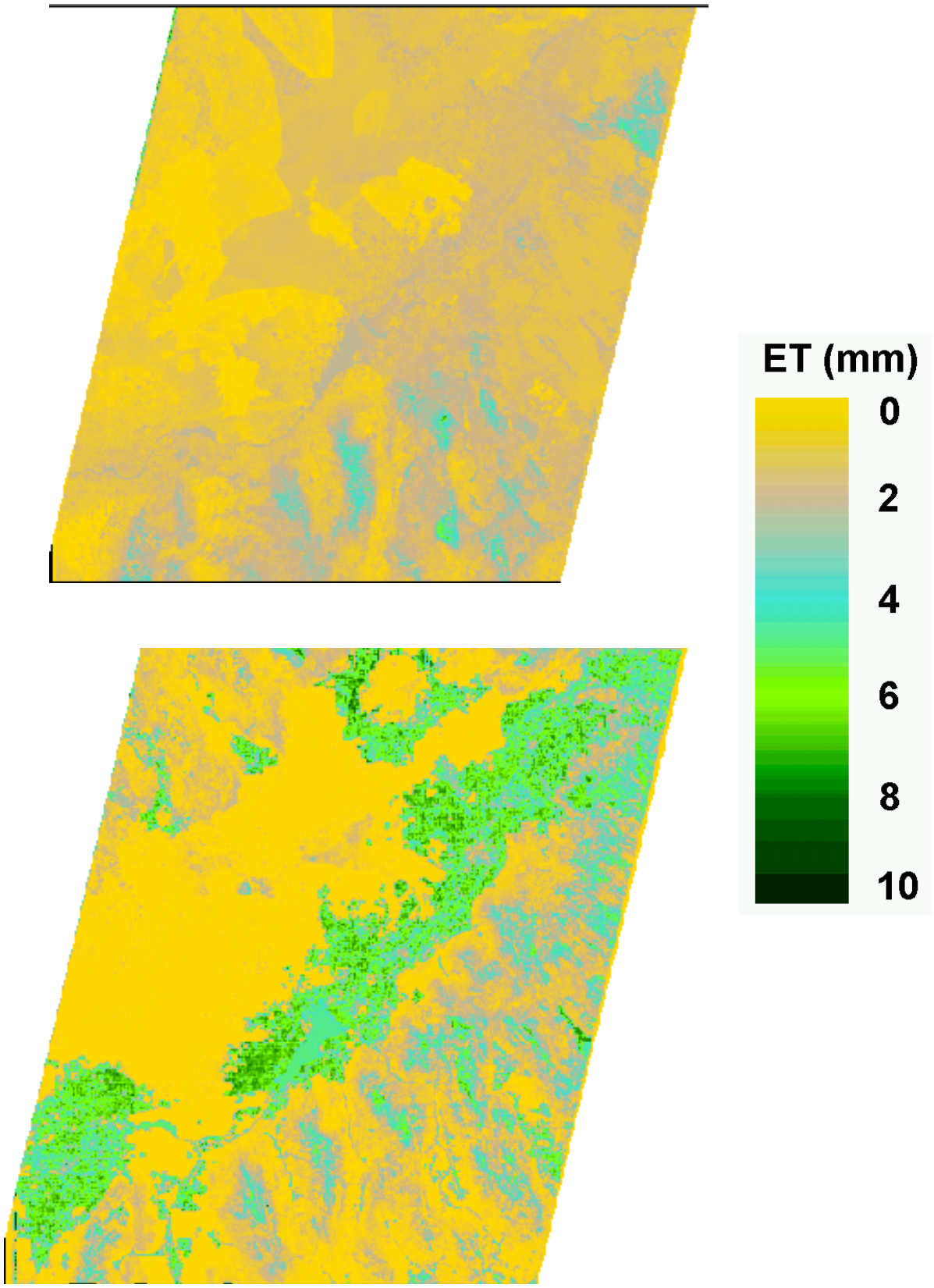

Figure 12. ET "maps" for the American Falls area of path 39 for dates April 1 (top) and July 6 (bottom), 2000.

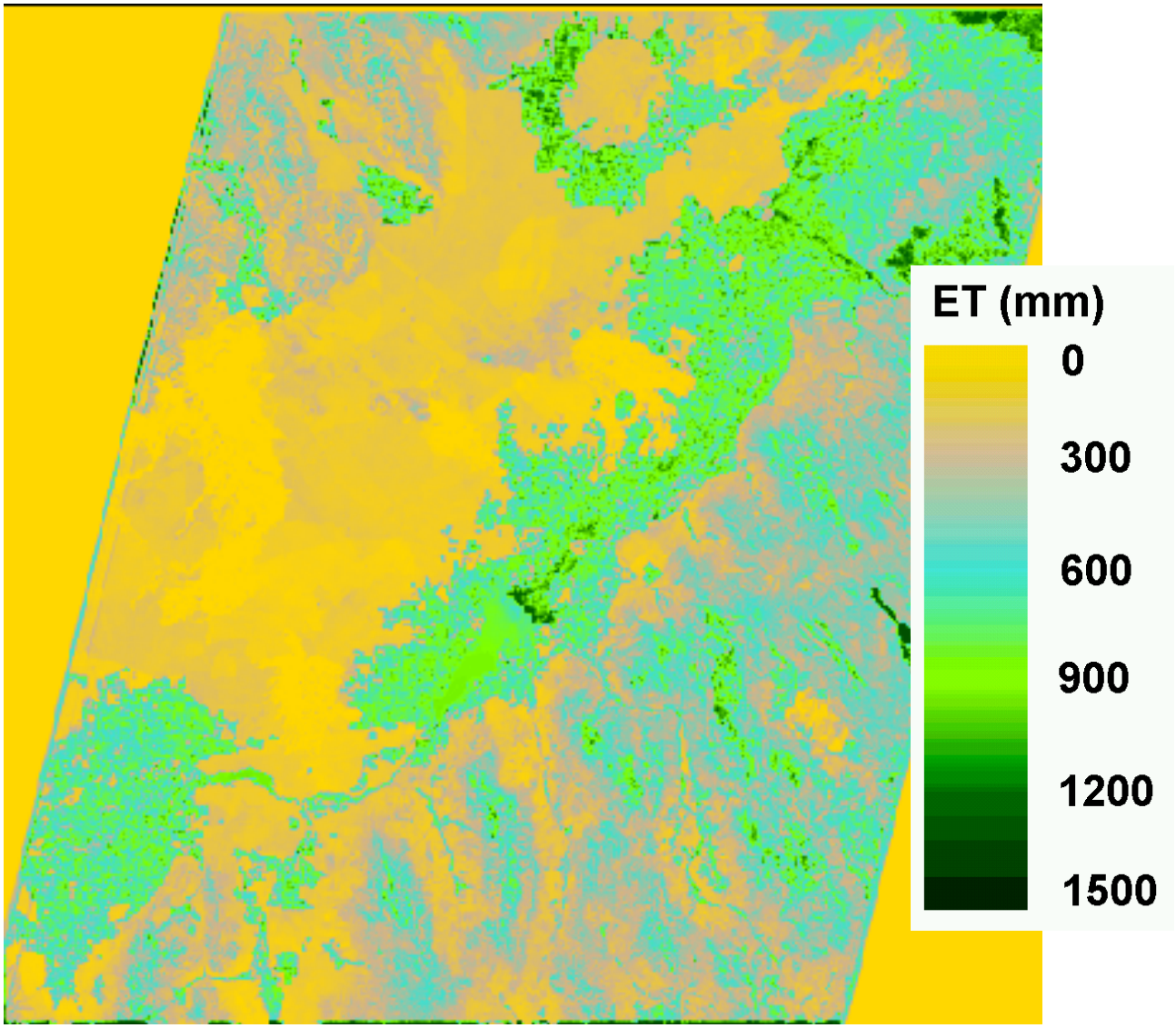

Figure 13. Seasonal ET (April - October) for year 2000 for the ESPA portion of path 39. The dark green (i.e., high ET) strip along the NE edge of American Falls Reservoir (center of image) represents a wetland area.

Figure 14 shows a close-up of 24-hour ET for for 05/03/2000. The spatial resolution of ET differences within individual fields irrigated by center pivots (circular shaped areas) is visible. Differences in ET within a field are caused by variation in crop density, soil fertility, disease, or water application uniformity, all of which impact ET and crop yield. Impacts of wetness of soil on ET due to location and operating direction of the center pivot lateral are also visible. The striped ET lines in rectangular-shaped fields are caused by differences in evaporation from wet soil by wheel line sprinkler systems (these cover only 30 to 50 m strips at one time). The false color image shows the darker strips representing wet soil. These translate into larger ET values.

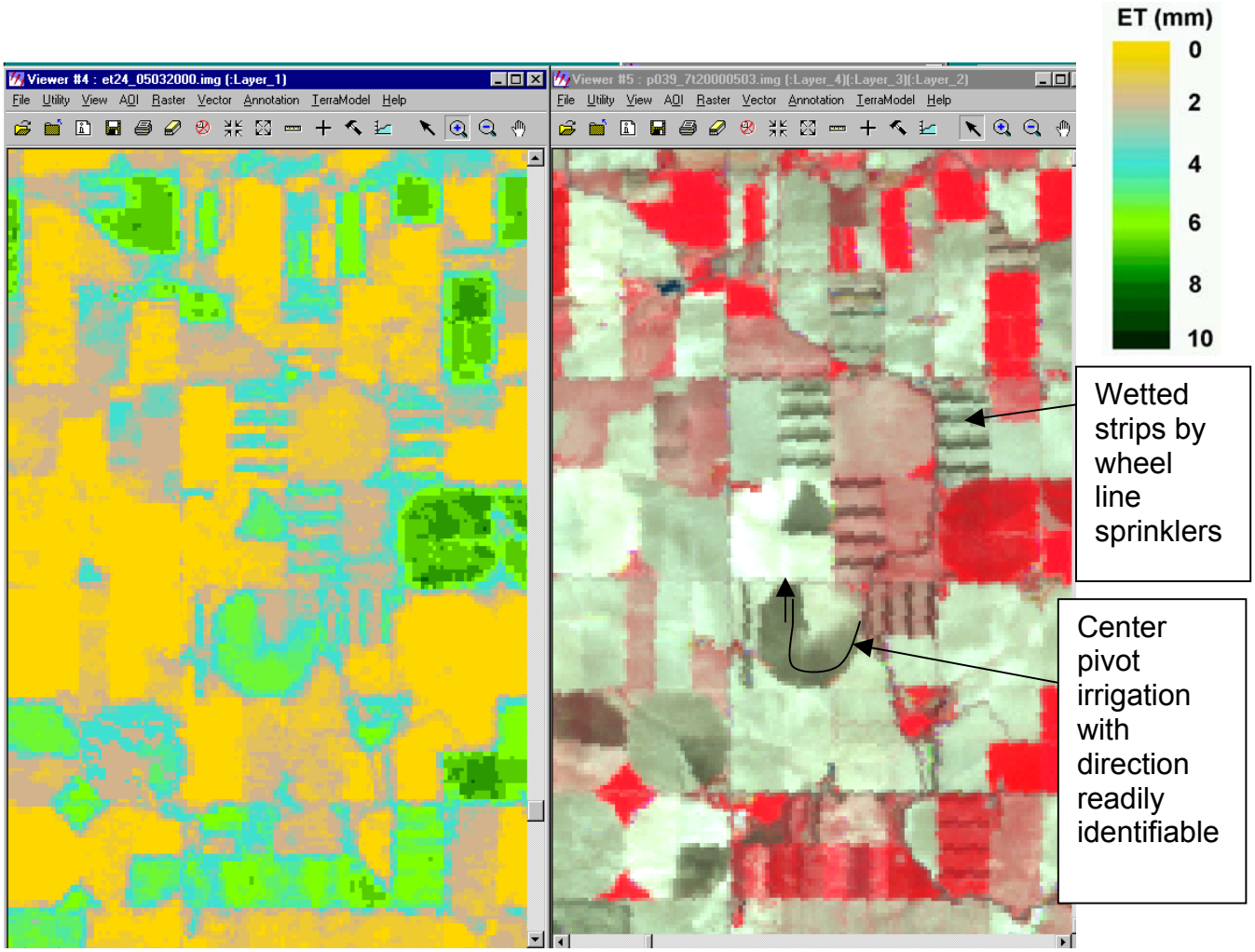

Figure 14. Close-up of ET from a Landsat 7 image showing ET variation within individual fields on May 5, 2000 in the American Falls area, Idaho.

The Relationship Between SEBAL-Derived ET and Ground Water Pumpage

The relationship between ET and ground water pumpage is important to IDWR regulatory business processes. The transition to conjunctive water management will require that there be parity in monitoring ground water and surface water diversions.

Historically, surface water diversions have been closely monitored while ground water diversions have not. This disparity is a function of 1) the relatively few number of surface water diversions compared to the number of wells, 2) the ease of locating surface water diversions, 3) the much greater volume of water diverted from surface sources, and 4) historical practices. There are approximately 300 monitored diversions from the Snake River above Milner Dam that irrigate approximately 1.6 million acres on the Eastern Snake River Plain (ESRP). The ESRP also supports approximately half a million acres of ground water irrigation, but from approximately 5,000 wells. From a logistical point alone, monitoring ground water pumpage is a large undertaking.

IDWR and other, associated organizations presently spend approximately $500,000 per year on monitoring ground water pumpage from the ESRP. The Water Distribution Section of IDWR has visited the approximately 5,000 wells on the ESRP over the last 5 years to record the GPS location and to measure the well flow and simultaneous power consumption. These data are stored in the Water Management Information System (WMIS). WMIS is designed to estimate ground water pumpage given the power-meter records for its constituent wells.

This task hypothesizes that there is a correlation between SEBAL ET and ground water pumpage, and that for a given water right, the ET for the field or fields covered by that water right can be used to estimate the volume of water pumped. The data used in this task are 1) the polygons that define the actual place of use (POU) for water rights, 2) the location of each associated well (or point of diversion, POD) as recorded in the WMIS, 3) the original power records for the wells in WMIS, 4) the flow-volume/power coefficients computed by the WMIS program for each WMIS well, and 5) the April-to-October, cumulative ET as computed by SEBAL.

The significance of a strong correlation between pumpage and SEBAL ET is that IDWR would be able to estimate the pumpage from each individual water right, allowing the present, intensive and expensive data-gathering effort to be scaled-back, potentially saving IDWR tens-of-thousands of dollars.

The initial results of the analysis were not encouraging. There were 184 POUs for which the SEBAL-pumpage was made. Figure 15 shows the scatter plot of the two variables. No clear relationship is obvious, and a first-order polynomial regression confirms the lack of correlation with an $r^2 = 0.14$. Nevertheless, a close examination of the two data sets is revealing.

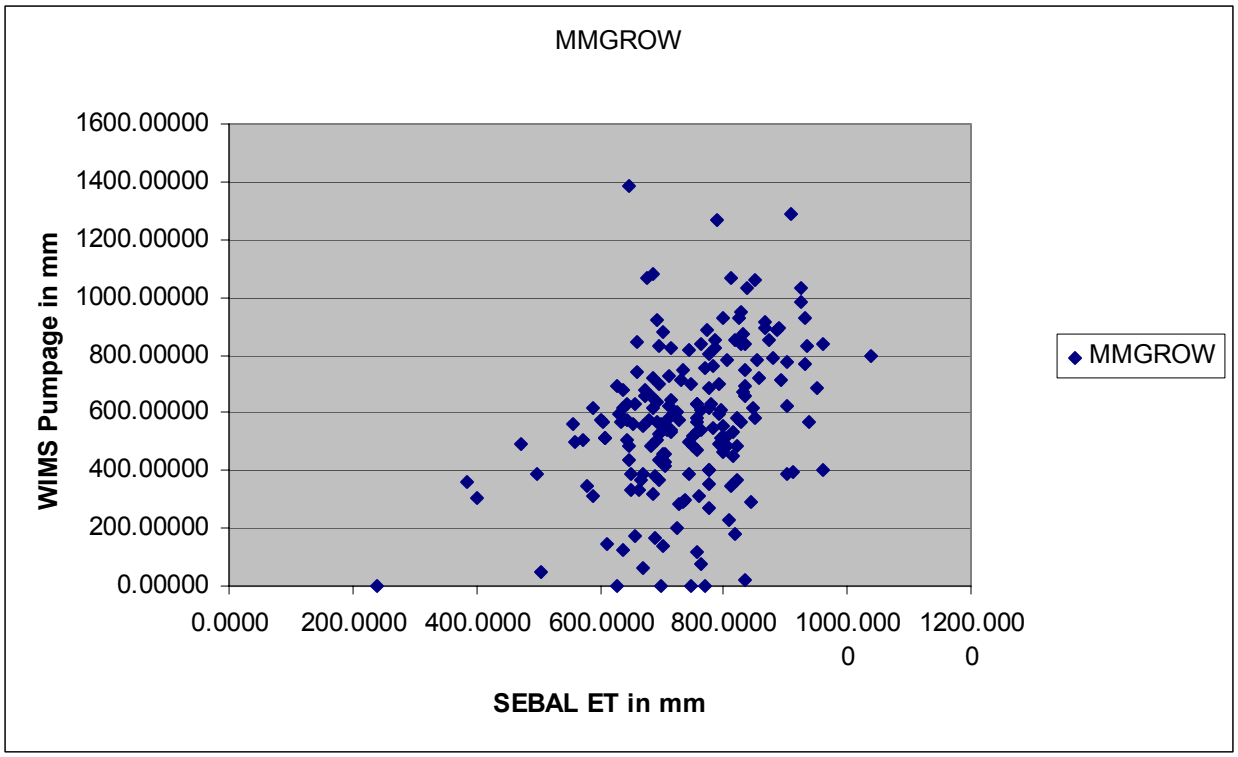

Figure 15. The scatter plot of pumpage versus SEBAL ET in millimeters for the period April – October, 2000.

Figures 16 and 17 show the scatter within each individual variable in the dataset plotted with AgriMet ET data. The AgriMet data show the ET extremes of Alfalfa and peas, and were recorded recorded for the year 2000 at the U.S. Bureau of Reclamation AgimMet station in Aberdeen, Idaho. The Aberdeen Station is within approximately twenty miles of these fields, and is representative of them.

The two plots reveal useful information. Nearly all the SEBAL ET observations fall between the extremes of ET, which is the lowest at 365 mm for peas and highest at 890 mm for alfalfa. Further, there is a distinct “floor” at approximately 600 mm of ET, which is an indication of a minimum level of ET from irrigated agriculture. Most of the data fall well above the minimum ET for peas because grains, which have a higher minimum ET, in the range of 556 mm to 576 mm, are a more common crop than peas in the Aberdeen area. The reason that the “floor” is approximately 50 mm above the ET level for grains is that the AgriMet figures are crop ET, not field ET. They are adjusted to account for precipitation, and do not account for the fact that, after harvest, many farmers will continue to irrigate bare soil to build soil moisture. This practice is clearly evident in Figure 18, which is a Landsat FCC image taken September 16, 2000.

Contrast the SEBAL ET pattern of Figure 16 with the pattern for pumpage as illustrated by Figure 17. The pumpage data are not consistent at either the high end of the chart or at the low end. There is no “floor” evident to show that there is a minimum level of pumping that is a minimum level of irrigation needed to support an irrigated

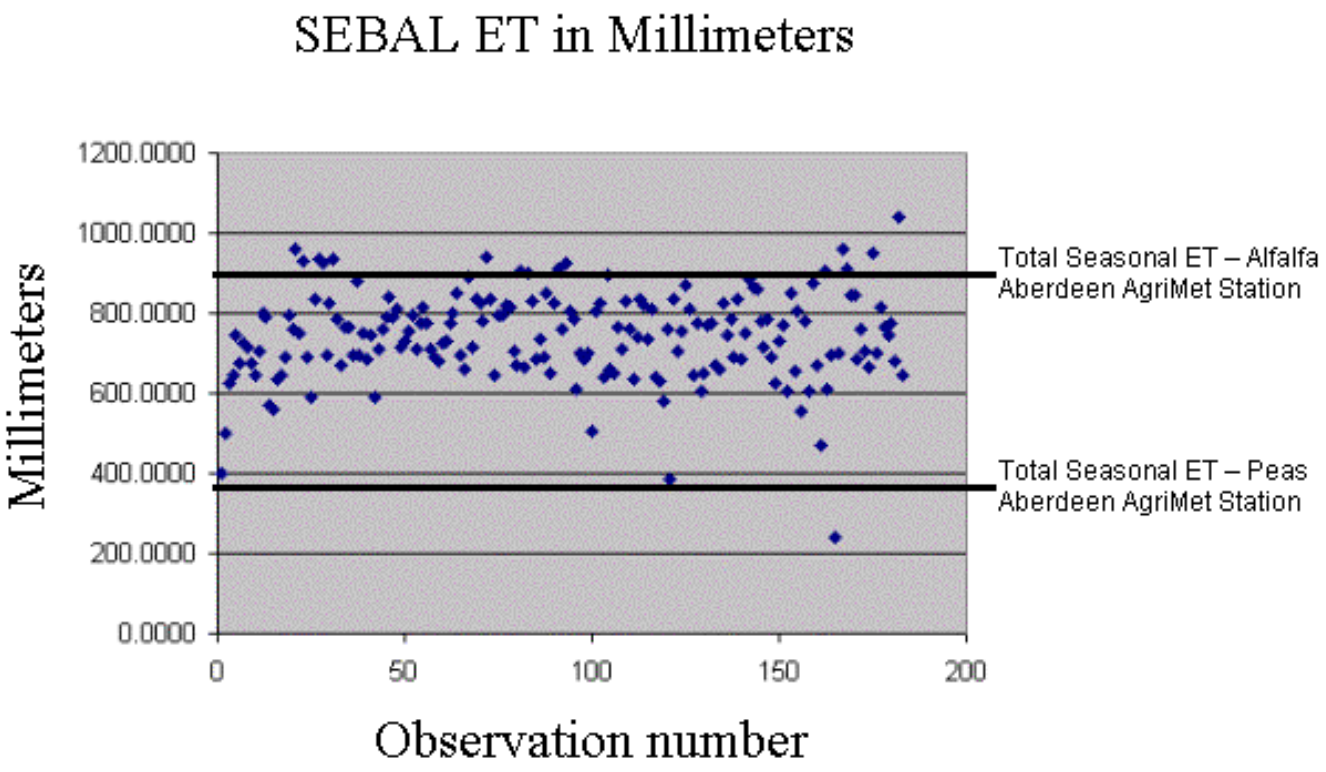

Figure 16. April to October, 2000 SEBAL ET compared with AgriMet ET extremes.

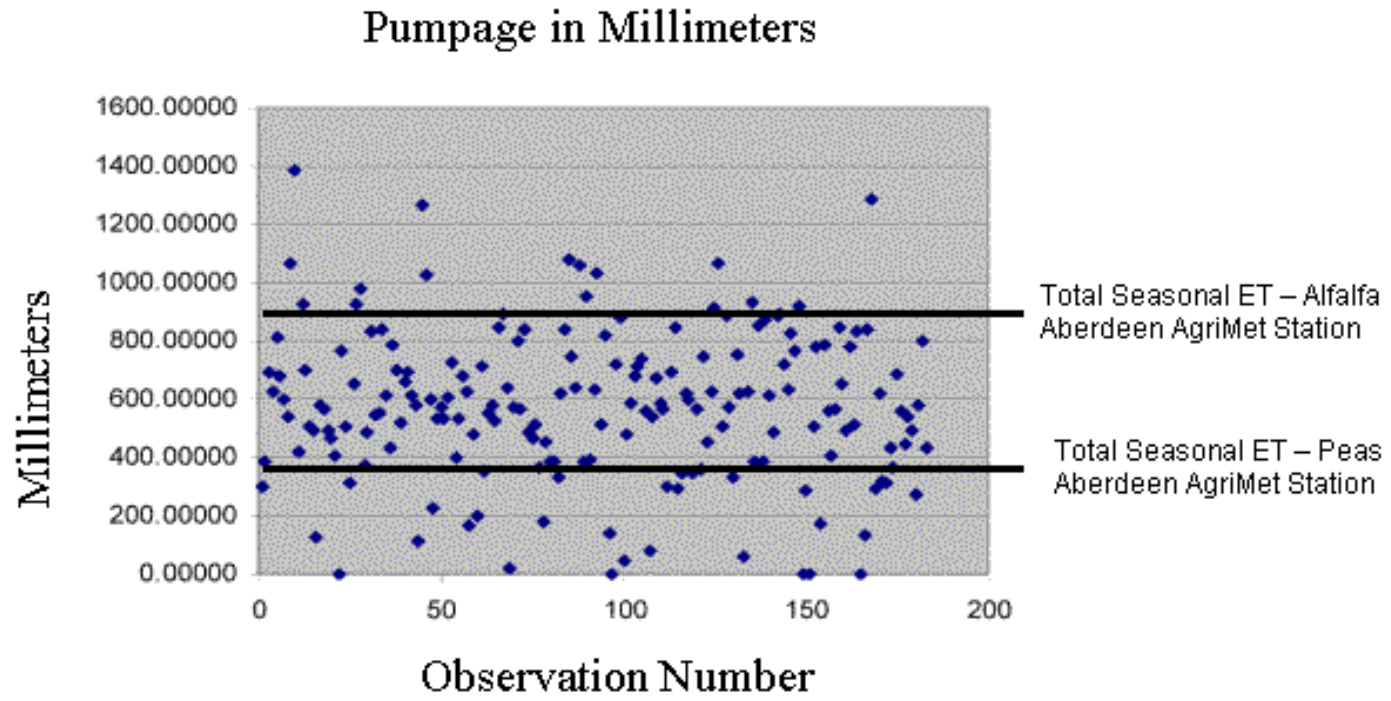

Figure 17. April to October, 2000 pumpage compared with AgriMet ET extremes.

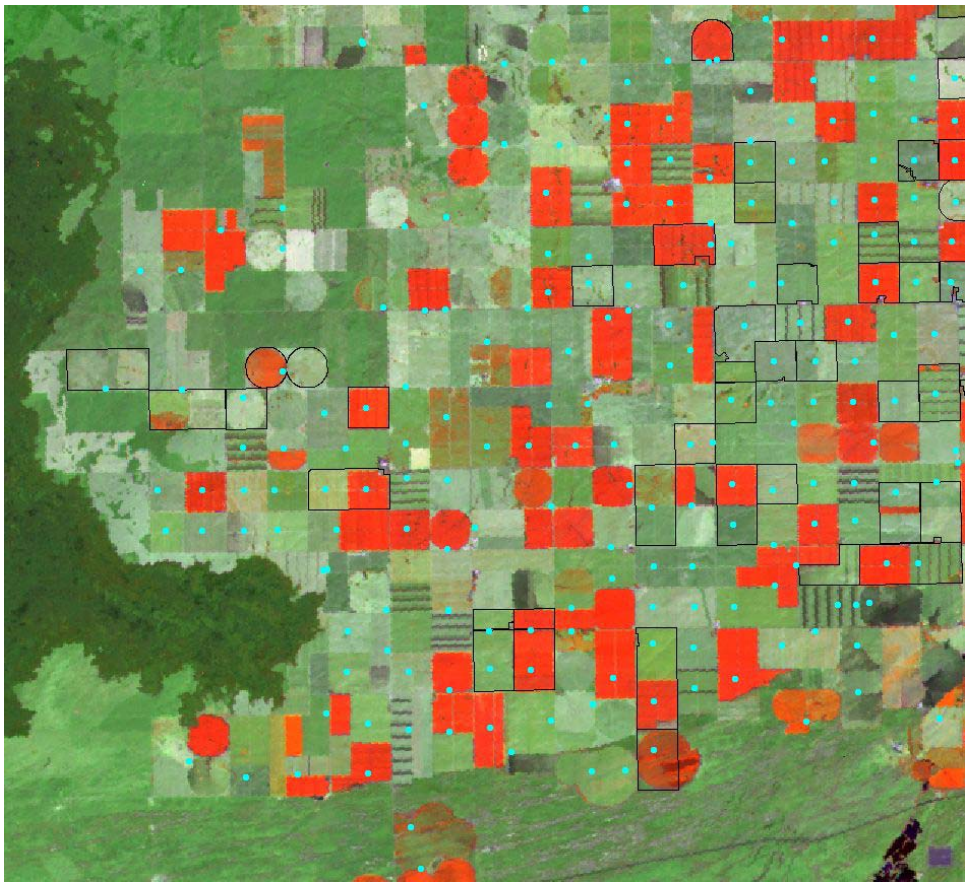

Figure 18. Landsat FCC image showing the dark-and-light stripe pattern characteristic of continued irrigation of harvested fields in order to build soil moisture.

crop. In fact, the pumpage data set indicates that there are fields getting no pumpage at all. The reliability of the dataset is called into question by the lack of patterns that reflect irrigation practice on the ESRP, and by the abundance of data at the extreme low end of the chart. With these questions in mind, a small part of the study area was chosen arbitrarily, and the pumpage data were examined field-by-field. The results of this examination bear out the unreliability of the pumpage data.

In an effort to understand data, regression analysis was run on 32 POUs as shown in Figure 19 as a baseline. The result was an $r^2 = 0.08$.

Figure 19 shows POUs and PODs for the fields being individually examined. The most significant problem discovered stemmed from the inconsistent connectivity between the wells (PODs) and associated water rights (POUs). This inconsistency is not a problem for the WMIS program, which monitors pumpage, but is a problem for any analysis needing to link pumpage to a specific water right and, hence, a specific field or fields being irrigated by that pumpage. For example, the fields designated as POU 609 and POU 610 had only one POD listed in the database, but, in fact, have two PODs. For

POU 609, POD 609 has a pumpage of 332 mm and a SEBAL ET of 663 mm. The pumpage for POU 609 was increased to 590 mm by adding the 258 mm of pumpage from the second POD that served POU 609.

Another type of problem was found with POU 708. The POU is a rectangle, but

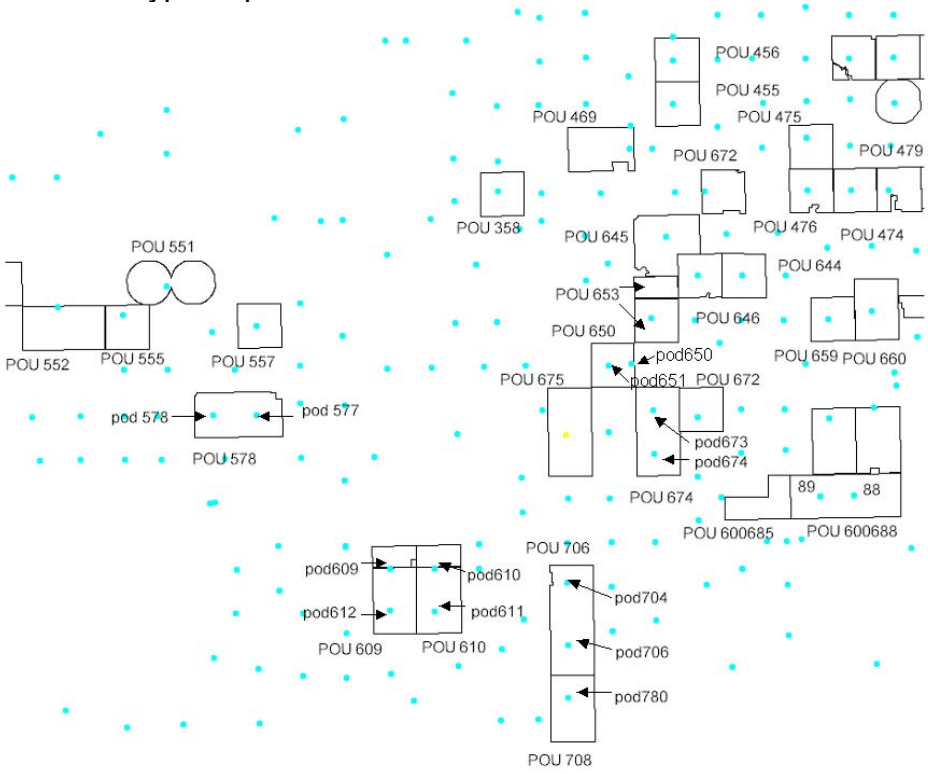

Figure 19. POUs and PODs for the fields being individually examined.

the area being irrigated is actually a center-pivot that extends well out of the defined POU. The result is that the SEBAL ET for POU 708 is 686 mm, significantly below the pumpage of 1079 mm for the field that is actually irrigated. Figure 20 illustrates the problem with POU 708. Since the recorded POU does not match the actual POU, this field was removed from the analysis.

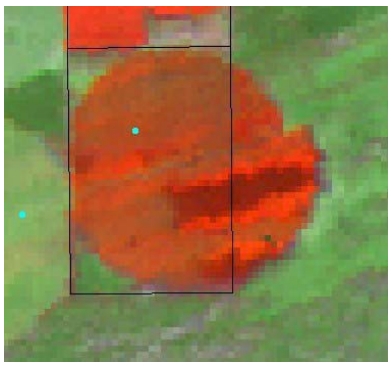

Figure 20. POU 708 plotted on a Landsat FCC image showing the difference between the POU and actual area irrigated.

The other field removed from the analysis was POU 551. The pumpage was listed as zero millimeters, but as seen in Figure 18, there was a crop grown in the POU.

After making the appropriate adjustments in the pumpage data by removing two fields and adding the missing PODs for five POUs, the analysis was re-run on the remaining 31 of the original 33 fields. The result was an $r^2 = 0.24$. Figure 21 is the associated scatter plot. Two facts are clear: 1) the link is weak between water right places of use and the WMIS points of diversion, and 2) even when the link between POUs and PODs is clean, the relationship between SEBAL ET and pumpage is poor.

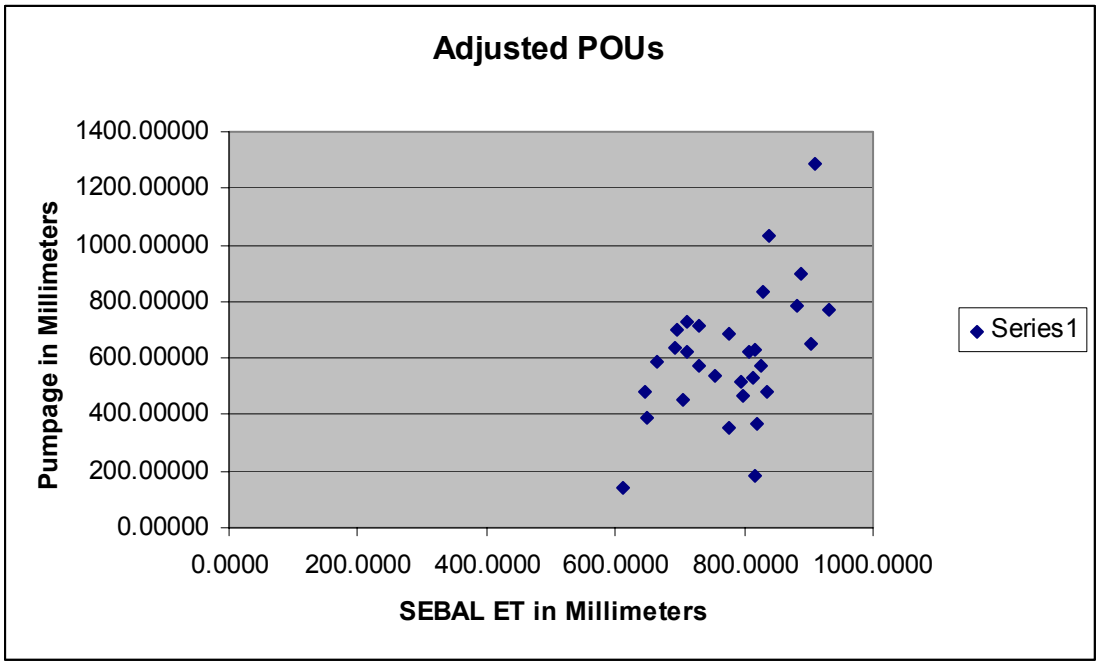

Figure 20. The scatter plot of SEBAL ET with pumpage for the adjusted POUs.

The results of the analysis of SEBAL ET with pumpage might seem to preclude using SEBAL in this application. However, this is not necessarily the case. The analysis indicates that the problem seems to lie with the pumpage data, not with the SEBAL data. The SEBAL data are consistent with irrigation conditions on the ESRP. Deriving pumpage from power records appears to be less than exact. At least part of the problem appears to stem from the power conversion coefficient (PCC), The PCC is the ratio of power to water-volume for an irrigation system. The PCC, even if perfect when measured, changes every time there is a change in the system configuration (e.g. when another wheel line is added of when one is removed), or with any fluctuation in the depth to water in the well. The PCCs for the wells in this analysis have never been reexamined, some going unchanged over a three-year period.

The results of the analysis for the other objectives indicate that SEBAL is a reliable means of computing ET. SEBAL ET may be a reliable predictor of pumpage, but before

that conclusion can be made, the ET-pumpage analysis needs to be rerun on a dataset that is more closely monitored that the data in this analysis. The new data set needs to be clearly ground water only with no supplemental surface water; has to have all the PODs identified and monitored; has to have the PCC inspected regularly and adjusted on as necessary; and has to have information from the farmer as to crop grown and irrigation practices.

Appendix A Publications and Presentations

Allen, R.G., M Tasumi, W. Bastiaanssen, W. Kramber, A. Morse, R. Trezza, J.L. Wright; 2002; Evapotranspiration from Satellite and SEBAL for the Snake Plain Aquifer in Idaho; Proceedings of the Conference on Energy, Climate, Environment, and Water; U.S. Committee on Irrigation and Drainage; California Polytechnic State University, San Luis Obispo, CA

Allen, R.G., A. Morse, M. Tasumi, W. Bastiaanssen, W.J. Kramber, H.N. Anderson; 2001; Evapotranspiration from Landsat (SEBAL) for Water Rights Management and Compliance with Multi-State Water Compacts; Proceedings of IGARSS 2001; Sydney, Australia

Allen, R.G., A. Morse, M. Tasumi, W. Bastiaanssen, W.J. Kramber, H.N. Anderson; 2001; Landsat Thematic Mapper for Evapotranspiration from via SEBAL process for Water Rights Management and Hydrologic Water Balances; Proceedings of the Conference of the American Geophysical Union; Boston, MA.

Allen, R.G., M. Tasumi, A. Morse, W. Bastiaanssen, W.J. Kramber, H.N. Anderson; 2001; Evapotranspiration from Landsat (SEBAL): Applications in the U.S. Proceedings of the Annual Conference of the International Commission on Irrigation and Drainage, Seoul, Korea.

Morse, A.; 2001; SEBAL Evapotranspiration from Landsat for Water Rights Management in Idaho; presented at the 2001 meeting of the National States' Council on GIS; St. Louis, MO

Morse, A.; 2001; Managing Idaho Water Rights with Remote Sensing; presented to The World Bank; Washington, D.C.

Morse, A, R.G. Allen, M. Tasumi, and W.J. Kramber; 2001; SEBAL Evapotranspiration from Landsat for Water Rights Management; presented at the IGARSS 2001 Symposium; Sydney, Australia

Morse, A and R.G. Allen; 2001; Application of the SEBAL Methodology for Estimating ET and Consumptive Water-Use Through Remote Sensing; presented at Raytheon Company, Upper Marlboro, MD.

Morse, A.; 2001; SEBAL Phase II: Now What?; presented at the Western States Water Council Water Information Management Systems 2001 Workshop; Reno, NV.

Morse, A.; 2000; Mapping Evapotranspiration with SEBAL and Landsat TM; presented at the Western States Water Council Water Information Management Systems 2000 Workshop; Sun Valley, ID.

Morse, A.; 2000; Using SEBAL and Landsat TM to Estimate Evapotranspiration; presented at the 2000 meeting of the National States Geographic Information Council Meeting; North Lake Tahoe, CA.

Morse, A., M. Tasumi, R.G. Allen, and W.J. Kramber; 2000; Application of SEBAL Methodology for Estimating Consumptive Use of Water and Streamflow Depletion in the Bear River Basin of Idaho through Remote Sensing; Final Report

Tasumi, M.; 2000; Preliminary Results on Computing Evapotranspiration Using SEBAL; research report to University of Idaho

Appendix B
Student Involvement

This project has supported three graduate students. Masahiro Tasumi has been supported for the length of his PhD studies in Biological and Agricultural Engineering at the University of Idaho, and is writing his dissertation on SEBAL. Tasumi has been working on the project from the beginning and has had extensive input on SEBAL refinement.

Two graduate students from Utah State University, Ricardo Trezza and Maria Gloria Romero, began working full-time on Phase II of the project beginning in June 2001. Both are Ph.D. students in Biological and Irrigation Engineering at Utah State University. Trezza was heavily involved in data processing and SEBAL application.

Romero has conducted various data analyses on Kimberly lysimeter and micro-meteorological data, including development of an albedo data model, which is not referred to in the report. It is used as background information for modeling and evaluating the evaporative fraction in SEBAL.

Appendix C
Inventory of Purchased Equipment

Under Phase I of this project, the University of Idaho purchased 2 copies of ERDAS Imagine software. No hardware was purchased.

Appendix D
Literature Citations

ASCE, 2000 (Walter, I.A. et al.), ASCE's Standardized reference evapotranspiration equation. ASCE Standardization of Reference Evapotranspiration Task Committee. Proceedings of the 4th Decennial Irrigation Symposium, ASAE, Phoenix, AZ, Nov., 2000.

Bastiaanssen, W.G.M., M. Menenti, R.A. Feddes, and A.A.M. Holtslag. 1998. A remote sensing surface energy balance algorithm for land (SEBAL): 1. Formulation. *J. Hydrology* 212-213, p. 198-212.

Bastiaanssen, W.G.M. 2000. SEBAL-based sensible and latent heat fluxes in the irrigated Gediz Basin, Turkey. *J. Hydrology* 229:87-100.

Jensen, M.E., R.D. Burman, and R.G. Allen (ed). 1990. *Evapotranspiration and Irrigation Water Requirements.* American Society of Civil Engineers, Engr. Pract. Manual No. 70. 332 p.

Morse, A., M. Tasumi, R.G. Allen, and W.J. Kramber; 2000; Application of SEBAL Methodology for Estimating Consumptive Use of Water and Streamflow Depletion in the Bear River Basin of Idaho through Remote Sensing; Final Report

Wright, J.L. 1982. New Evapotranspiration Crop Coefficients. *J. of Irrig. and Drain. Div.* (ASCE), 108:57-74.

Wright, J.L. 1996. Derivation of Alfalfa and Grass Reference Evapotranspiration. in. Evapotranspiration and Irrigation Scheduling, C.R. Camp, E.J. Sadler, and R.E. Yoder (ed.). Proc. Int. Conf., ASAE, San Antonio, TX. p. 133-140.

Appendix 1. Matching Band 6 of Landsat 5 TM images with lysimeter fields.

Because of the relatively small dimensions of the lysimeter fields at Kimberly (about 140 m x 190 m on average), it was not possible to find a complete Band 6 pixel of the Landsat 5 TM (120 m x 120 m) lying completely inside a lysimeter field. Often, portions of four band 6 pixels fell onto a lysimeter field. This caused "blurring" or contamination of the Band 6 pixel from surface temperatures of surrounding crops (or bare soil conditions) that were different from those for the lysimeter field, so that no single pixel could be found for many of the images that completely represented conditions and environment for the lysimeter field, and therefore the lysimeter itself. In some situations, no Band 6 pixels had more than 8 out of 16 30 m pixels lying on the lysimeter field (green area in figure below). The fields adjacent to the lysimeter fields were planted to beans (to the south) and wheat (to the north) during 1989, for example, when the lysimeter 2 field was planted to sugar beets. Planting dates and development rates of vegetation differ substantially between beans, wheat and sugar beets. The crop planted to the west of the lysimeter 2 field during 1989 was unidentifiable.

*TM Band6 DN values in Lysimeter fields (each number has an area of 30m*30m)for July 7, 1989.*

159	159	159	159	157	157	157	157	152	152	152	157
159	159	159	159	157	157	157	157	152	152	152	152
168	159	159	157	157	157	157	152	152	152	152	152
168	167	167	167	167	164	157	152	152	152	152	162
168	167	167	167	167	164	164	164	164	165	165	162
168	167	167	167	167	164	164	164	164	165	165	165

This difference in DN values between north and south portions of the Lys2 Field represented a 4-5 degree difference in surface temperature as shown in the following image:

Tab. Surface Temperature (K)

309	310	310	310	309	308	307	308	307	307	307	309
309	309	309	309	308	307	308	307	305	305	305	307
312	309	309	308	308	308	306	305	305	305	305	305
313	312	312	312	312	311	308	306	306	305	306	311
315	312	312	313	313	312	310	310	310	311	311	311
315	314	314	315	315	313	312	312	313	313	313	312

For the July 7, 1989 image, the 4-5 degree difference in surface temperature between pixels in Lys2Field created about 1 mm difference (about 20%) in daily ET (note the values in the following image are slightly out of date):

Tab. Daily ET in mm

5.76	5.92	5.85	5.82	5.94	5.88	7.08	7.06	7.01	6.62	6.06	6.11
5.62	5.84	5.75	5.59	6.01	6.04	6.3	6.47	6.87	6.99	7.17	6.37
5.28	5.72	5.88	6.13	6.12	6.11	6.73	6.99	7.12	6.9	6.73	7.37
5.1	5.22	5.16	5.18	5.18	5.49	6.17	6.54	6.74	6.73	6.58	5.97
4.54	5.3	5.02	4.91	4.84	4.95	5.86	5.91	5.88	5.61	5.58	6
4.54	4.67	4.69	4.23	3.94	4.36	5.23	5.24	5.31	5.47	5.42	5.47

The actual ET for the lysimeter field may have been higher than shown for either portion of the image, as the true temperature may have been lower than for any of the band six pixels, since all pixels contained some information from outside.

Example values for various surface characteristics for pixels inside and surrounding the Kimberly lysimeter fields

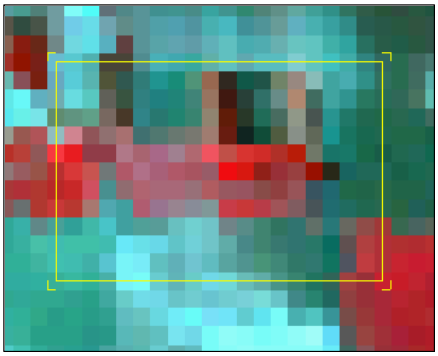

The following figures provide a sample of the type of variation in background characteristics and energy balance parameters computed during application of SEBAL. Each figure contains pixel values from the original TM image for the area surrounding the Kimberly lysimeter fields during 07/07/89. Each value shown represents a 30m*30m pixel.

Band 6 digital number:

B6

169	169	169	169	169	166	166	166	166	159	159	159	159	157	157	169	169	165	165	165
169	169	169	169	166	166	166	166	159	159	159	159	157	157	157	157	157	166	166	166
160	160	160	160	159	166	166	166	159	159	159	159	157	157	157	157	166	166	166	166
160	160	160	160	159	159	159	159	157	157	159	159	157	157	157	157	166	166	166	166
160	160	160	160	159	159	159	159	157	157	157	157	152	152	152	157	166	166	166	166
160	160	160	160	159	159	159	159	157	157	157	157	152	152	152	152	162	162	162	162
161	168	168	168	168	159	159	157	157	157	157	152	152	152	152	152	162	162	162	162
161	168	168	168	168	167	167	167	167	164	157	152	152	152	152	162	162	162	162	163
161	168	168	168	168	167	167	167	167	164	164	164	164	165	165	162	162	162	162	163
161	168	168	168	168	167	167	167	167	164	164	164	164	165	165	165	165	153	153	153
168	168	168	168	168	167	167	167	167	164	164	164	164	165	165	165	165	153	153	153
186	186	186	186	167	167	167	167	164	164	164	164	165	165	165	165	165	153	153	153
186	186	186	186	174	174	174	174	170	164	164	164	165	165	165	165	153	153	153	153

Albedo

0.27	0.26	0.22	0.17	0.17	0.23	0.24	0.23	0.23	0.24	0.25	0.24	0.25	0.25	0.27	0.26	0.24	0.23	0.2	0.18
0.26	0.26	0.23	0.17	0.18	0.2	0.21	0.2	0.21	0.19	0.14	0.16	0.17	0.22	0.22	0.26	0.23	0.23	0.2	0.18
0.26	0.27	0.24	0.18	0.18	0.2	0.2	0.19	0.2	0.2	0.14	0.16	0.19	0.22	0.23	0.2	0.22	0.2	0.18	0.18
0.21	0.22	0.22	0.19	0.16	0.2	0.19	0.19	0.2	0.21	0.14	0.15	0.17	0.2	0.23	0.19	0.21	0.18	0.17	0.17
0.26	0.24	0.2	0.21	0.22	0.19	0.2	0.21	0.21	0.22	0.14	0.13	0.15	0.19	0.23	0.2	0.2	0.18	0.17	0.17
0.21	0.19	0.2	0.2	0.23	0.22	0.22	0.23	0.22	0.22	0.2	0.19	0.19	0.18	0.16	0.2	0.18	0.18	0.17	0.16
0.18	0.2	0.21	0.22	0.21	0.23	0.22	0.21	0.21	0.21	0.18	0.18	0.17	0.18	0.19	0.15	0.14	0.17	0.17	0.17
0.18	0.18	0.21	0.22	0.22	0.22	0.22	0.22	0.22	0.22	0.2	0.2	0.19	0.19	0.2	0.18	0.18	0.17	0.17	0.17
0.19	0.19	0.22	0.24	0.22	0.22	0.23	0.23	0.23	0.24	0.2	0.2	0.2	0.2	0.2	0.18	0.18	0.18	0.17	0.17
0.23	0.22	0.24	0.26	0.22	0.23	0.23	0.25	0.27	0.27	0.22	0.21	0.2	0.19	0.19	0.2	0.19	0.2	0.19	0.18
0.24	0.24	0.24	0.24	0.29	0.28	0.28	0.26	0.27	0.27	0.24	0.21	0.2	0.2	0.19	0.19	0.17	0.18	0.19	0.18
0.24	0.24	0.24	0.26	0.3	0.3	0.26	0.25	0.27	0.25	0.24	0.22	0.21	0.21	0.19	0.19	0.18	0.18	0.19	0.18
0.23	0.24	0.23	0.24	0.3	0.31	0.27	0.25	0.26	0.28	0.28	0.25	0.24	0.22	0.2	0.18	0.18	0.19	0.18	0.18

Evaporative Fraction (EF = ET / (R_n – G)):

EF

0.58	0.56	0.61	0.71	0.71	0.67	0.63	0.64	0.63	0.74	0.72	0.74	0.72	0.74	0.74	0.58	0.56	0.65	0.69	0.72
0.61	0.56	0.6	0.7	0.72	0.68	0.65	0.65	0.76	0.8	0.82	0.78	0.81	0.79	0.8	0.76	0.75	0.64	0.67	0.7
0.72	0.67	0.7	0.79	0.8	0.68	0.67	0.67	0.76	0.8	0.84	0.8	0.79	0.79	0.8	0.8	0.65	0.66	0.69	0.7
0.75	0.75	0.74	0.79	0.82	0.76	0.76	0.75	0.78	0.8	0.84	0.81	0.79	0.8	0.79	0.81	0.65	0.68	0.7	0.7
0.73	0.78	0.8	0.78	0.79	0.78	0.78	0.78	0.8	0.81	0.86	0.84	0.85	0.86	0.84	0.81	0.64	0.69	0.7	0.7
0.82	0.83	0.81	0.81	0.79	0.8	0.8	0.78	0.82	0.83	0.83	0.85	0.89	0.89	0.9	0.85	0.73	0.73	0.74	0.75
0.81	0.74	0.72	0.68	0.71	0.79	0.8	0.83	0.83	0.82	0.87	0.9	0.89	0.89	0.88	0.9	0.79	0.75	0.75	0.74
0.82	0.75	0.72	0.65	0.69	0.71	0.71	0.71	0.71	0.75	0.82	0.87	0.87	0.88	0.87	0.76	0.74	0.75	0.75	0.74
0.81	0.74	0.69	0.62	0.62	0.72	0.7	0.69	0.68	0.7	0.78	0.78	0.77	0.75	0.74	0.77	0.74	0.74	0.75	0.74
0.72	0.62	0.59	0.57	0.62	0.65	0.65	0.62	0.59	0.65	0.72	0.71	0.71	0.71	0.7	0.72	0.69	0.85	0.87	0.88
0.59	0.57	0.57	0.59	0.54	0.57	0.58	0.6	0.59	0.65	0.67	0.7	0.71	0.7	0.7	0.7	0.7	0.86	0.87	0.88
0.28	0.29	0.31	0.27	0.54	0.55	0.61	0.63	0.65	0.66	0.68	0.69	0.68	0.69	0.7	0.7	0.69	0.85	0.88	0.88
0.3	0.29	0.31	0.32	0.42	0.39	0.48	0.52	0.56	0.63	0.63	0.66	0.66	0.68	0.69	0.7	0.84	0.87	0.88	0.89

Emissivity

0.95	0.94	0.94	0.98	0.98	0.96	0.94	0.94	0.94	0.95	0.94	0.95	0.94	0.94	0.95	0.94	0.93	0.94	0.95	0.96
0.95	0.94	0.95	0.97	0.97	0.95	0.94	0.94	0.95	0.98	0.98	0.96	0.96	0.97	0.97	0.95	0.94	0.94	0.95	0.96
0.95	0.94	0.94	0.97	0.97	0.95	0.95	0.95	0.95	0.97	0.99	0.97	0.96	0.96	0.97	0.96	0.94	0.95	0.95	0.96
0.96	0.96	0.95	0.97	0.98	0.95	0.95	0.95	0.95	0.97	0.99	0.97	0.95	0.96	0.97	0.97	0.94	0.95	0.96	0.96
0.96	0.98	0.98	0.97	0.98	0.96	0.96	0.97	0.97	0.97	0.99	0.98	0.96	0.97	0.97	0.97	0.94	0.95	0.95	0.96
0.99	0.99	0.98	0.98	0.98	0.98	0.98	0.97	0.98	0.99	0.98	0.99	0.99	0.99	0.99	0.97	0.95	0.95	0.95	0.96
0.99	0.99	0.98	0.97	0.98	0.98	0.98	0.98	0.98	0.98	1	0.99	0.99	0.99	0.98	0.99	0.98	0.96	0.96	0.96
0.99	0.99	0.99	0.95	0.97	0.98	0.98	0.98	0.98	0.98	0.98	0.98	0.98	0.98	0.98	0.97	0.96	0.96	0.96	0.96
0.99	0.99	0.97	0.95	0.95	0.98	0.97	0.97	0.97	0.96	0.99	0.99	0.99	0.98	0.98	0.97	0.95	0.96	0.96	0.96
0.95	0.94	0.94	0.93	0.95	0.95	0.95	0.95	0.94	0.95	0.97	0.96	0.96	0.96	0.96	0.97	0.95	0.97	0.98	0.99
0.94	0.93	0.93	0.94	0.93	0.94	0.94	0.94	0.94	0.95	0.95	0.96	0.95	0.96	0.96	0.95	0.95	0.98	0.99	0.99
0.93	0.94	0.94	0.94	0.93	0.94	0.94	0.95	0.95	0.95	0.95	0.95	0.95	0.95	0.95	0.95	0.95	0.97	0.99	0.99
0.93	0.93	0.93	0.94	0.93	0.93	0.94	0.95	0.94	0.94	0.94	0.95	0.95	0.95	0.95	0.95	0.96	0.99	0.99	0.99

24 hour ET from an early run of SEBAL, mm d^{-1}

ET24

3.92	3.83	4.46	5.72	5.72	4.88	4.45	4.55	4.6	5.22	4.96	5.18	4.93	5.1	4.87	3.92	3.92	4.69	5.26	5.66
4.16	3.77	4.31	5.63	5.67	5.18	4.88	4.99	5.65	6.18	6.84	6.31	6.48	5.79	5.78	5.17	5.37	4.57	5.02	5.48
4.93	4.45	4.91	6.15	6.25	5.19	5.16	5.16	5.74	6	7.01	6.46	6.06	5.71	5.8	6.03	4.71	4.99	5.39	5.55
5.56	5.47	5.38	6.05	6.56	5.69	5.85	5.78	5.87	6	7	6.68	6.29	6.1	5.62	6.26	4.86	5.35	5.6	5.62
4.95	5.46	6.01	5.76	5.76	5.92	5.85	5.82	5.94	5.88	7.08	7.06	7.01	6.62	6.06	6.11	4.85	5.43	5.6	5.62
6.11	6.45	6.16	6.16	5.62	5.84	5.75	5.59	6.01	6.04	6.3	6.47	6.87	6.99	7.17	6.37	5.68	5.74	5.96	6.07
6.3	5.65	5.34	5.01	5.28	5.72	5.88	6.13	6.12	6.11	6.73	6.99	7.12	6.9	6.73	7.37	6.59	5.92	5.94	5.89
6.4	5.88	5.33	4.78	5.1	5.22	5.16	5.18	5.18	5.49	6.17	6.54	6.74	6.73	6.58	5.97	5.84	5.96	6	5.88
6.18	5.76	5.01	4.37	4.54	5.3	5.02	4.91	4.84	4.95	5.86	5.91	5.88	5.61	5.58	6	5.76	5.83	5.93	5.86
5.17	4.53	4.23	3.93	4.54	4.67	4.69	4.23	3.94	4.36	5.23	5.24	5.31	5.47	5.42	5.47	5.32	6.4	6.62	6.8
4.11	4.05	4.05	4.1	3.46	3.7	3.77	4.05	3.93	4.36	4.72	5.19	5.34	5.36	5.42	5.43	5.54	6.65	6.67	6.86
1.97	2.04	2.2	1.88	3.36	3.42	4.14	4.41	4.34	4.49	4.82	5.08	5.09	5.19	5.38	5.4	5.43	6.62	6.66	6.86
2.19	2.09	2.26	2.26	2.64	2.42	3.19	3.63	3.76	4.08	4.08	4.55	4.65	5	5.24	5.45	6.58	6.71	6.91	6.94

Soil Heat Flux (G) from an early run of SEBAL, W m^{-2}

G

128	129	139	149	149	141	137	139	141	144	140	143	140	142	136	130	133	141	150	154
131	128	136	150	153	148	146	148	152	150	158	163	163	149	147	140	147	139	147	153
138	133	141	155	157	149	149	150	153	149	149	160	157	149	145	155	142	147	152	154
149	148	147	151	155	153	156	156	155	151	145	161	162	155	146	155	146	152	156	156
137	137	144	145	143	155	153	150	150	146	145	166	171	160	151	153	146	154	156	156
120	115	139	139	140	141	140	142	143	133	141	129	132	140	132	156	156	157	160	161
132	123	131	140	133	141	141	142	142	145	106	120	139	142	147	131	157	158	159	158
129	122	128	142	138	134	134	135	138	135	145	149	151	148	150	155	157	159	159	158
131	129	136	136	140	134	136	136	137	139	128	129	131	138	143	152	156	157	158	157
145	141	136	131	140	140	139	133	128	132	143	146	148	152	151	147	151	156	149	144
134	134	134	134	122	125	126	130	128	132	138	146	149	150	151	152	156	156	142	137
119	120	121	115	119	120	132	135	132	135	140	144	146	147	151	151	154	159	139	137
122	121	124	121	114	111	122	128	128	128	128	136	138	144	149	153	163	145	143	128

Sensible Heat Flux to the Air (H), W m^{-2}

H

126	132	127	109	109	110	118	119	120	89.8	93	88.6	93.5	86.7	83.7	129	137	115	110	103
122	132	127	111	104	112	120	121	87	74.8	73.2	84.8	75.1	74	71.9	80	86.8	117	116	109
89.8	101	100	81	78.5	112	115	116	86.5	76.1	70.4	77.5	78.1	76.2	70.6	75.4	117	116	111	109
87.1	89	90.9	80	73.9	88.3	88.4	90.9	81.1	72.2	69.7	76	79.6	74.2	74.1	71.4	120	113	110	109
88.3	78.1	77	79.5	75.2	82.9	82.2	79.8	71.9	70.2	63.2	68.7	59.7	55.8	57.8	72.3	123	114	111	109
71.4	70.4	74.4	74.4	75.5	73.8	74.2	76.9	67.3	64.2	65	62.3	46.4	47.2	45.9	56.7	99.5	101	97.3	94.3
75.8	99.3	102	110	103	74.6	73.5	66.1	66.2	67.2	59.7	45	46.8	47.8	49.5	45.4	83.8	95.5	95.7	95.8
75.2	98.7	101	118	106	100	101	101	102	89.6	67.1	51.1	50.6	49.6	51.2	89.3	95.4	95.4	94.2	97.8
76.1	100	106	123	123	99.7	103	105	107	99	86.3	86.2	86.7	93	95.3	87.1	96.4	96	94.8	97.4
97.1	127	130	131	123	117	115	120	121	109	97.6	101	103	106	106	99.9	109	58.6	53.6	51.5
130	134	134	130	133	127	125	122	121	109	106	103	104	106	106	108	111	56.1	51.5	50.2
201	199	197	196	129	127	121	118	109	109	106	104	109	107	107	107	111	57.9	50.9	50.2
200	201	200	194	153	156	148	144	133	112	112	108	110	108	108	109	62.4	52	51	48.9

Normalized Difference Vegetation Index:

NDVI

0.27	0.22	0.26	0.49	0.49	0.32	0.25	0.24	0.23	0.28	0.25	0.29	0.24	0.24	0.27	0.24	0.19	0.24	0.28	0.36
0.31	0.22	0.26	0.47	0.4	0.3	0.23	0.22	0.31	0.5	0.54	0.34	0.38	0.39	0.43	0.31	0.24	0.25	0.26	0.33
0.31	0.21	0.22	0.44	0.43	0.3	0.27	0.26	0.31	0.48	0.62	0.45	0.33	0.36	0.46	0.37	0.25	0.26	0.31	0.33
0.35	0.32	0.3	0.46	0.53	0.29	0.29	0.27	0.3	0.43	0.64	0.48	0.32	0.39	0.39	0.44	0.23	0.29	0.32	0.33
0.33	0.5	0.53	0.47	0.5	0.36	0.37	0.41	0.43	0.46	0.64	0.5	0.37	0.43	0.4	0.42	0.21	0.28	0.31	0.33
0.7	0.74	0.6	0.6	0.49	0.53	0.52	0.46	0.53	0.61	0.59	0.67	0.69	0.66	0.7	0.42	0.28	0.27	0.31	0.34
0.66	0.67	0.58	0.42	0.56	0.51	0.53	0.56	0.56	0.53	0.78	0.74	0.67	0.64	0.59	0.72	0.52	0.33	0.33	0.32
0.68	0.69	0.6	0.31	0.48	0.53	0.52	0.52	0.49	0.55	0.53	0.54	0.55	0.58	0.54	0.42	0.33	0.33	0.34	0.34
0.65	0.64	0.48	0.26	0.26	0.55	0.48	0.45	0.41	0.37	0.64	0.65	0.63	0.55	0.49	0.46	0.32	0.32	0.34	0.35
0.27	0.23	0.21	0.2	0.26	0.29	0.31	0.26	0.25	0.26	0.39	0.34	0.32	0.33	0.32	0.41	0.29	0.44	0.56	0.62
0.21	0.19	0.19	0.21	0.19	0.21	0.22	0.24	0.25	0.26	0.28	0.32	0.31	0.32	0.32	0.3	0.28	0.49	0.62	0.66
0.2	0.21	0.22	0.23	0.2	0.21	0.25	0.28	0.26	0.26	0.29	0.31	0.3	0.31	0.31	0.32	0.27	0.46	0.63	0.66
0.2	0.2	0.2	0.24	0.2	0.19	0.24	0.27	0.24	0.24	0.24	0.27	0.28	0.3	0.3	0.3	0.38	0.6	0.63	0.71

Net Radiation (R_n) from an early run of SEBAL, W m^{-2}

Rn

430	431	467	527	527	477	457	465	470	484	470	480	468	474	456	434	444	471	503	522
441	428	457	523	522	498	488	496	510	533	575	552	556	508	506	472	492	465	493	515
464	443	473	536	542	500	500	502	515	522	582	554	530	505	505	526	474	491	512	520
503	499	495	528	557	514	524	522	521	521	580	567	547	530	497	537	487	512	524	525
464	487	522	508	505	524	518	514	516	510	583	588	582	553	517	528	489	517	525	525
519	540	528	528	496	509	503	496	516	514	533	540	560	569	579	537	522	527	538	543
537	508	493	483	491	502	511	523	522	523	552	566	577	564	554	592	566	534	535	532
542	521	491	478	484	486	482	484	486	495	527	543	556	555	546	531	528	536	538	532
529	516	479	457	468	490	477	472	470	471	514	517	516	506	507	530	524	529	534	531
486	472	456	437	468	470	469	445	427	442	489	493	500	512	510	506	506	540	549	559
448	448	448	448	409	418	420	435	427	442	464	492	502	505	510	512	522	554	550	561
397	399	406	385	398	400	440	454	441	452	470	486	490	495	508	509	516	554	549	561
409	405	413	405	380	369	407	430	428	428	428	455	463	484	500	514	555	554	566	565

Surftemp

315	316	316	313	313	313	314	315	315	311	312	311	312	311	310	316	317	314	314	313
315	316	315	313	313	314	315	315	311	309	309	310	309	309	309	310	311	314	314	313
311	313	313	310	310	314	314	314	311	309	308	309	310	309	308	309	314	314	314	313
311	311	311	310	309	311	311	311	310	309	308	309	310	309	309	309	315	314	313	313
311	309	309	310	309	310	310	310	309	308	307	308	307	307	307	309	315	314	314	313
308	308	309	309	309	309	309	309	308	307	308	307	305	305	305	307	312	312	312	312
309	312	312	313	312	309	309	308	308	308	306	305	305	305	305	305	310	312	312	312
309	311	312	314	313	312	312	312	312	311	308	306	306	305	306	311	312	312	312	312
309	312	313	315	315	312	312	313	313	312	310	310	310	311	311	311	312	312	312	312
312	316	316	316	315	314	314	315	315	313	312	312	313	313	313	312	313	307	306	306
316	316	316	316	316	316	315	315	315	313	313	313	313	313	313	313	314	307	306	305
323	323	323	323	316	316	315	314	313	313	313	313	313	313	313	313	314	307	306	305
323	323	323	322	318	319	318	317	316	314	314	313	314	313	313	313	308	306	306	305

Aerodynamic Roughness, z_{om}, m (from an earlier SEBAL run)

z0m

0.01	0.01	0.01	0.03	0.03	0.02	0.01	0.01	0.01	0.01	0.01	0.02	0.01	0.01	0.01	0.01	0.01	0.01	0.01	0.02
0.02	0.01	0.01	0.02	0.02	0.02	0.01	0.01	0.02	0.03	0.03	0.02	0.02	0.02	0.02	0.02	0.01	0.01	0.01	0.02
0.02	0.01	0.01	0.02	0.02	0.02	0.01	0.01	0.02	0.02	0.04	0.02	0.02	0.02	0.02	0.02	0.01	0.01	0.02	0.02
0.02	0.02	0.02	0.02	0.03	0.02	0.02	0.01	0.02	0.02	0.04	0.02	0.02	0.02	0.02	0.02	0.01	0.02	0.02	0.02
0.02	0.03	0.03	0.02	0.03	0.02	0.02	0.02	0.02	0.02	0.04	0.03	0.02	0.02	0.02	0.02	0.01	0.01	0.02	0.02
0.04	0.05	0.03	0.03	0.03	0.03	0.03	0.02	0.03	0.04	0.03	0.04	0.04	0.04	0.04	0.02	0.01	0.01	0.02	0.02
0.04	0.04	0.03	0.02	0.03	0.03	0.03	0.03	0.03	0.03	0.05	0.05	0.04	0.04	0.03	0.05	0.03	0.02	0.02	0.02
0.04	0.04	0.03	0.02	0.02	0.03	0.03	0.03	0.03	0.03	0.03	0.03	0.03	0.03	0.03	0.02	0.02	0.02	0.02	0.02
0.04	0.04	0.02	0.01	0.01	0.03	0.02	0.02	0.02	0.02	0.04	0.04	0.04	0.03	0.03	0.02	0.02	0.02	0.02	0.02
0.01	0.01	0.01	0.01	0.01	0.02	0.02	0.01	0.01	0.01	0.02	0.02	0.02	0.02	0.02	0.02	0.02	0.02	0.03	0.04
0.01	0.01	0.01	0.01	0.01	0.01	0.01	0.01	0.01	0.01	0.01	0.02	0.02	0.02	0.02	0.02	0.01	0.03	0.04	0.04
0.01	0.01	0.01	0.01	0.01	0.01	0.01	0.01	0.01	0.01	0.02	0.02	0.02	0.02	0.02	0.02	0.01	0.02	0.04	0.04
0.01	0.01	0.01	0.01	0.01	0.01	0.01	0.01	0.01	0.01	0.01	0.01	0.01	0.02	0.02	0.02	0.02	0.03	0.04	0.04

3. Variation of Band 6 DN Values for a wider area (07/07/89)

The following figure and tabular map show surface temperature (expressed as digital numbers) for a larger area surrounding the lysimeter fields. Variation is quite large, due to the wide variation in vegetation cover of fields. Some fields were at full vegetation cover, others were bare.

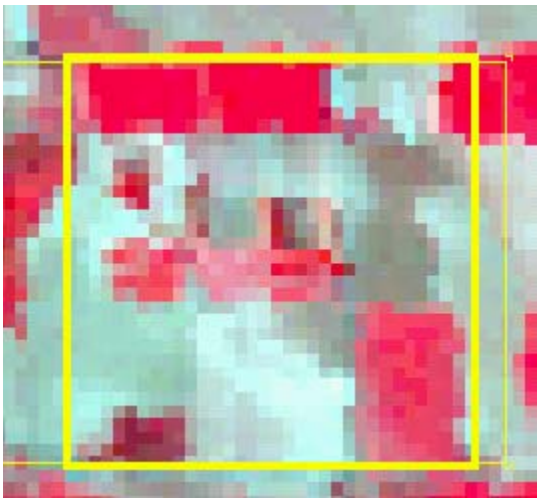

151	151	151	151	148	148	148	148	145	145	145	145	168	166	166	166	166	163	163	163	163	173	173	173	173	172	172	172	172	153	153	153
151	151	151	151	148	148	148	148	145	145	145	145	144	144	144	144	145	163	163	163	173	173	173	173	173	172	172	172	172	153	153	153
153	153	151	151	148	148	148	148	145	145	145	145	144	144	144	144	145	145	145	145	159	159	173	173	172	172	172	172	153	153	153	153
153	153	153	153	155	155	155	148	145	145	145	145	144	144	144	144	145	145	145	145	159	159	159	159	170	170	170	172	153	153	153	153
153	153	153	153	155	155	155	155	159	159	159	159	144	144	144	144	145	145	145	145	159	159	159	159	170	170	170	170	164	164	164	164
153	153	153	155	155	155	155	159	159	159	159	159	165	165	165	165	167	145	145	145	159	159	159	159	170	170	170	170	164	164	164	164
168	168	153	155	155	155	155	159	159	159	159	165	165	165	165	167	167	167	167	169	169	169	159	159	170	170	170	170	164	164	164	164
168	168	168	161	161	161	161	159	159	159	159	165	165	165	165	167	167	167	167	169	169	169	169	165	165	165	165	164	164	164	164	161
168	168	168	161	161	161	161	169	169	169	169	166	165	165	165	167	167	167	167	169	169	169	169	165	165	165	165	165	165	165	165	174
168	168	168	161	161	161	161	169	169	169	169	166	166	166	166	159	159	167	167	169	169	169	169	165	165	165	165	165	165	165	165	174
179	168	161	161	161	161	169	169	169	169	169	166	166	166	166	159	159	159	159	157	157	169	169	165	165	165	165	165	165	165	165	174
179	179	178	178	178	178	169	169	169	169	166	166	166	166	159	159	159	159	157	157	157	157	157	166	166	166	165	165	165	165	165	174
179	179	178	178	178	178	160	160	160	160	159	166	166	166	159	159	159	159	157	157	157	157	166	166	166	166	166	166	166	166	177	174
179	179	178	178	178	178	160	160	160	160	159	159	159	159	157	157	159	159	157	157	157	157	166	166	166	166	166	166	166	166	177	177
182	179	178	178	178	178	160	160	160	160	159	159	159	159	157	157	157	157	152	152	152	157	166	166	166	166	166	166	166	166	177	177
182	182	182	161	161	161	160	160	160	160	159	159	159	159	157	157	157	157	152	152	152	152	162	162	162	162	166	166	166	166	177	177
182	182	182	161	161	161	161	168	168	168	168	159	159	157	157	157	157	152	152	152	152	152	162	162	162	162	163	163	163	163	169	177
182	182	182	161	161	161	161	168	168	168	168	167	167	167	167	164	157	152	152	152	152	162	162	162	162	163	163	163	163	169	169	169
182	182	182	161	161	161	161	168	168	168	168	167	167	167	167	164	164	164	164	165	165	162	162	162	162	163	163	163	163	169	169	169
182	182	182	161	161	161	161	168	168	168	168	167	167	167	167	164	164	164	164	165	165	165	165	153	153	153	163	163	163	169	169	169
190	190	190	190	190	161	168	168	168	168	168	167	167	167	167	164	164	164	164	165	165	165	165	153	153	153	153	150	150	150	150	169
190	190	190	190	190	190	186	186	186	186	167	167	167	167	164	164	164	164	165	165	165	165	165	153	153	153	153	150	150	150	150	171
190	190	190	190	190	190	186	186	186	186	174	174	174	174	170	164	164	164	165	165	165	165	153	153	153	153	150	150	150	150	171	171
190	190	190	190	190	190	186	186	186	186	174	174	174	174	170	170	170	170	169	169	165	165	153	153	153	153	150	150	150	150	171	171
188	188	188	188	188	190	186	186	186	186	174	174	174	174	170	170	170	170	169	169	169	169	157	157	157	153	150	150	150	150	171	171
188	188	188	188	188	181	181	181	181	181	174	174	174	174	170	170	170	170	169	169	169	169	157	157	157	157	150	150	150	150	171	171
188	188	188	188	188	181	181	181	181	174	174	174	174	173	173	170	170	169	169	169	169	157	157	157	157	150	150	150	150	150	167	167
188	188	188	188	188	181	181	181	181	174	174	174	174	173	173	173	173	174	174	174	169	157	157	157	157	150	150	150	150	167	167	167
184	165	165	165	165	181	181	181	181	174	174	174	174	173	173	173	173	174	174	174	174	164	164	164	164	150	150	150	150	167	167	167
184	165	165	165	165	154	154	154	154	174	174	174	174	173	173	173	173	174	174	174	174	164	164	164	164	152	152	152	152	159	167	167
165	165	165	165	154	154	154	154	154	172	172	172	172	175	173	173	174	174	174	174	164	164	164	164	164	152	152	152	152	159	159	159
165	165	165	165	154	154	154	154	172	172	172	172	175	175	175	175	178	178	178	174	174	164	164	164	164	152	152	152	152	159	159	159

Selection of 30 m comparison pixels from lysimeter fields based on representation by thermal (band 6) pixels

The following figures show computer screen presentations within ERDAS Imagine of pixels surrounding the lysimeter fields during 1989. Four screens are shown. The upper left hand screen of each figure is a false color from bands 2, 3, and 4, so that brownish colors represent soil and reddish colors represent green vegetation. The lower left hand screen shows the orthophotoquad (taken during the mid-1990's), for reference. The upper right hand screen shows the band 6 pixels, as resampled to 30 m using nearest neighbor resampling (thus the non-square shapes). The lower right hand screen is the final 24-hour ET determined by SEBAL for the date.

These figures were used to determine, date by date, the appropriate 120 m band 6 pixel and 30 m short-wave pixels (bands 1-5, 7) that best represented the conditions of the lysimeter area. The selection of pixels varied from date to date, as the locations of boundaries between specific band 6 pixels varied with date.

In some instances, only a single row of pixels were selected that contained both the short wave, visual characteristics of the center portion of the lysimeter field and the band 6 pixel that was judged to contain the most appropriate surface temperature information. As illustrated in the ET portions of the following figures, substantial variation in ET for 30 m pixels within the boundaries of the lysimeter fields occurred for many dates, largely due to problems of smearing of band 6 pixels and also smearing of border 30 m pixels.

The specific 30 m pixels selected for comparison of ET from SEBAL with ET measured by lysimeter are listed in the main text in Table __. The selected pixels are also shown in the form of bar graphs Figures __ in the main text along with the lysimeter measurement.

In summary, the Kimberly lysimeter system was a well-designed and well-managed, world-class system for measuring evapotranspiration. It collected data that were valuable in developing and calibrating ET methods and computation procedures. However, the fields containing the lysimeters were too small for ideal application to validation of ET computations based on TM images. Ideally, the field sizes should have been a minimum of 480 m x 480 m to insure that a minimum of four band 6 pixels could have been located that completely represented conditions of the field and of the lysimeter. Four pixels would have provided statistical information concerning variability in measurement and repeatability of predictions.

With this said, the comparisons with the lysimeter field were still considered to be extremely valuable and successful.

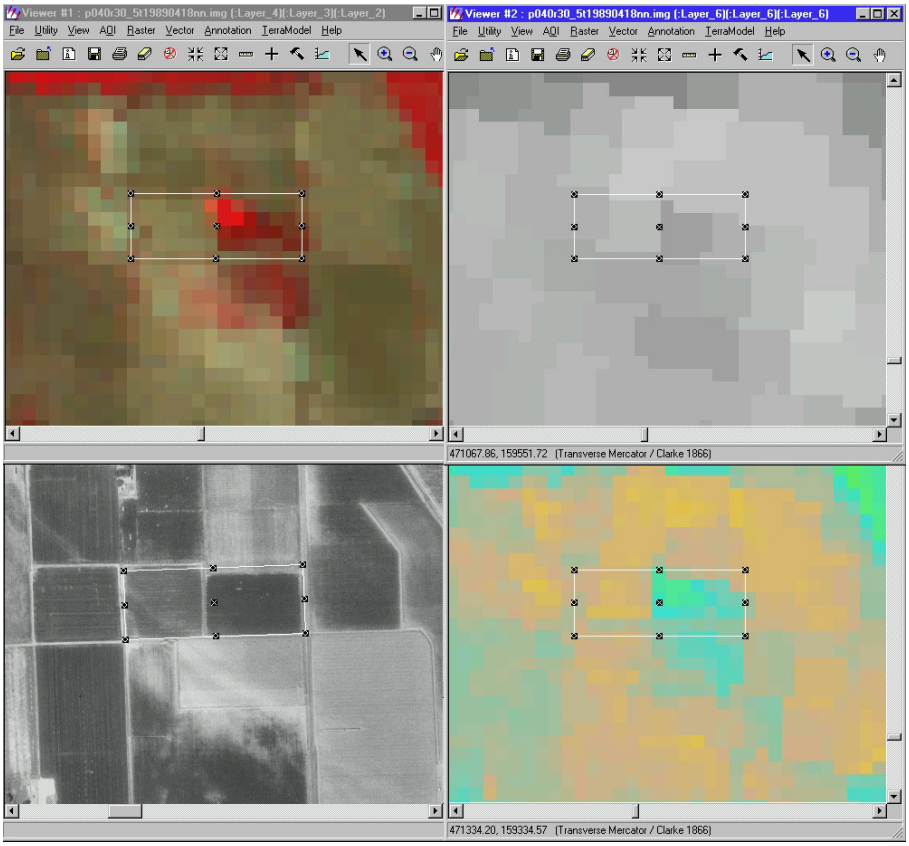
Viewer #1 : p040r30_5t19890418nn.img (:Layer_4)(:Layer_3)(:Layer_2)
Viewer #2 : p040r30_5t19890418nn.img (:Layer_6)(:Layer_6)(:Layer_6)
File Utility View AOI Raster Vector Annotation TerraModel Help
471067.86, 159551.72 (Transverse Mercator / Clarke 1866)
471334.20, 159334.57 (Transverse Mercator / Clarke 1866)


ET (mm)
0
2
4
6
8
10

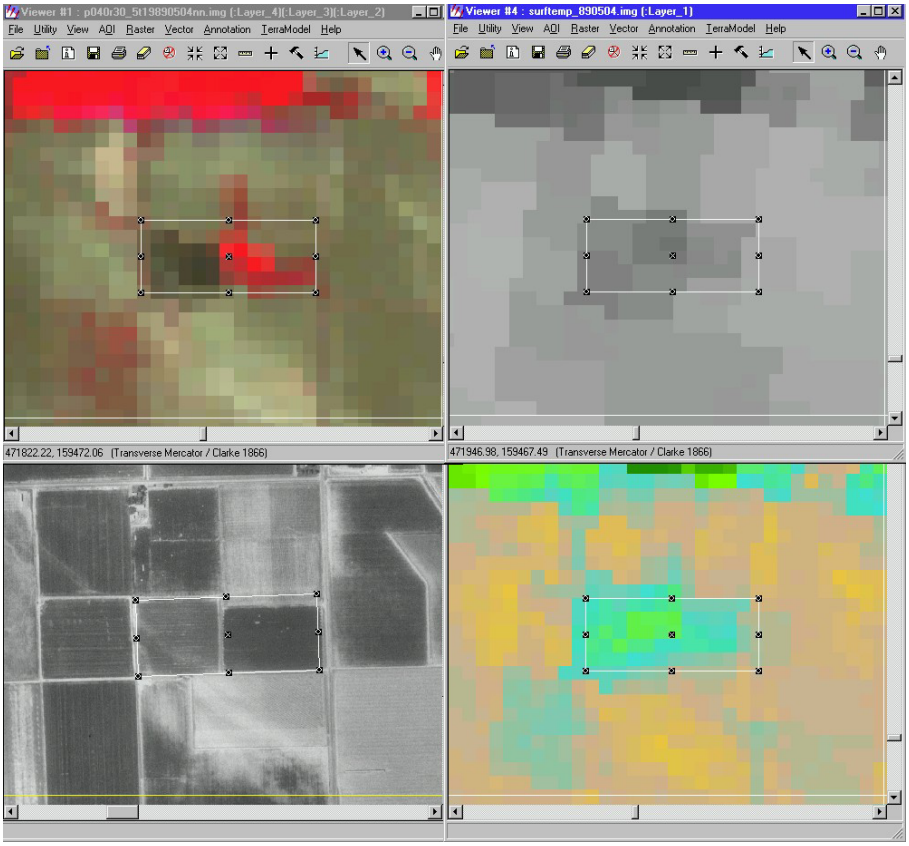
Viewer #1 : p040r30_5t19890504nn.img (:Layer_4)(:Layer_3)(:Layer_2)
Viewer #4 : surftemp_890504.img (:Layer_1)
File Utility View AOI Raster Vector Annotation TerraModel Help
471822.22, 159472.06 (Transverse Mercator / Clarke 1866)
471946.98, 159467.49 (Transverse Mercator / Clarke 1866)

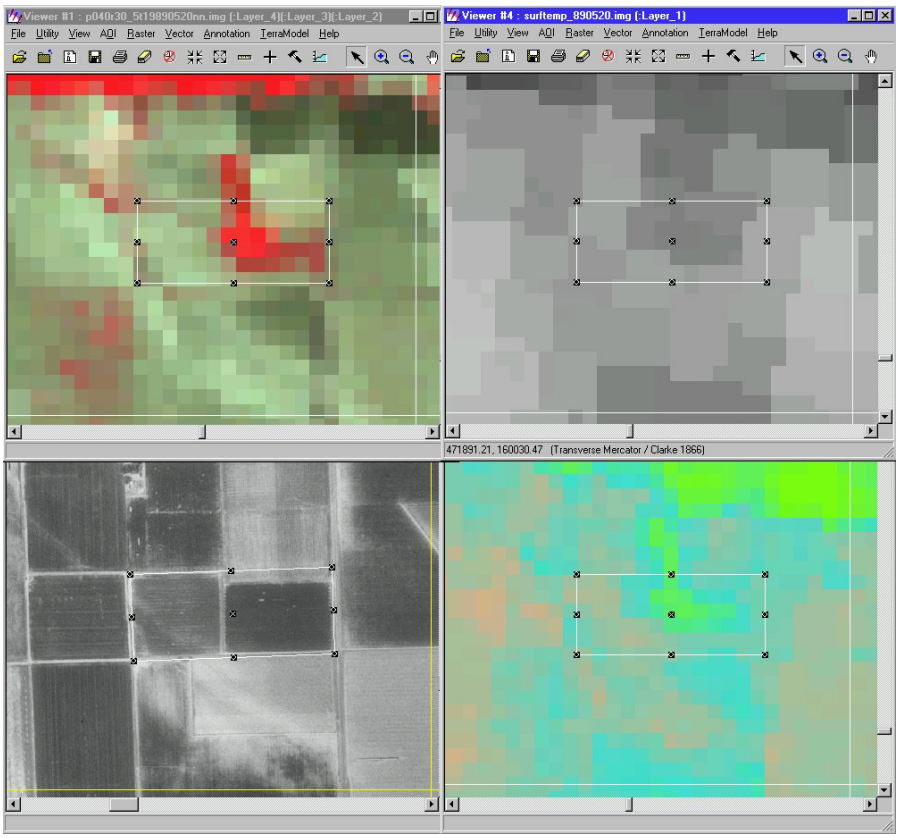
Viewer #1 : p040r30_5t19890520nn.img (:Layer_4)(:Layer_3)(:Layer_2)
Viewer #4 : surftemp_890520.img (:Layer_1)
File Utility View AOI Raster Vector Annotation TerraModel Help
471891.21, 160030.47 (Transverse Mercator / Clarke 1866)


ET (mm)
0
2
4
6
8
10

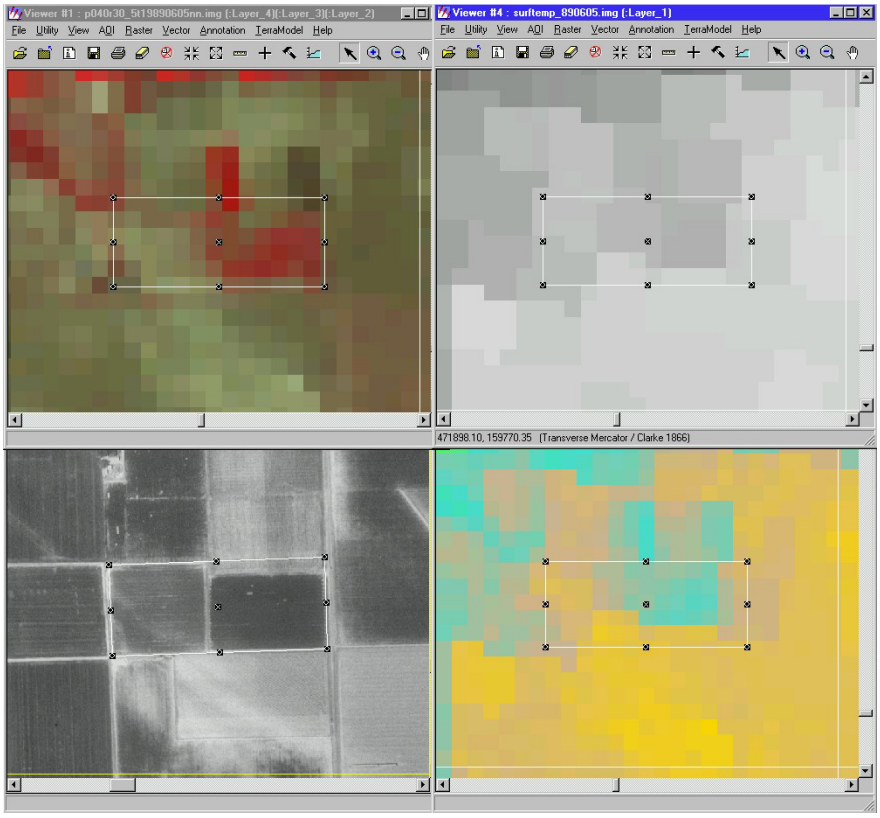
Viewer #1 : p040r30_5t19890605nn.img (:Layer_4)(:Layer_3)(:Layer_2)
Viewer #4 : surftemp_890605.img (:Layer_1)
File Utility View AOI Raster Vector Annotation TerraModel Help
471898.10, 159770.35 (Transverse Mercator / Clarke 1866)

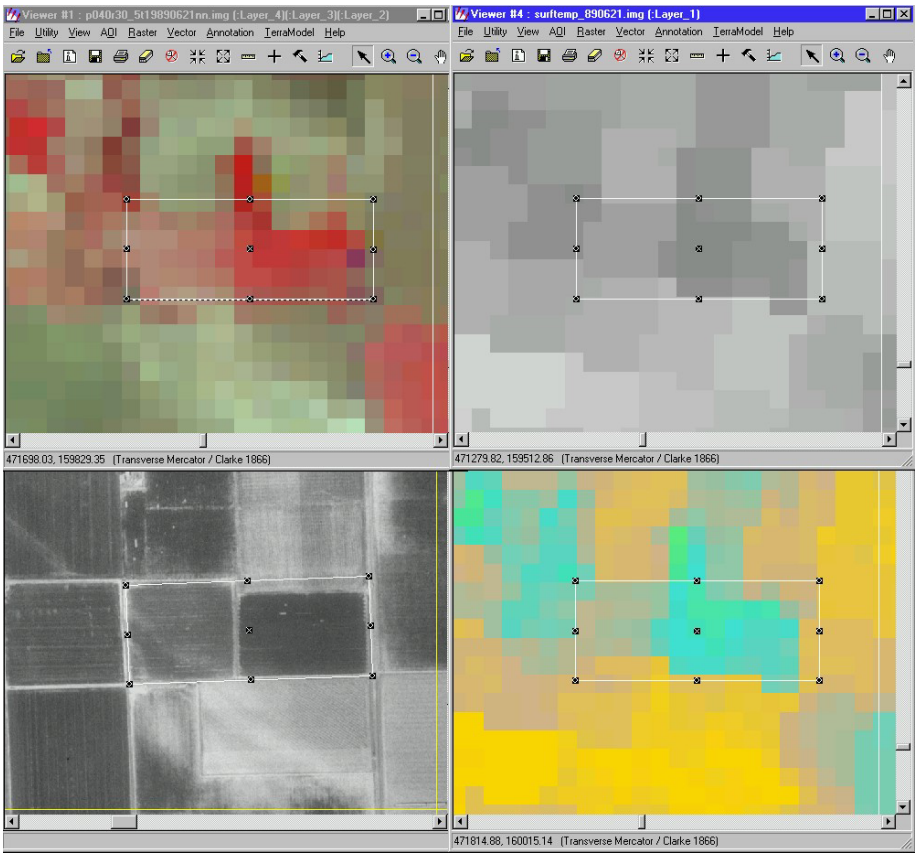
Viewer #1 : p040r30_5t19890621nn.img (:Layer_4)(:Layer_3)(:Layer_2)
Viewer #4 : surftemp_890621.img (:Layer_1)
File Utility View AOI Raster Vector Annotation TerraModel Help
471698.03, 159829.35 (Transverse Mercator / Clarke 1866)
471279.82, 159512.86 (Transverse Mercator / Clarke 1866)
471814.88, 160015.14 (Transverse Mercator / Clarke 1866)


ET (mm)
0
2
4
6
8
10

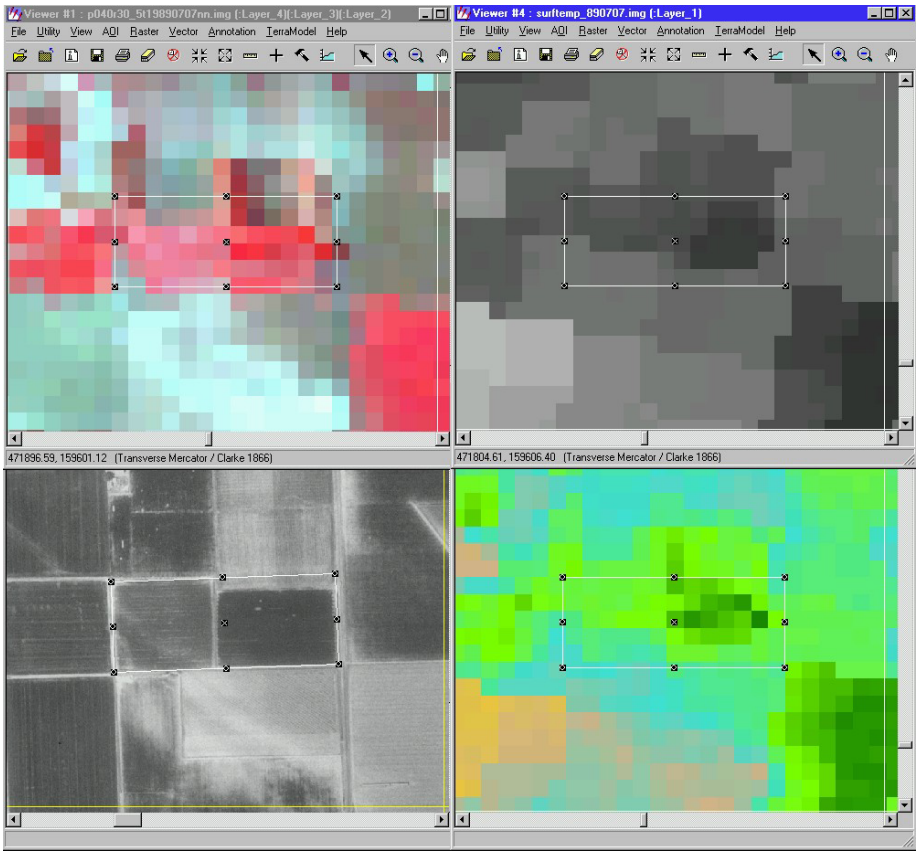
Viewer #1 : p040r30_5t19890707nn.img (:Layer_4)(:Layer_3)(:Layer_2)
Viewer #4 : surftemp_890707.img (:Layer_1)
File Utility View AOI Raster Vector Annotation TerraModel Help
471896.59, 159601.12 (Transverse Mercator / Clarke 1866)
471804.61, 159606.40 (Transverse Mercator / Clarke 1866)

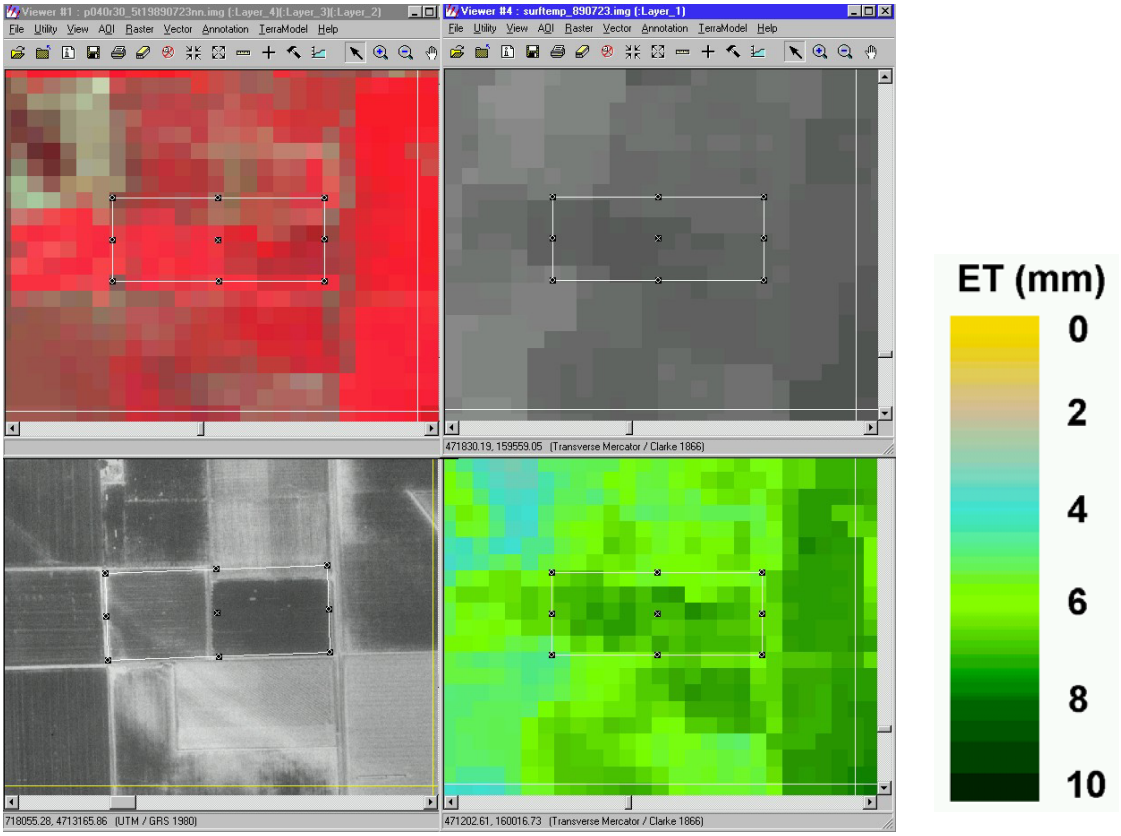
Viewer #1 : p040r30_5t19890723nn.img (:Layer_4)(:Layer_3)(:Layer_2)
Viewer #4 : surftemp_890723.img (:Layer_1)
File Utility View AOI Raster Vector Annotation TerraModel Help
471830.19, 159559.05 (Transverse Mercator / Clarke 1866)
718055.28, 4713165.86 (UTM / GRS 1980)
471202.61, 160016.73 (Transverse Mercator / Clarke 1866)
ET (mm)
0
2
4
6
8
10

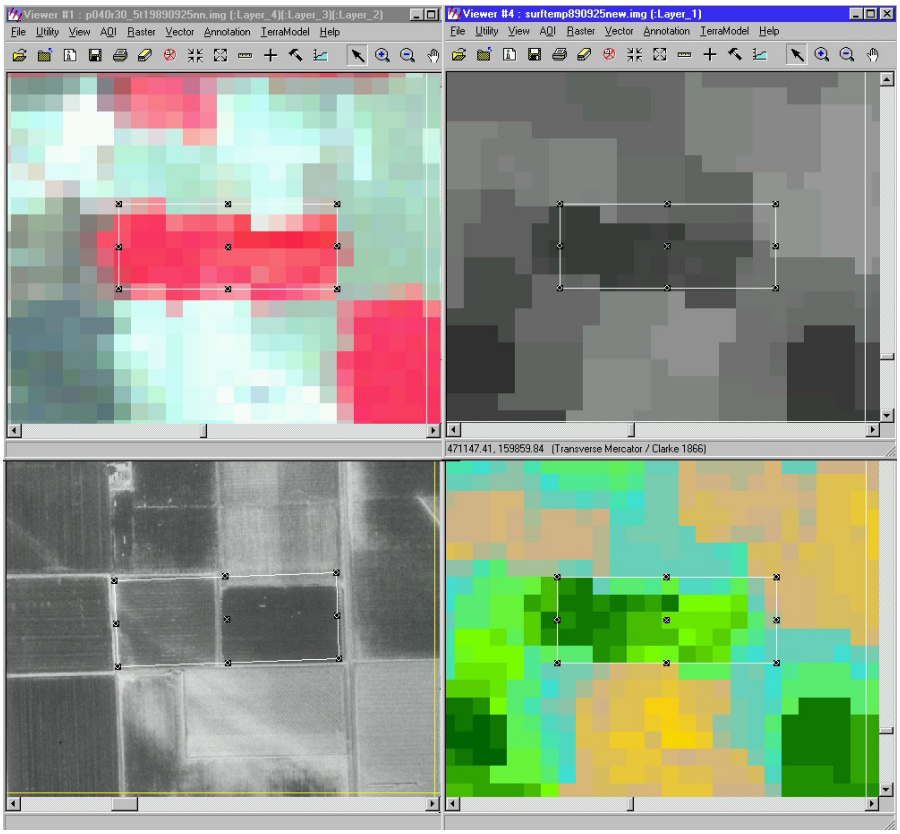
Viewer #1 : p040r30_5t19890925nn.img (:Layer_4)(:Layer_3)(:Layer_2)
Viewer #4 : surftemp890925new.img (:Layer_1)
File Utility View AOI Raster Vector Annotation TerraModel Help
471147.41, 159859.84 (Transverse Mercator / Clarke 1866)

Technique to Estimate actual DN values for Lysimeter fields

In addition to careful selection of the most representative thermal pixel (120 m) for the lysimeter fields, and the selection of resulting 30 m pixels for ET comparison (described above), we have attempted to manually "correct" the DN value for the Lysimeter fields (results to be available by 1 Dec., 2001). We estimated the Band6-DN value using a simple linear correction method by describing the factors affecting the spatial mixture for the band 6 pixels shown:

$DN_{Mixture} = DN_{Outside}$ * *(weight of outside field in the Mixture pixel)* + DN_{Lys2F} * *(weight of inside)*

The DN values for areas of larger fields adjacent to the lysimeter fields were evaluated and representative values were selected, for example, for July 7, 1989:

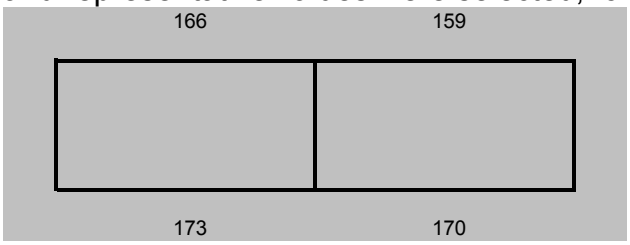

The estimated DN value for Lys2Field was determined by solving the above equation, for example, for the 167 DN pixel:

$167 = 173*12/20 + DN_{Lys2}*8/20$
$\rightarrow DN_{Lys2} = 158$

This value is less than the DN values for the outside fields and is lower than the pixel lying partially inside the Lysimeter field 2.

When the DN for the field north of the lysimeter 2 field was used instead, the estimated DN value becomes 145

$159 = 166*10/15 + DN_{Lys2}*5/15$
$\rightarrow DN_{Lys2} = 145$

This DN value may be too low as the north field was also a relatively small and experimental field.

Appendix 2. Estimation of Soil Heat Flux

This appendix details the refinement of algorithms for predicting soil heat flux (G) for various land classes and vegetation conditions. In general, G is predicted as some function of R_n.

Data from a literature search

In this section, we review some soil heat flux data from Kustas and Daughtry(1990). Kustas and Daughtry measured a heat balance over bare soil, alfalfa and cotton fields in Arizona. The data collected represented four days for bare soil and alfalfa, and three days for three cotton fields (all tables and figures scanned from Kustas and Daughtry (1990).

TABLE 2

Gravimetric soil moisture in bare soil, alfalfa, and cotton fields ($g\ g^{-1}$)

Field	DOY	Location		
		Bed	Side	Bottom
Bare soil	162	0.04	NA	NA
	163	0.04	NA	NA
	164	0.04	NA	NA
	165	0.04	NA	NA
Alfalfa	162	0.17	NA	NA
	163	0.15	NA	NA
	164	0.14	NA	NA
	165	0.13	NA	NA
Cotton 28E	163	0.14	0.13	0.13
	164	0.14	0.13	0.13
	165	0.14	0.12	0.12
Cotton 28W	163	0.16	0.13	0.14
	164	0.15	0.11	0.12
	165	0.14	0.10	0.10
Cotton 29	163	0.10	0.10	0.10
	164	0.35	0.35	0.35
	165	0.35	0.35	0.35

NA = not applicable.

The above table repreents soil moisture in each field. In bare soil field, soil moisture was almost the same and apparently quite dry during the four days. In the alfalfa field, the soil appeared to be moderately wet and became gradually drier during the four days. In the cotton 28 fields, soils were moderately wet, and almost the same during the four days. The cotton 29 field was drier than the other cotton fields on DOY=163, but was very wet on DOY=164 and 165 (probably because of irrigation).

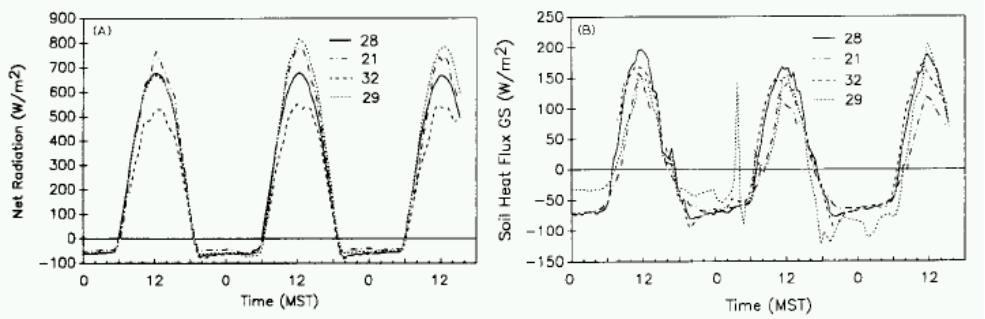

Fig. 2. Values of Rn (a) and $\overline{GS}$ (b) for DOY 163–165 in bare soil Field 32, and alfalfa Field 21, cotton Field 28E and 28W (averaged) and cotton Field 29.

Fig2 shows the R_n and G (their GS is the calculated soil heat flux at the surface) values for the bare field for four days.

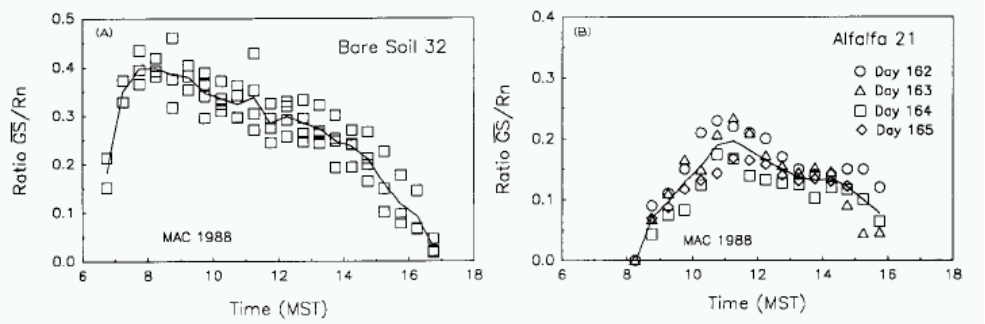

Fig. 3. Daytime values of $\overline{GS}/Rn$ for DOY 162–165 in (a) Field 32 bare soil and (b) Field 21 alfalfa. For the alfalfa field, each day is represented by a symbol.

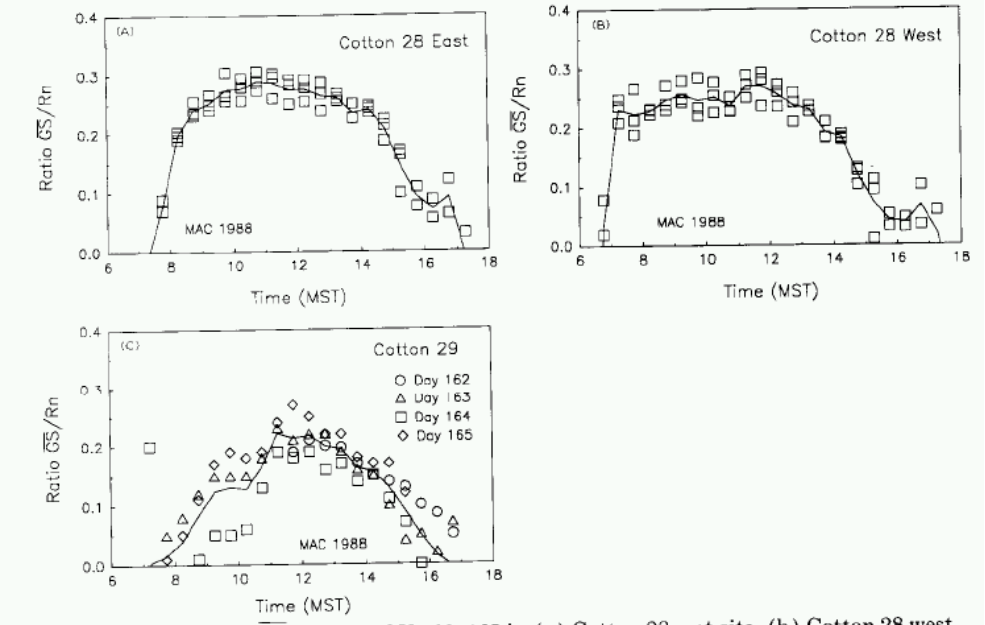

Fig. 4. Daytime values of $\overline{GS}/Rn$ for DOY 163–165 in (a) Cotton 28 east site, (b) Cotton 28 west site, and (c) Cotton 29.

Fig3 and Fig4 (from Kustas and Daughtry) show that the G/Rn ratios for each field. These graphs indicate that:

(1) G/Rn ratio changes by time within same day
G/Rn ratio was not constant during a day. In the very dry bare soil, G/Rn was high in morning and lower in evening. The authors stated that this decrease over time is because of the time lag in surface temperature. A higher proportion of R_n is used as G during morning because soil is cooled during the previous night time. The G/Rn ratio is reduced and more energy is used as H from noon to evening as the soil warms. The daily averaged values of G/Rn ratio were higher (G ~ 0.3Rn) in bare soil than in vegetated areas (G ~ 0.2Rn).

In dense alfalfa and cotton (Cotton29) field, G/Rn was highest at noon and lower in morning and evening. In partially covered cotton fields (Cotton28 E&W), G/Rn was almost constant in morning and decreased toward evening. This trend is in between that for bare soil and high-density vegetated fields.

(2) G/R_n ratio changes by day for the same time of day
The G/R_n ratio is not a constant for the same time of day, when evaluating different days. A ratio difference of 0.1 was often found. The authors mentioned that the changes in G/R_n for the alfalfa field was because of the rapid growth of the alfalfa, and also in the Cotton29 field, wet soil in the morning of DOY164 reduced G/R_n ratio.

It is understandable that the rapid growth of vegetation and difference of soil moisture contributes to reduce G. However, the change of G/R_n ratio from day to day probably cannot be explained only by the rapid growth of vegetation and changes of soil moisture. For example, the bare soil field had no vegetation, and had very similar R_n values for every day (See Fig2) and very similar soil moisture conditions (See Table2). However, the G/R_n ratio at the same times of day vary much by day.
In another example, the Cotton29 field is very wet not only on DOY164 but also on DOY165. However, G/Rn ratio did not decrease (or even higher than dry days) in the morning of DOY165.

Therefore, the authors' explanations may not be fully complete and appropriate. It is possible that difference of temperature gradient or windspeed affected the G/R_n ratio.

TABLE 4

Acquisition dates and times for vegetation indices calculated from reflectance factor data using Barnes 12-1000 multiband radiometer. Estimates of midday (1030–1430 h MST) values of $\overline{GS}/Rn$ are listed

Field	DOY	Time (h MST)	Solar angle (°)		NIR/Red	NDVI	$\overline{GS}/Rn$	$\overline{GS}/Rn$[a] Corrected
			Zenith	Azimuth				
Alfalfa	162	1239–1242	11	201	5.45	0.64	0.19	0.21
	163	1009–1014	31	101	8.65	0.79	0.175	0.20
	165	1215–1220	11	164	9.51	0.80	0.14	0.16
Bare soil	162	1300–1303	13	216	1.20	0.09	0.32	0.32
	165	1426–1429	28	257	1.21	0.09	0.29	0.29
Cotton 28E	162	1330–1338	17	237	1.82[b]	0.29[b]	0.26[c]	–
	163	0905–0913	45	90	2.30	0.39	0.28	0.33
	165	0906–0913	45	90	2.39	0.41	0.27	0.33
Cotton 28W	162	1330–1338	17	237	1.40[b]	0.17[b]	0.27[c]	–
	163	0905–0913	45	90	1.86	0.30	0.25	0.30
	165	0906–0913	45	90	1.84	0.30	0.24	0.30
Cotton 29	162	1344–1348	19	244	2.27[b]	0.38[b]	0.26[c]	–
	163	0919–0923	42	92	3.20	0.52	0.19	0.19
	165	0918–0922	42	92	4.06	0.60	0.20	0.23

[a] $\overline{GS}/Rn$ corrected for differences in diffusivities between soil, transducer and calibrating medium.
[b] Values of NIR/Red and NDVI not used in deriving equations shown in Fig. 5.
[c] $\overline{GS}/Rn$ computed with NIR/Red values and the expression in Fig. 5.

This table shows that the G/R_n along with NDVI values. It is surprising that the NDVI values for some fields changed so much by date. For example, in the Cotton28W field, NDVI on DOY=162 was 0.17, and it became 0.30 on the next day. It looks like the authors rejected some low NDVI values from further analysis. Therefore, it is possible that there might be some problems in observation.

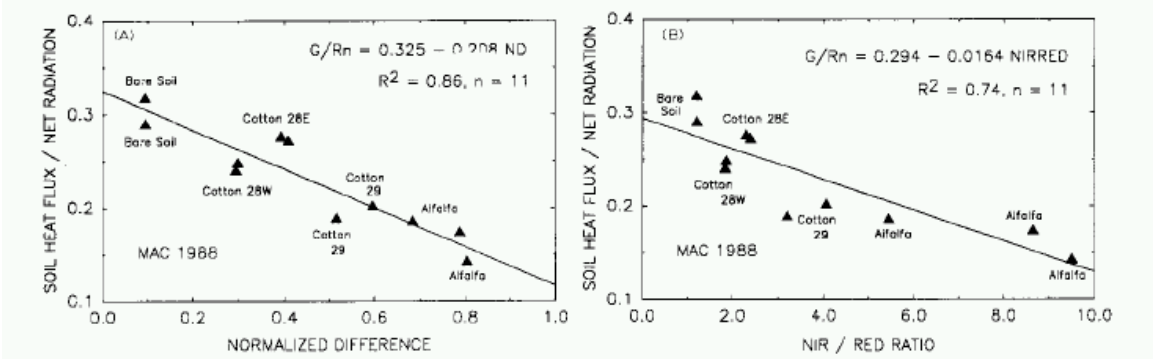

Fig. 5. Comparison of GS/Rn averaged around midday (i.e. from 1030 to 1430 h MST) for each field versus the NIR/Red vegetation index (a) and the NDVI (b). The lines are linear least squares fit to the data. The equation and coefficient of determination, R^2, are given.

Kustus and Daughtry compared the G/R_n ratios at noon time with NDVI, and obtained a linear relation. The authors mention the possibility of predicting G from satellite image using NDVI.

For SEBAL

From the above results, we have considered using one of the following methods to estimate G/R_n ratios in SEBAL:

(1) G/R_n = f(NDVI)
This is the current method used in the SEBAL-2000 version. NDVI has an obvious relationship with G/R_n. In SEBAL-2001, we are using a modified SAVI and LAI instead of NDVI, similar to Choudhury (19__).

(2) G/R_n = f(NDVI, T_s)
Surface temperture, T_s, can impact the relationship with NDVI and somewhat represents the soil moisture. We expect a lower G/R_n ratio when T_s is low.

(3) G/R_n = f(NDVI, albedo)
The G/R_n ratio in a vegetated area might become highest at noon time and lower in morning and evening. This trend might be explained by applying albedo^{-1} as a factor.

(4) Combination: G/Rn = f(NDVI, albedo, T_s)

Reference
Kustas,W.P. and Daughtry,C.S.T. (1990), Estimation of the soil heat flux/net radiation ratio from spectral data, Agricultural and Forest Met., 49, 205-223

Data from the 1999 RAPID Study, Kimberly Idaho

In this section, we introduce some results of an analysis of soil heat flux collected from the Idaho RAPID study, conducted in 1999 between the University of Idaho (R.G. Allen, P.I.) and scientists from Wageningen Agricultural University of the Netherlands (H. deBruin). Measurements were made during August and September, 1999, over growing alfalfa.

1. Background information

The alfalfa height during the study period is shown in the following graph:

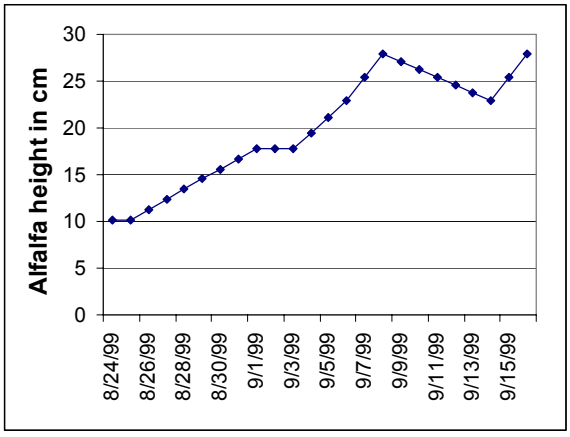

We estimated LAI from the following LAI estimation equation for Alfalfa based on LAI – ht information from J.L. Wright, USDA, Kimberly, Idaho:

LAI = 10h for h < 0.4m

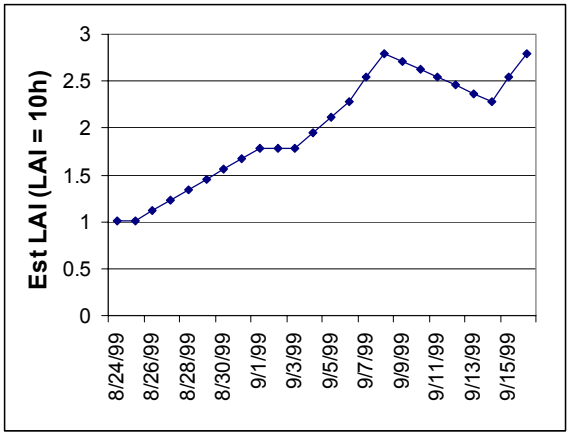

The alfalfa field was somewhat dry during the first one week of study , and then center pivot irrigation with a 2.5 day interval was started so that soil was fairly wet after the first week.

2. G/R_n ratio in the RAPID study

The RAPID study showed some valuable trends of G/R_n ratio:

2-1. Hourly change in G/R_n ratio

The hourly change in G/R_n (within a day) had a strong relation with vegetation cover. The following graph shows the change of the trend of G/R_n ratio.

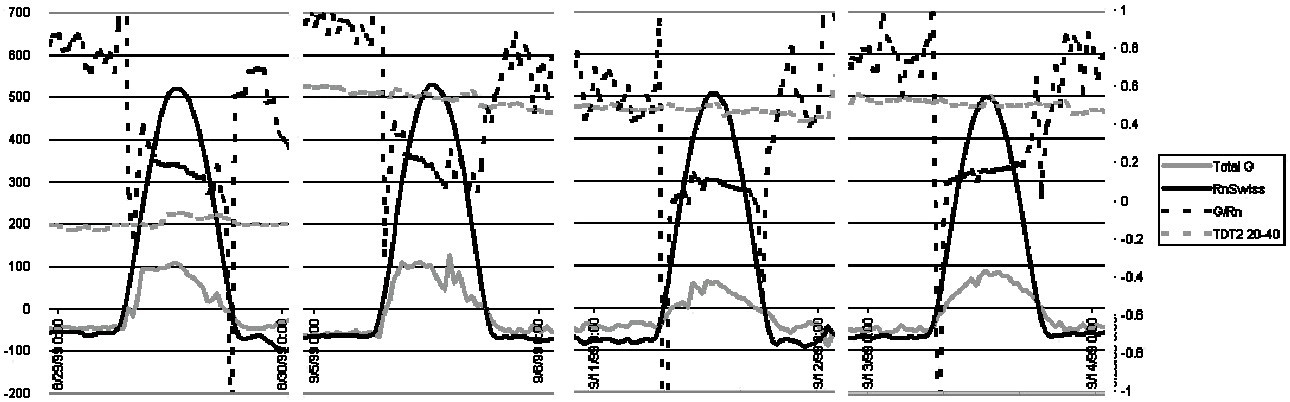

Figure. Change of the trend of G/R_n ratio

On 8/29, G/R_n was higher in morning and lower in evening. 9/5 had the same trend. On 9/11, G/R_n was lower in morning and evening, and higher in noon. On 9/13, G/R_n was higher in evening and lower in morning.

The following graph shows the plot of the slope of G/R_n between 9:00am and 5:00pm. The slope value represents the slope of the linear regression equation (which had the highest r-square) using 30 minute data for all periods. The negative slope values indicate that the G/R_n is higher in morning and lower in evening, and positive slope values indicate the opposite trend. As shown in the graph, the daytime slope of G/R_n had a relation with the height of alfalfa. A similar trend is reported in the Payero (2001). The results from Kustas and Daughtry (above) show a similar trend also.

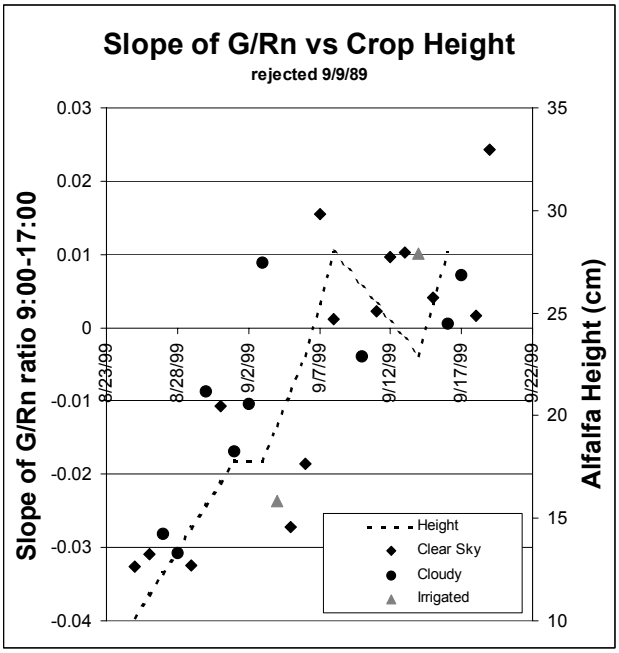

Figure. Slope of G/R_n vs Crop height.

2-2. Irrigation effect

During the study period, there were four days when the G observation point was irrigated during day time. It was observed that G and the G/R_n ratios increased each time irrigated (See. the graph below). The reason is unclear. Generally, an opposite trend would be expected (for example, the results of Kustas and Daughtry: G goes down when irrigated). In the RAPID study site, the irrigation water might be warmer than the soil or the irrigation water conveyed some heat from the hotter soil surface to the lower depth of the thermisters buried in the soil. The inclement increase in G following irrigation was only for a few hours.

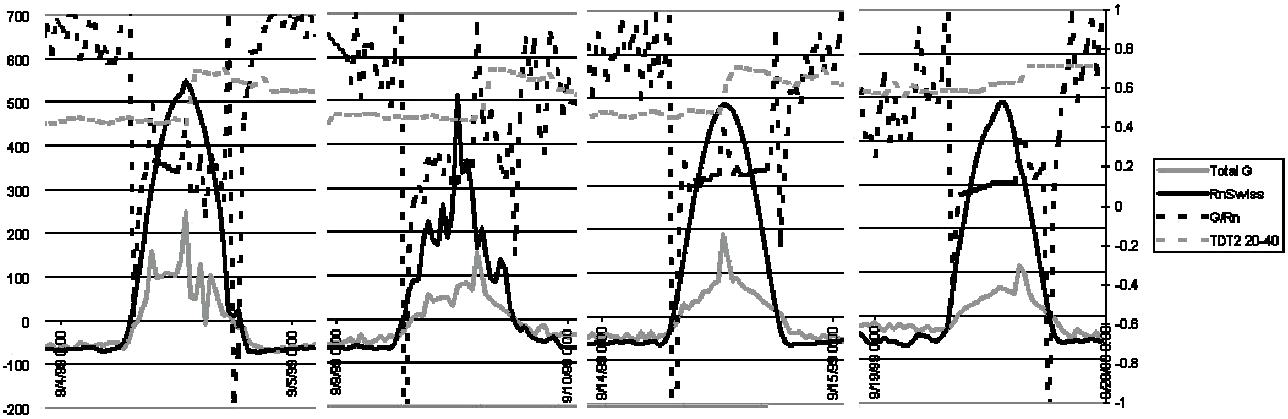

Figure. G and G/Rn jumped up every time when irrigated.

2-3. Soil moisture effect

The following graph shows G and R_n two days before and after the first irrigation. As shown in the following graph, no significant change in G/Rn ratio was observed. Therefore, soil moisture might not be a strong factor impacting the G/Rn ratio. The period shown in the following graph is a cloudy period. However, if one compares the data between 8/29 (dry soil, clear sky) and 9/5 (wet soil, clear sky), a very similar value range and the trend of G/Rn occur.

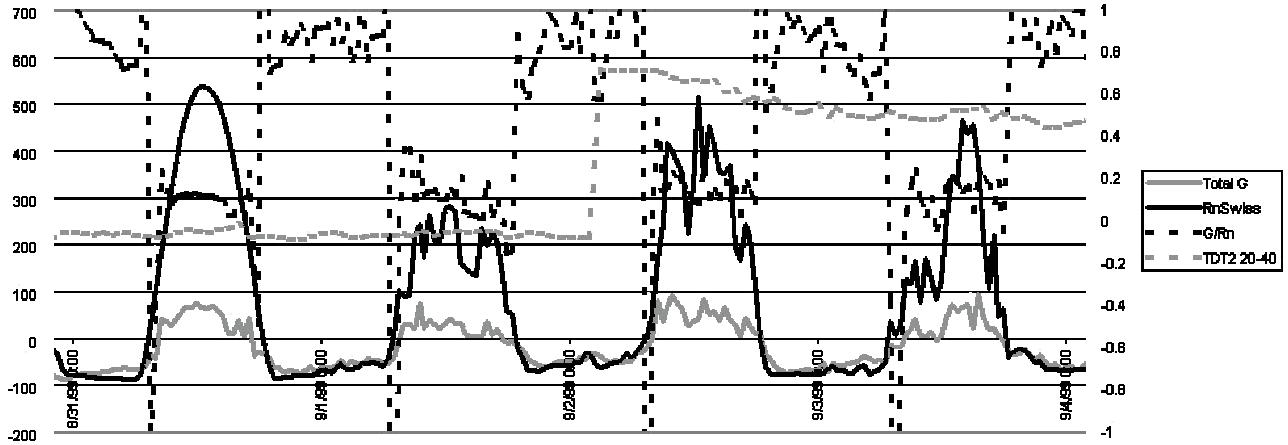

Figure, Rn, G, Rn/G and Soil moisture from 8/31 to 9/3

2-4. Change of G/R_n ratio by crop growth

The G/Rn ratio decreased when vegetation indices increased. The following is the G/R_n vs LAI graph. The LAI were estimated as described earlier.

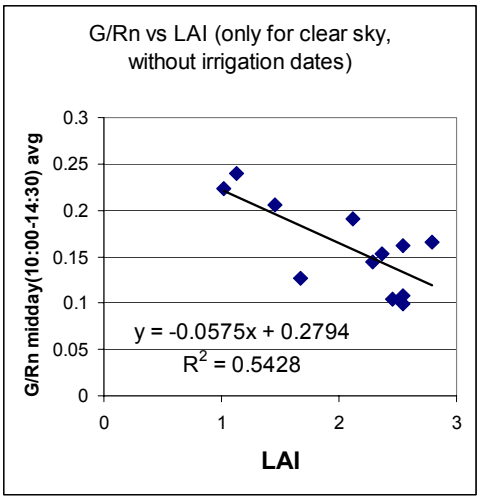

Figure. G/R_n ratio vs LAI

2-5. Effect of sky-clearness (or intensity of Rn)

Although no detailed analysis was done, the graphs of G/R_n over time indicateed that sky-clearness (or intensity of R_n) was not a strong factor impacting G/R_n ratio.

3. Estimation of G

3-1. Linear equation with the crop height

For alfalfa, Clothier et.al. (19__) reported the following equation for midday, for alfalfa.

$$G/Rn = 0.283 - 0.4096h \quad (r^2=0.77)$$

However, this equation did not work well for the results of RAPID study (See. the following graph).
It appears that a simple linear equation using crop height will not work well for the results of the RAPID study.

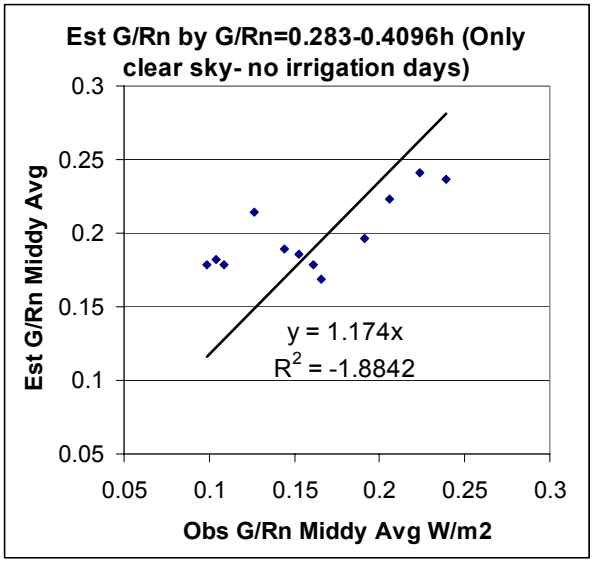

Figure. Observed and estimated values of G/Rn by Clothier's eqn.

3-2. Choudhury's eqn.

Choudhury's equation for predicting G/Rn from LAI works well for grass and alfalfa and has been adopted by the ASCE for standardization of reference evaporation:

$$G/Rn = 0.4 * e^{-0.5LAI}$$ *for night time, coefficient 1.6 is used instead of 0.4*

The following graphs are the observed and estimated G/Rn ratios for the beginning, middle and final periods of the RAPID study;

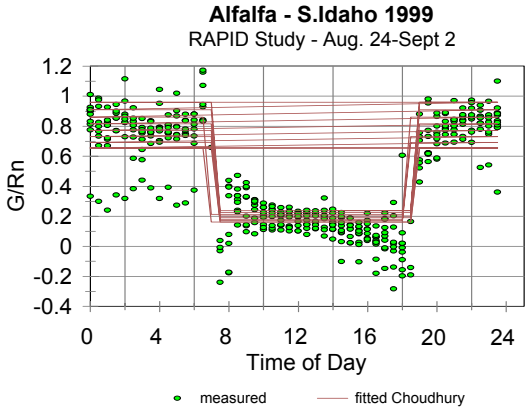

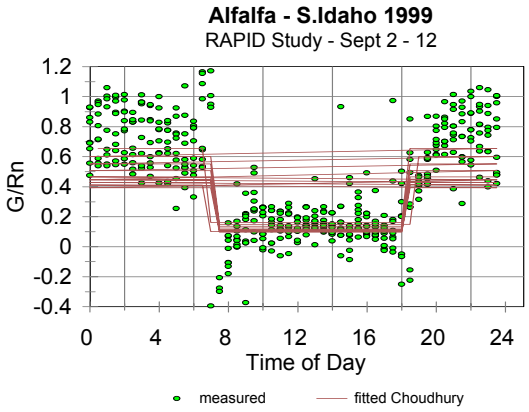

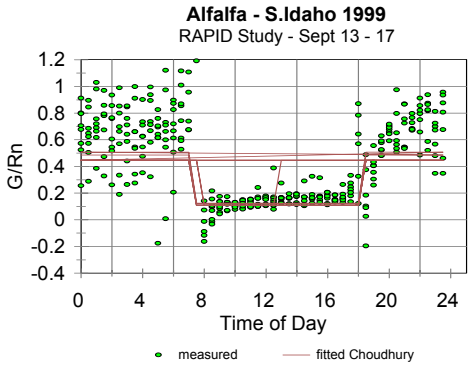

Figure. Observed and estimated G/Rn ratios

For the estimation of G/R_n, LAI was estimated from crop height using the equation given previously.
As shown in the graph, Choudhury's equation estimated G/Rn ratios quite well, but did not account for change in G/R_n during a specific day.

The three figures above also show that the slope of G/R_n vs. time of day changes with LAI.

4. Comments
It is concluded that the G/R_n ratio strongly depends on vegetation indices such as LAI. G might not be substantially affected by soil moisture and by the absolute value of R_n. Clothier et.al. (1986) indicated that the effect of soil moisture on values of G/Rn may be small or negligible.

G/R_n observations were predicted will with the estimation values by Choudhury's estimation. The observed G/Rn ratios varied in same relation to time over different time periods, especially in the beginning and middle periods of study. These results agree with the Payero's results that G/R_n is unstable during daytime when the field is not fully covered with alfalfa.

Model for Hourly G estimation for alfalfa fields based on data from the RAPID Study, Kimberly ID

In this section, we introduce prediction results for hourly G estimation based on using data from the 1999 RAPID study for alfalfa.

1. Basic Idea

The analysis in the previous section showed that the Choudhury's equation of G/R_n vs LAI estimated daily G for an alfalfa field quite well. Also, the analysis showed that hourly change of G/R_n depends on the crop height (or LAI). A better estimation method for

hourly soil heat flux might be developed if the hourly change of G/R_n ratio is explained by a simple regression equation.

2. Equation Development

The daily G for the alfalfa field can be estimated by following Choudhury's equation:

$G/Rn = 0.4 * e^{-0.5LAI}$ for night time, the coefficient 1.6 is used instead of 0.4 following ASCE.

G/Rn ratio by this equation agrees with the observed "midday" ratio (i.e., 13:00). 13:00 is the middle of the 9:00 to 17:00 period, which was selected since on many days, G/Rn ratio formed a sloped line within 9:00 and 17:00.

When alfalfa is short, the G/R_n ratio tends to be higher in morning and lower in evening. The slope of G/Rn ratio becomes moderated as the crop grows. (This trend is also reported by Payero and supported by Kustas's results, although he did not mention it). Also, Kondo (19__) shows an observed heat balance in desert area that indicates a steep slope of G/Rn for desert.

If the hourly change of G/Rn ratio can be explained as a "slope", hourly G can be predicted by the following equation;

$$G/Rn(hour) = 0.4e^{-0.5LAI} + (hour - 13) \times Slope$$

where, the number 13 in the equation is 13:00. The "hour", is expressed as 1 – 24. (ex. 15:30 is 15.5).

Since the primarily factor of the G/Rn slope is a vegetation index such as crop height and LAI, the slope is predicted by the following simple linear equation;

Slope = ah + b

where, a and b are constants, h is the height (m) of alfalfa

By applying a LAI estimation equation LAI = 10h, the variable of hourly G/Rn estimation equation finally becomes a function of "hour" and "crop height" only;

$$G/Rn(hour) = 0.4e^{-5h} + (hour - 13) \times (0.2229h - 0.0526)$$

2-1. Determination of the slope of G/Rn

The slope of G/Rn was determined by a linear regression method. The following graphs show examples for 8/25, 9/6 and 9/15.

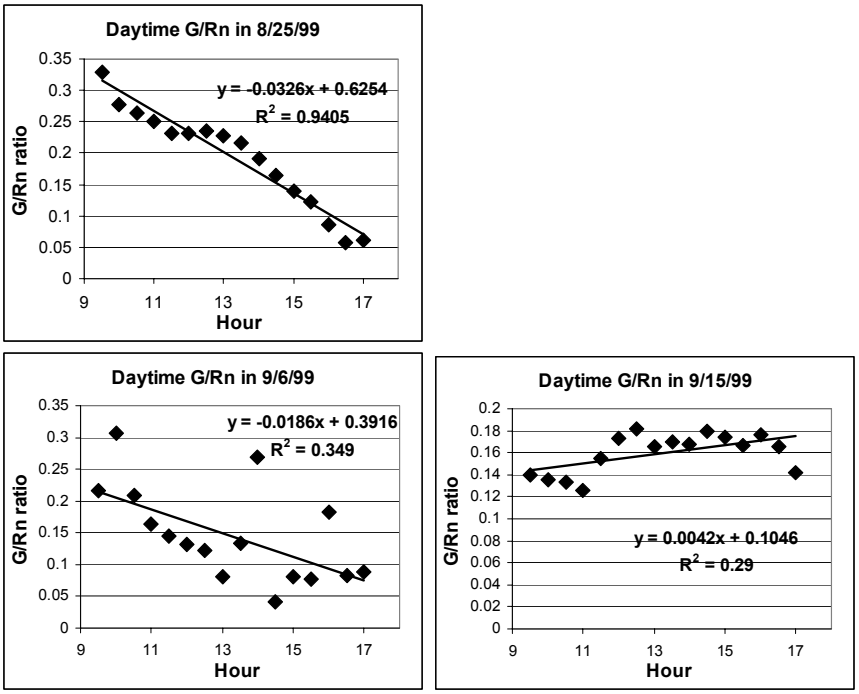

Figure. Examples of slope determination – G/Rn slope was -0.0326 in 8/25/99, -0.0186 in 9/6/99 and 0.0042 in 9/15. (The slope reduces and finally becomes opposite in sign as alfalfa grows)

2-2. Combination of G/Rn slope and crop height

The calculated G/Rn slope values were plotted with the alfalfa height;

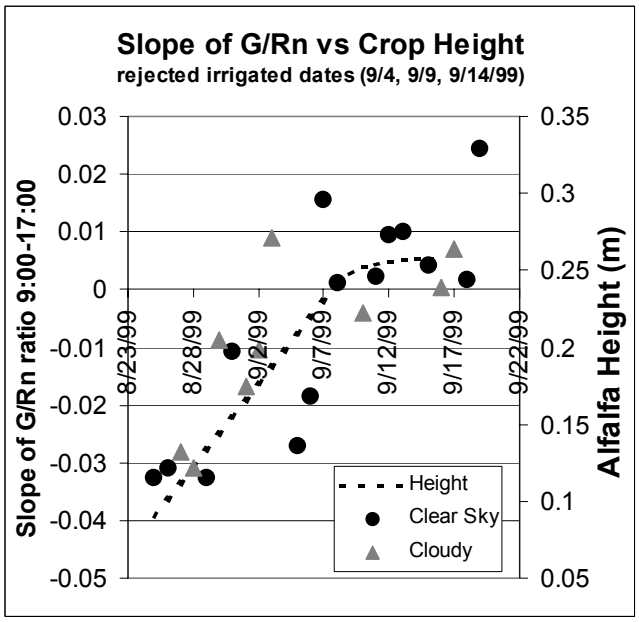

Figure. G/Rn daytime slope and Alfalfa height

Also, the G/Rn slopes were plotted vs the crop height;

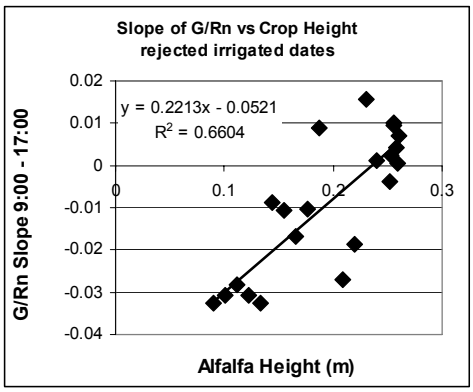

Figure. G/Rn slope vs Crop height

Although the above graph shows a clear relation between G/Rn slope and the crop height, the r-square value of 0.66 indicates that G/Rn values are not a singular function of crop height. To get a sort of "averaged" relation between the G/Rn slope and the crop height, we used 4-day averaged values instead of daily values (the total study period was 24days).

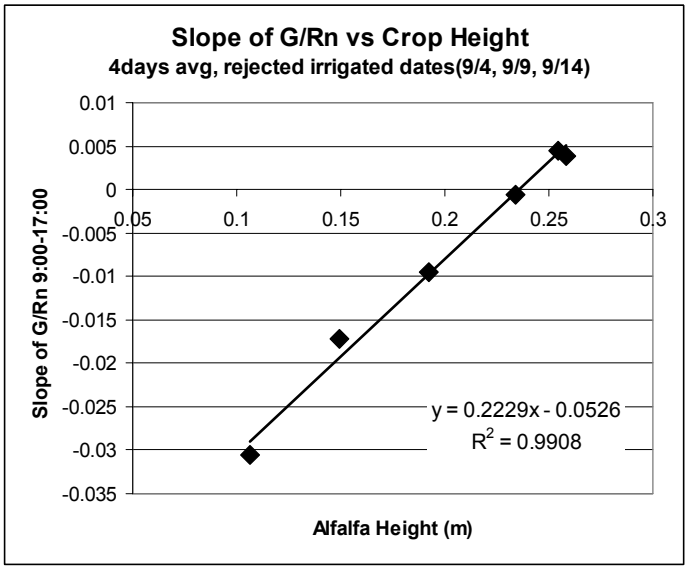

Figure. G/Rn slope vs Crop height (4 days average)

The constants of regression equation derived by the 4days_avg data were very similar with the ones by the daily data, and the G/Rn ratio showed a strong linear relation with crop height.

The averaged G/Rn slope is predicted by;

$$Slope = 0.2229h - 0.0526$$ for Alfalfa (less than 0.3 or 0.4m)

3. Conclusions

Hourly G/Rn ratio can be estimated by the following equation;

$$G/Rn(hour) = 0.4e^{-5h} + (hour - 13) \times (0.2229h - 0.0526)$$

The following figures show the fit between predicted and observed G/R_n for the RAPID study:

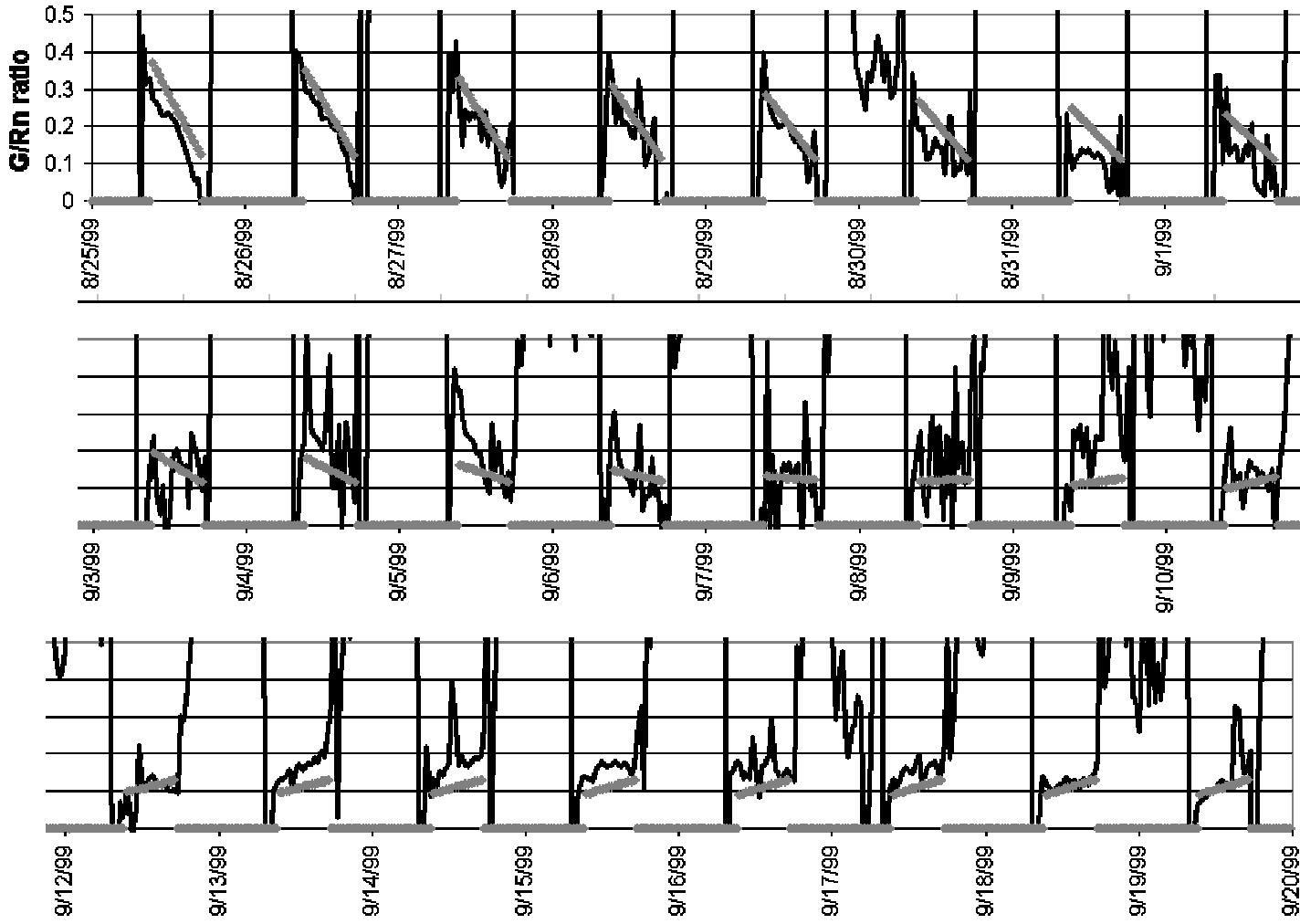

Note: Estimated G/Rn in the above figures is for daytime only . Irrigation dates, which were rejected from the analyses, were 9/4, 9/9 and 9/14.

Hourly G estimation for alfalfa fields (data from RAPID study and 1970's study, Kimberly ID)

Part 1. Additional analyses

1. Using LAI instead of crop height

In the previous section, we used crop height as the vegetation index. However, LAI may be a better indicator for extending the developed equation for other crops or for all crops.

For short alfalfa (less than 0.4m), LAI can be estimated by the following equation;

$$LAI = 10h$$

Therefore, the developed equation becomes;

From: $G/Rn(hour) = 0.4e^{-5h} + (hour - 13) \times (0.2229h - 0.0526)$

To: $G/Rn(hour) = 0.4e^{-0.5LAI} + (hour - 13) \times (0.02229LAI - 0.0526)$

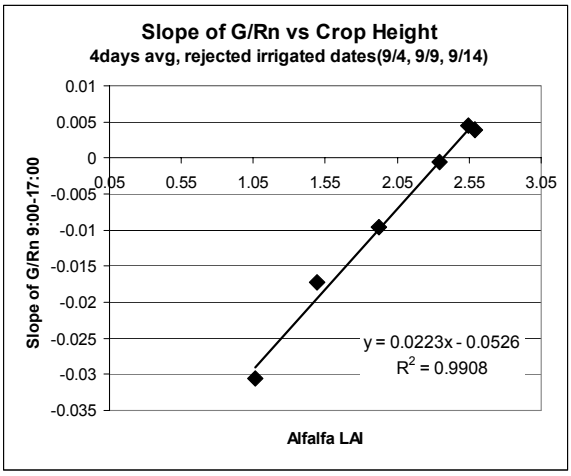

Figure. LAI vs daytime slope of G/Rn

By using the LAI equation, the same estimation results are obtained.

2. Modification of composition of the equation

In the previous section, we applied the following composition of equation;

$$G/Rn(hour) = 0.4e^{-5h} + (hour - 13) \times (0.2229h - 0.0526)$$

This equation means that;
$$G/Rn(hour) = (middayG/Rn\_by\_Choudhury) \pm (hour\_from\_midday) \times (G/Rn\_Slope)$$

However, if considered to apply this kind of equation for all crops, we might better to consider G/Rn slope as a function of LAI. Therefore, we evaluated the following format of the equation;

$$G/Rn(hour) = C_1 e^{C_2 LAI}(1 + (hour - 13) \times (C_3 LAI + C_4))$$

where, C1 to C4 are constants. C1 and C2 might be 0.4 and –0.5 respectively (by Choudhury). C3 and C4 are constants relate to G/Rn slope.

After a regression analysis, the following equation was suggested:

$$G/Rn(hour) = 0.4e^{-0.5LAI}(1 + (hour - 13) \times (0.109LAI - 0.2508))$$

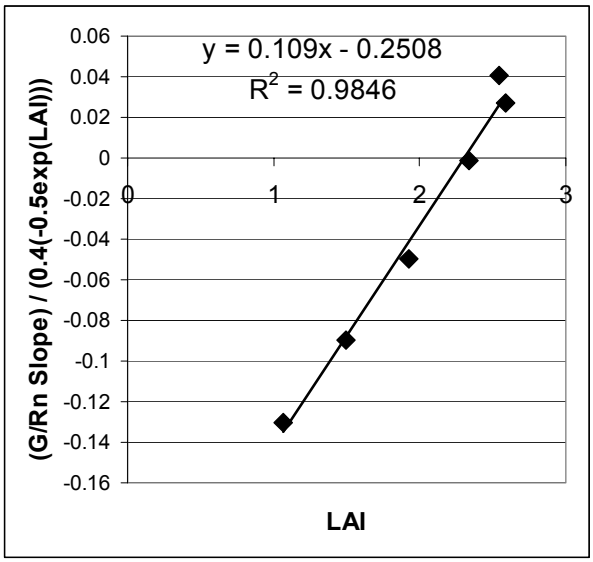

Figure. Plot of (daytime G/Rn slope)/(0.4(-0.5exp(LAI)))

This equation can be used to predict G/R_n for any hour and for any type of LAI.

Development of an equation for predicting G for all crop types

Part 1. G estimation from R_n (or R_s) and LAI for Alfalfa, Potato, Beans and Wheat

1. Introduction

This section develops G estimation equations from R_n or R_s and LAI, for several crops. Papers by Choubdhury, Kustas etc. indicate that G/Rn ratio is strongly related to LAI. Therefore, in this section we develop regression equations using LAI and G data collected during the 1970's by Dr. James L. Wright of the USDA-ARS at Kimberly. Dr. Wright was a cooperator for this Raytheon study. In addition to G/R_n, G/R_s was evaluated to see if one can estimate G by R_s. Rs data are easier to obtain.

2. Limitations

a) G estimation in the beginning of cultivation (bare soil condition)

Although it seems that the surface temperature affects G/Rn and G/Rs ratios until fields are covered by vegetation, this development does not include the effect of surface temperature.

b) Hourly G estimation

This analysis contains only the results for daytime (9:00-17:00) periods. The previous analysis of 1999 alfalfa data (RAPID study) indicated that there is a trend of G/Rn within a day and that the hourly trend could be explained by LAI.

c) G estimation during periods of crop senescence and death

The G/Rn ratio is a factor of both green-leaf LAI and whole LAI which includes dead leaves, since all leaves are effective in shading the ground surface. Therefore, when G/Rn is plotted against green-leaf LAI, the trends are different for crop growing period and senescent (end of season) periods. This report focuses only growing periods. In this report, we consider the LAI as including only green-leaf LAI.

3. Data and methods

3-1. Data

The meteorological data which Dr.J.L. Wright corrected during the 1970's were used for the analyses. The data include hourly Rs, Rn, and G, crop height and LAI, and rain/irrigation. Also, log book records by Dr. Wright were used for background information.

Data were evaluated as follows:

We used both G measured in lysimeter fields and G measured in the lysimeter itself. These two G measurements were compared to determine consistency of measurements. The daytime ratio of G_{lys}/G_{field} normally showed specific trends. However, some data were away from the trend. Most of the outlying values for G_{lys}/G_{field} ratios occurred at rain/irrigation dates and we kept these data. Other outlying G/G ratios occuring during periods of no rain or irrigation were rejected. The average of two G measurements were used for the soil heat of the field sites. Hourly Rs and Rn data were plotted to verify that measurements were correct.

LAI data were not observed everyday. Daily LAI values were calculated by interpolating the observed LAI data.

3-2. Method

The original data were in the form of hourly averages collected by Dr. Wright and assembled onto disk files by Vanderkimpen (1990). Averages for the daytime period (9:00 – 17:00) were derived from the hourly data by accumulation. All of the heat balance components are the aggregation of fluxes during 9:00-17:00 with units in MJ/m^2. 9:00 – 17:00 was specified as "daytime" following the 1999 alfalfa (RAPID) study. In the 1999 study, a trend of G/Rn was generally observed between 9:00 and 17:00. Therefore, the results represent midday periods rather than morning/evening periods.

G/Rn and G/Rs ratio were calculated and compared with LAI. Distinction was made between ratios for rain and irrigation dates, one day after rain/irrigation, cloudy days and clear sky days. The rainy days and irrigated days were rejected for final development of G estimation equations because it was confirmed that G/Rn values became inconsistent during such days.

4. Alfalfa 1971

4-1. LAI

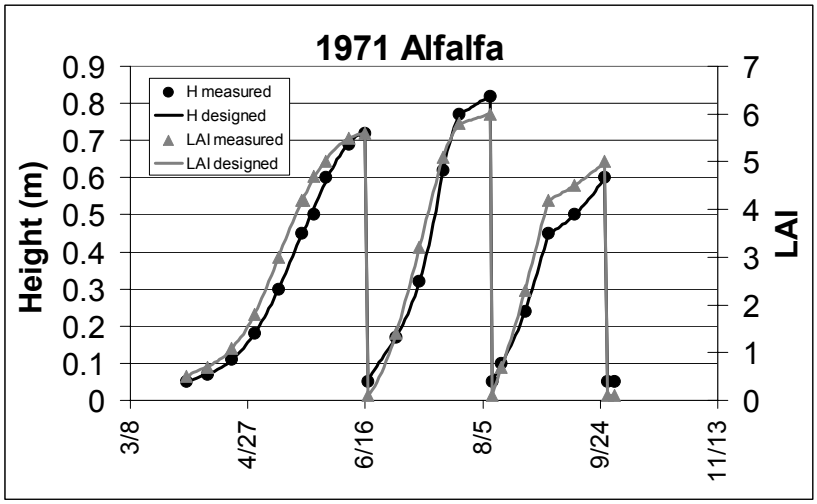

Figure 4-1-1. Crop heights and the LAI in 1971. Dots are the observation and the lines are “interpolated” height & LAI, which are used in the analysis in this report.

In 1971, alfalfa was cropped three times. The cropping periods are referred as 1971-1, 1971-2 and 1971-3.

4-2. Data evaluation

The following graphs show G/G ratios for each cropping periods in 1971. Also, the following information are noted under the title of each graph;

1) Cropping period
2) Number of days lacking
3) Date and the reason for rejecting data

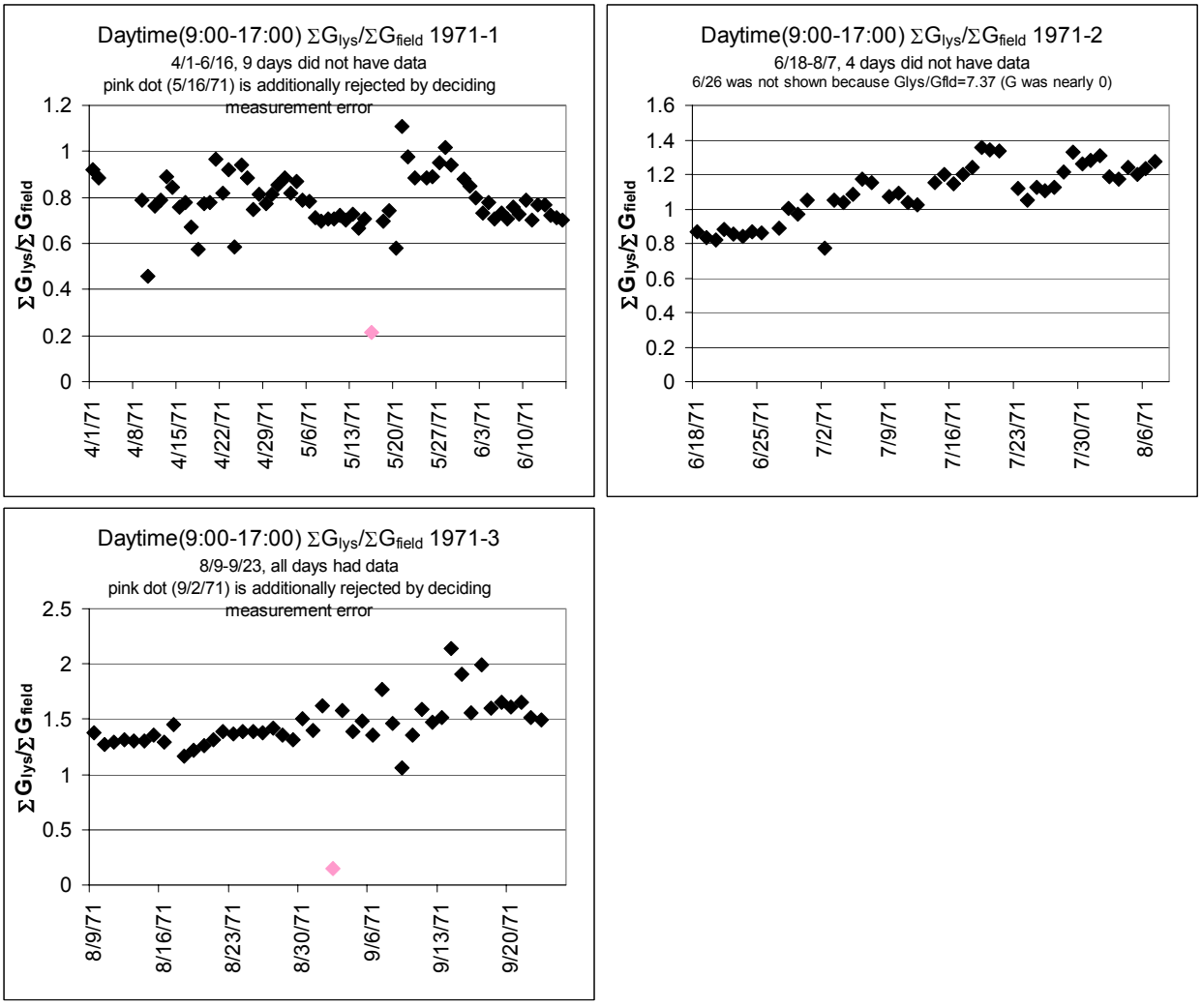

Figure4-2-1. Comparison of G at Lysimeter and G at field. The original G values used for calculating the ratios are accumulation of daytime in MJ/m^2 (9:00-17:00 which means 10:00-17:00 in the data; 10:00 data includes observation from 9:00 to 10:00).

As shown in Fig.4-2-1, G/G ratio ranges from 0.7 to 1.6. The primary reason of this difference is that the two Gs were observed at different locations under somewhat different field conditions.

4-3. Results: Effect of soil/sky conditions

The following graphs show G/Rn vs LAI for each cropping period.

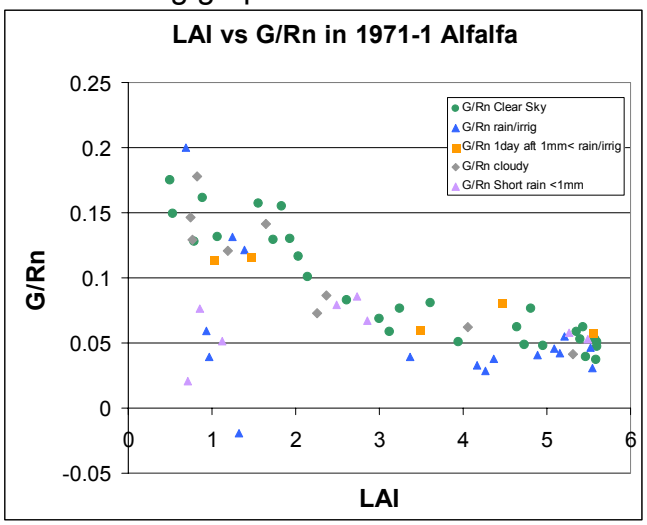

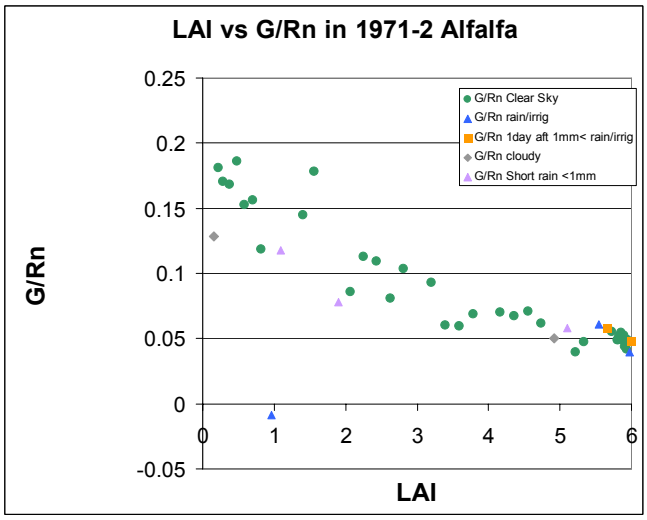

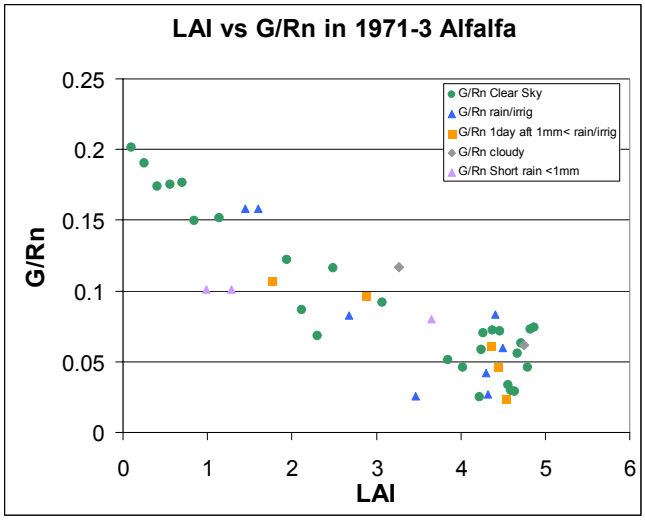

Figure 4-3-1. Daytime G/Rn ratio for Alfalfa including all soil/sky conditions

The following conclusions are made from the above figures:

(a) G/Rn is a strong factor of LAI

(b) Soil moisture does not affect G/Rn ratios, especially when a field is densely covered – Clothier (Clothier et.al. 1986) also reported that soil moisture did not affect to G/Rn ratio in a densely covered field. However, the analyses for other crops indicates that soil moisture might reduce G/Rn and G/Rs ratios under bare to sparse conditions.

(c) Cloudy days (which would have a smaller magnitude of Rn) can make G/Rn ratios unstable because both G and Rn inputs are smaller. However, there is no trend (which means that the magnitude of Rn itself might not be a significant factor of G/Rn)

(d) Rainfall or Irrigation impact G/Rn very much. Cold water might cool the top of heat flux plates or water might convey heat from near the soil surface to the heat plate (these two would cause G measurement errors). Also, increased soil water content will increase the thermal conductivity of the soil. Snow and short-but-very-cold rains reduced G/Rn ratio significantly. The three "G/Rn Short rain < 1mm" in the first figure for LAI ~1 represented snow.

4-4. Developed G estimation equation for Alfalfa

The following graph is the plot of G/Rn vs LAI and the regression line.

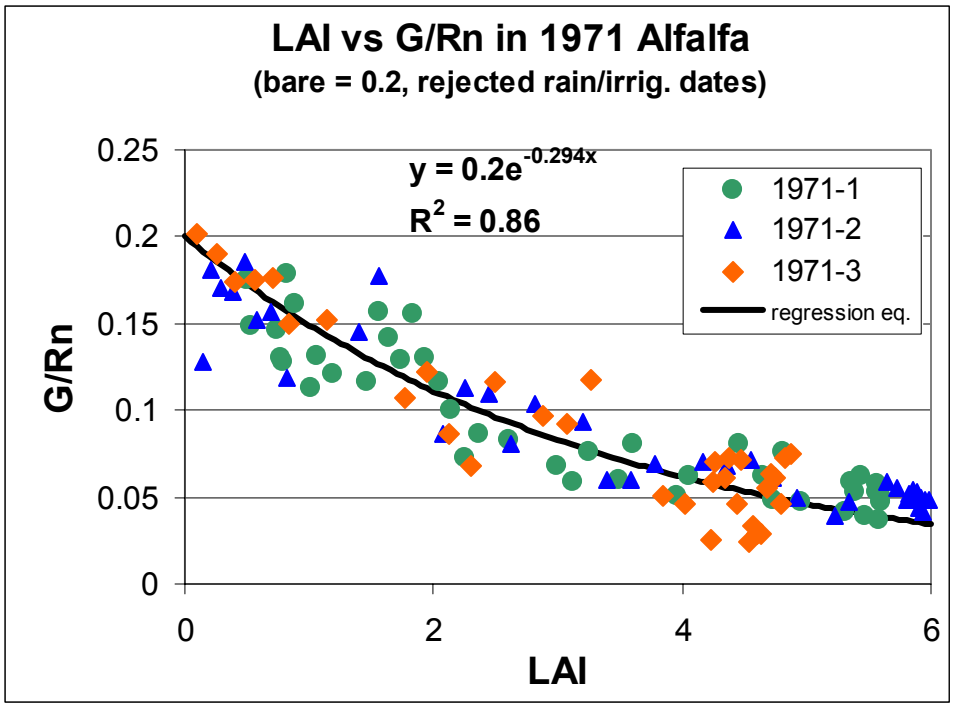

Figure.4-4-1 LAI vs daytime G/Rn ratio in 1971 alfalfa (all three cropping periods)

In the graph, G/Rn when LAI = 0 was manually assigned as 0.2, and the decay constant –0.294 represents the best regression.

The developed equation for alfalfa is;

$$G / Rn = 0.2e^{-0.294LAI} \qquad R^2=0.86$$

Measurements for the three cropping periods agree well with each other. However, there is some scatter in the G/Rn observations. One reason for the scatter might be in the measurement of G.
For example, a large scatter occurred around 1<LAI<2 in period 1971-1. Figure 4-2-1 shows that G/G ratio at that time was not stable and showed scatter, which might indicate that the G measurement had a problem or the field condition was instable.

5. Potatoes in 1972

5-1. LAI

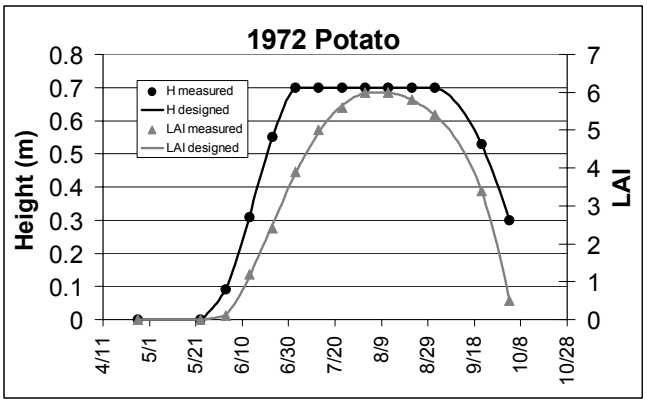

Figure 5-1-1. Crop heights and the LAI in 1972. Dots are the observation and the lines are "interpolated" height & LAI

5-2. Data evaluation

1) The following graphs represent $G_{lysimeter}$ /G_{field} ratios for potatoes in 1972.

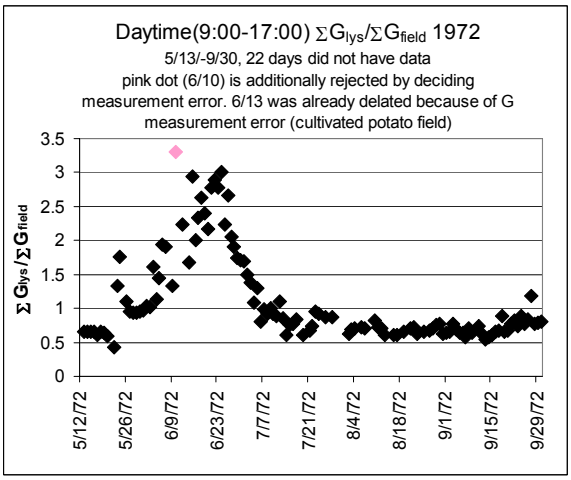

Figure5-2-1. Comparison of G at Lysimeter and G at field. The original G values used for calculating the ratios are accumulation of daytime in MJ/m^2 (9:00-17:00 which means 10:00-17:00 in the data; 10:00 data includes observation from 9:00 to 10:00).

G_{lys}/G_{field} ratios for Potatoes began at 0.7, increased to 3, and returned to 0.7 during the growing season. The very high ratios occurred when the crop was still small and field was partially covered. The different location of G measurements – i.e, within shadows of leaves would affect the magnitude of G substantially during this peirod, and slope/aspect of the soil surface above the G plate would change the amount of G also. G measurements only one from field location and one from lysimeter location are probably not sufficient to estimate the actual G of the field. However, the averaged value of two Gs may reasonably represent the spatial distribution of G in the field.

5-3. Results: Effect of soil/sky condition

The following graph shows G/Rn vs LAI.

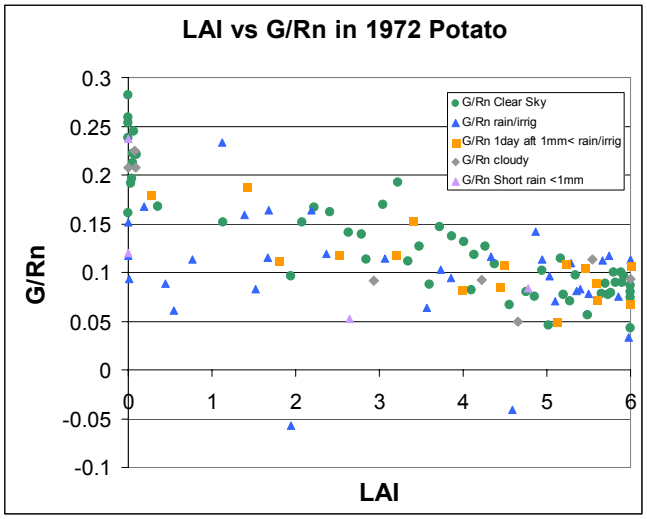

Figure5-3-1. Daytime G/Rn ratio for potato including all soil/sky conditions

As for alfalfa, G/Rn is a strong factor of LAI, and the soil moisture and sky conditions do not affect G/Rn ratio, especially when a field is densely covered. Rainfall and irrigation impact the G/Rn measurement significantly.

In addition to comments for alfalfa (part 4-3), there are two additional trends found for potatoes:

(1) There is a wide spread of G/Rn values when LAI is zero or close to zero, and,
(2) The G/Rn or G/Rs vs LAI curve might be different between the growing period and the senescent (wilting) period of the crop (See. Figure 5-3-2).

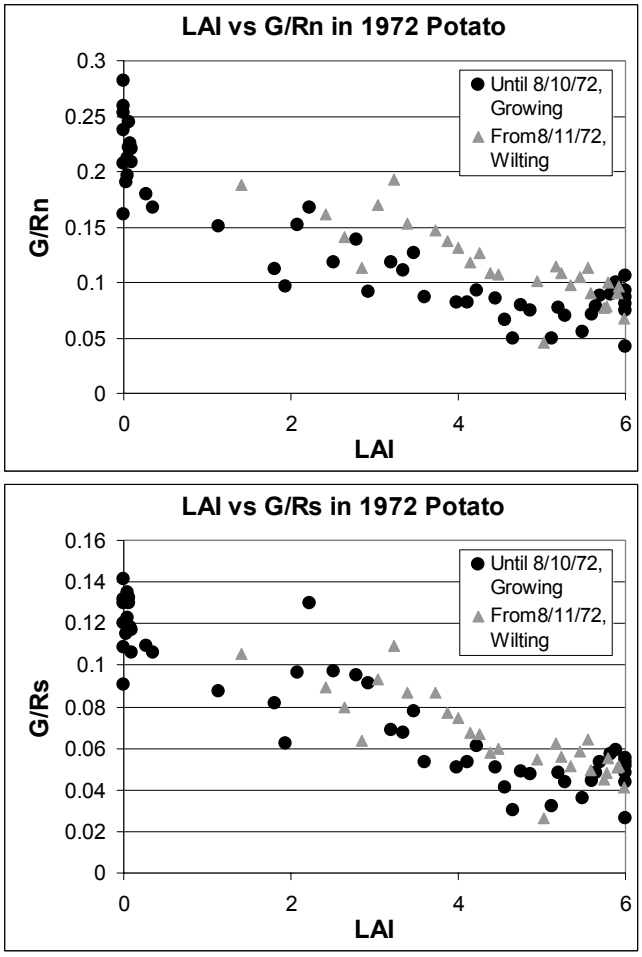

Figure 5-3-2. G/Rn vs LAI (left) and G/Rs vs LAI (right) in two phases

In Figure 5-3-2, G/Rn measurements are slightly higher in the senescent period than in the growing period, while G/Rs measurements in the two periods agree each other.

The detail for G/Rn and G/Rs in the senescent period is described later in the 1978-79 wheat section.
In the equation development, only growing period was used.

5-4. Developed G estimation equation for Potato

The following graphs are the plots of G/Rn and G/Rs vs LAI with the regression line.

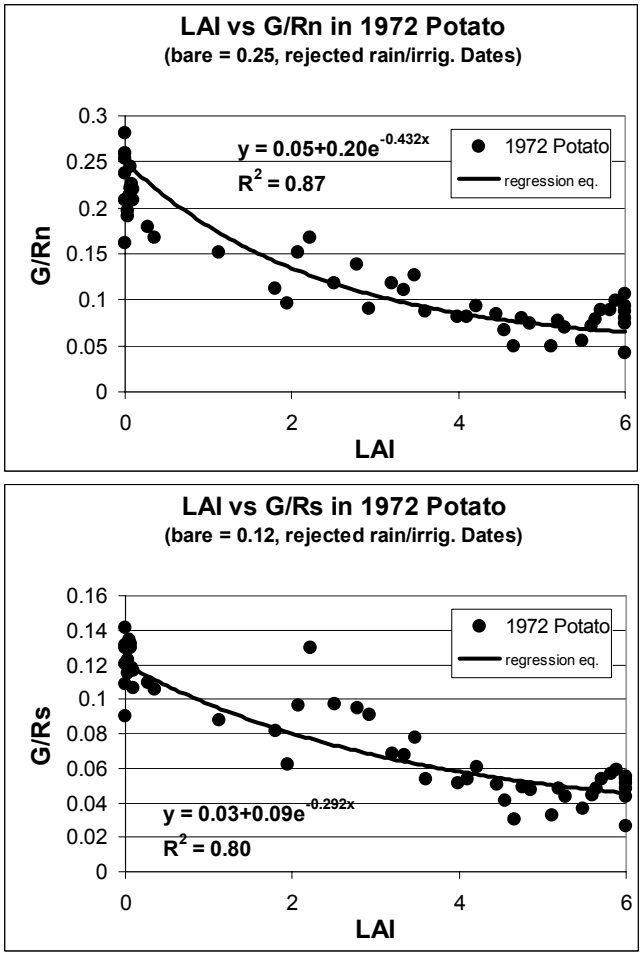

Figure.5-4-1 LAI vs daytime G/Rn ratio (left) and G/Rs ratio (right) in 1972 potato (only growing period)

In this figure, the starting point (when LAI = 0) and the ending point (when LAI = 6) were manually assigned. Therefore, only the decay constant was determined by a regression method.

The developed equations for potato are;

$$G/Rn = 0.05 + 0.25e^{-0.432\,LAI} \qquad R^2=0.87$$

$$G/Rs = 0.03 + 0.09e^{-0.292\,LAI} \qquad R^2=0.80$$

There is a wide range of G/Rn values at around LAI = zero. The analysis indicates that G/Rn depends on the surface temperature when soil is bare. A set of equations that use a surface temperature function are described later. The surface temperature affects G/Rn and G/Rs only when LAI is very small – less than 0.1 or 0.5.

6. Beans 1973-74

6-1. LAI

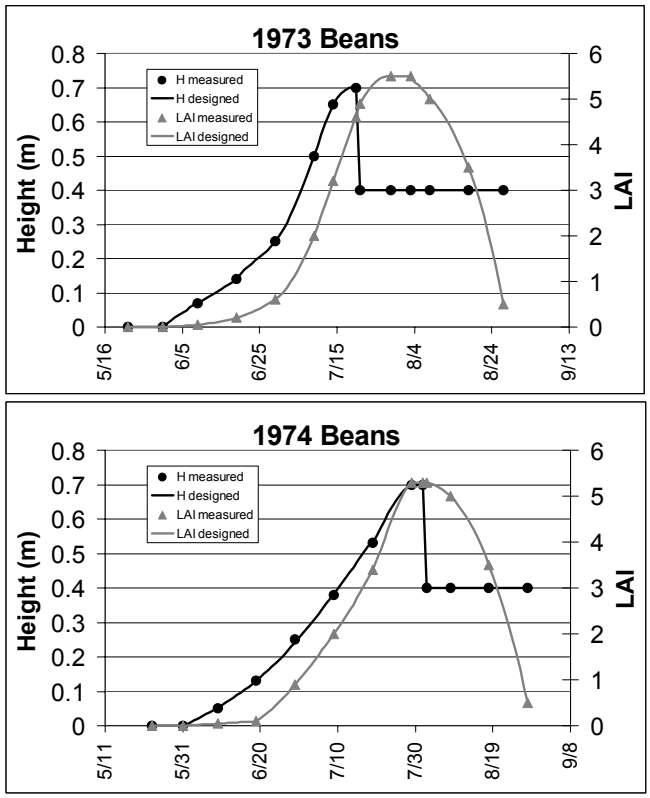

Figure 6-1-1. Crop heights and the LAI in 1973 and 74. Dots are the observation and the lines are "interpolated" height & LAI

In 1973 and 1974 (beans), crop height suddenly droped in the middle of the cropping periods due to a strong wind that lodged the crops. For the analysis of G, only the period before crop lodging was used Therefore, no senescent period included in the result.

6-2. Data evaluation

1) The following graphs are G/G ratios for beans during 1973 and 1974.

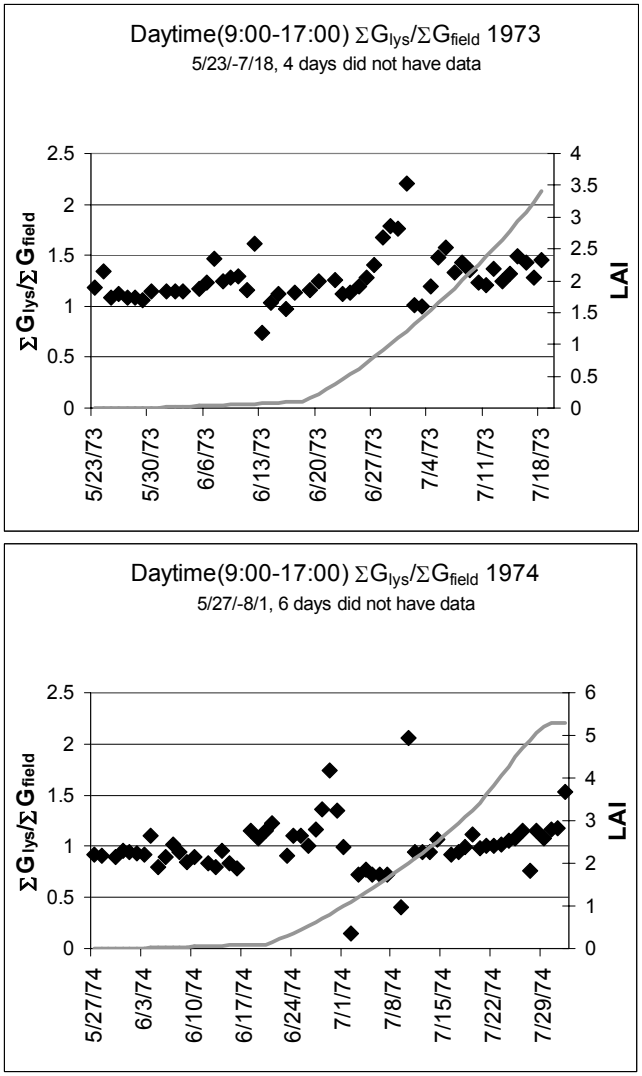

Figure6-2-1. Comparison of G at Lysimeter and G at field. The original G values used for calculating the ratios are accumulation of daytime in MJ/m^2 (9:00-17:00 which means 10:00-17:00 in the data; 10:00 data includes observation from 9:00 to 10:00).

As shown in Fig.6-2-1, the G_{lys}/G_{field} ratios for beans were unstable, especially when 0.5<LAI<1.5 (in 1973) and 0.5<LAI<1 (in 1974).

6-3. Results: Effect of soil/sky condition

The following graphs show G/Rn vs LAI.

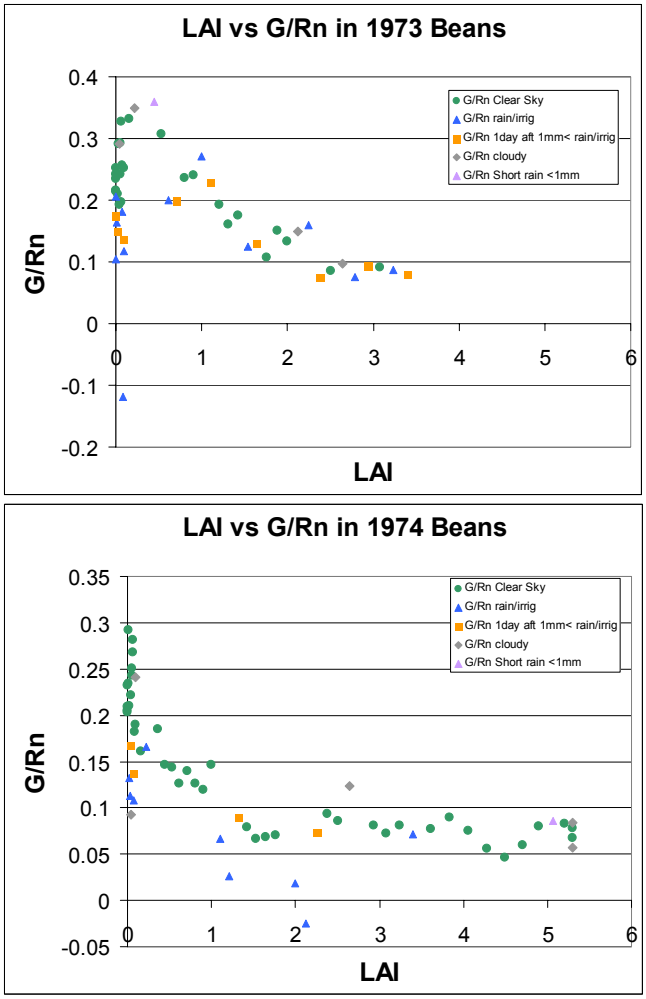

Figure6-3-1. Daytime G/Rn ratio for beans including all soil/sky conditions

These graphs support conclusions made for alfalfa and potatoes.

6-4. Developed G equation for Beans

The following graphs are plots of G/Rn and G/Rs vs LAI with the regression line.

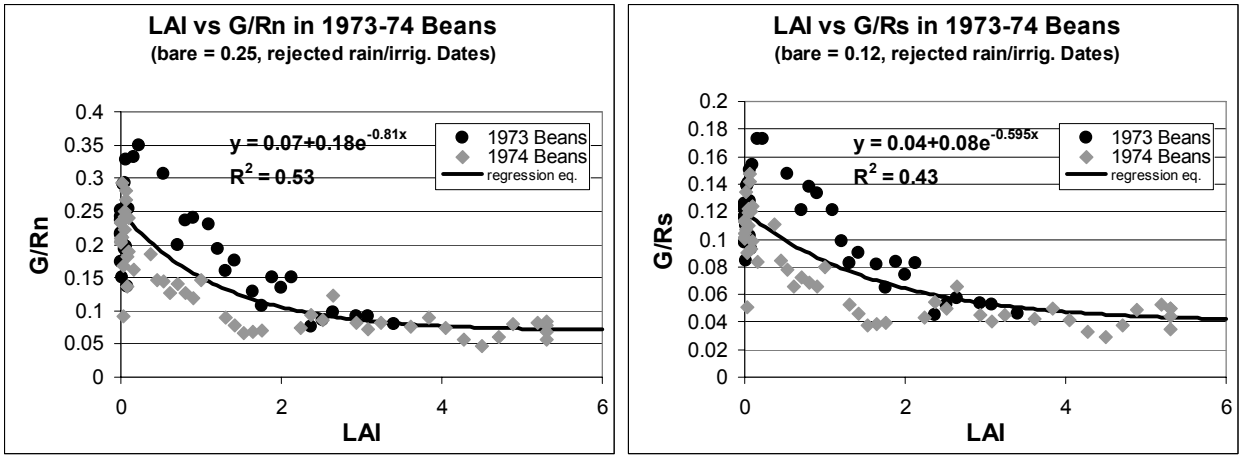

Figure.6-4-1 LAI vs daytime G/Rn ratio (left) and G/Rs ratio (right) in 1973-74 beans

The regression equation shown in the right (G/Rs) graph was determined by regression as explained in the Potato section. However, for the equation in the left graph (G/Rn), all three constants were manually assigned, to control the shape and behavior of the curve. Manual determination of the constants only reduced theR-square by 0.02.

The problem for beans is that the G/Rn and G/Rs ratios were considerably different between years, especially when LAI is around 0.5 to 2.
Measurements of G in the field and lysimeter attempt to measure the same G. Therefore, differences indicate problems with repeatability caused by placement, plates, technique, local vegetation. Therefore, by assuming that G/Rn should be similar in two years, only G_{field} was used for 1973 and only G_{lys} was used for 1974 instead of the averaged G values as used for potatoes and alfalfa. The similarity in these two data sets was confirmed by an analysis of surface temperature and surface heat storage. Surface temperature was computed by inverting the energy balance equation.

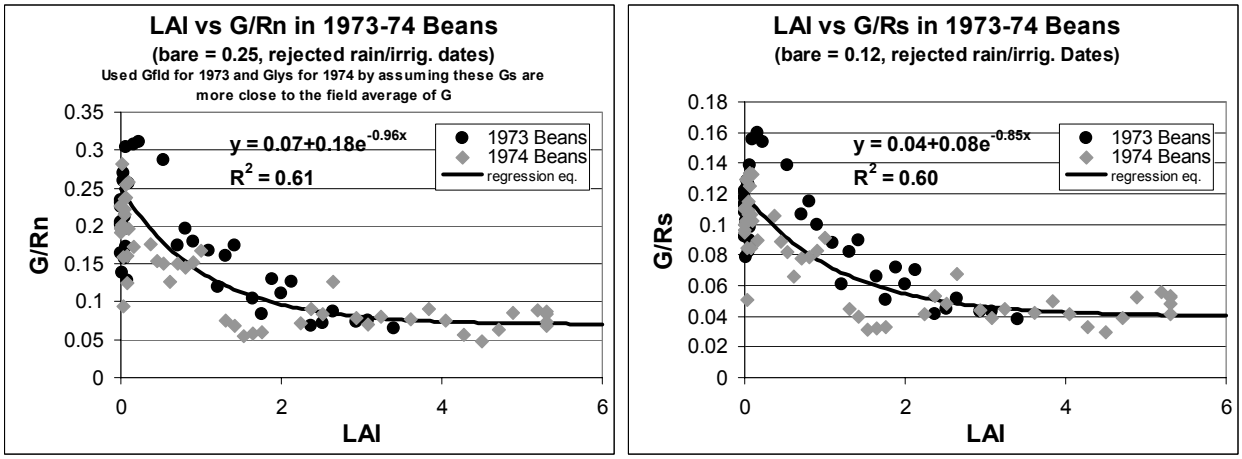

Figure.6-4-2. G Adjusted LAI vs daytime G/Rn ratio (left) and G/Rs ratio (right) in 1973-74 beans.

All three constants were manually assigned for the equations in both of the graphs. Compared to the regression method, the R^2 values were only 0.015 lower in the G/Rs curve while R^2 did not change for the G/Rn curve.

The equations for estimating G in Beans are:

$$G/Rn = 0.07 + 0.18e^{-0.96LAI} \qquad R^2=0.61$$

$$G/Rs = 0.04 + 0.08e^{-0.85LAI} \qquad R^2=0.60$$

7. Wheat 1978-79

7-1. LAI

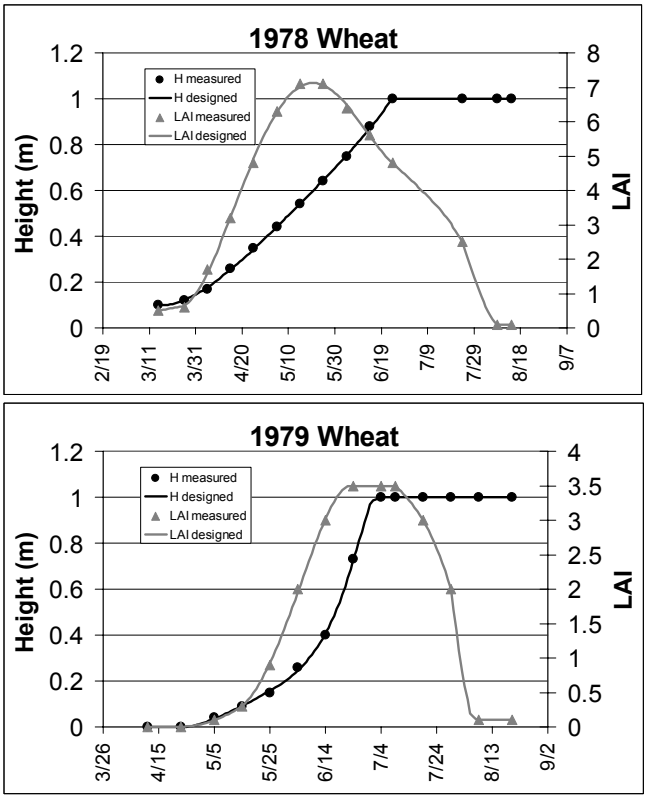

Figure 7-1-1. Crop heights and the LAI in 1978-79. Dots are the observation and the lines are "interpolated" height & LAI

7-2. Data evaluation

1) The following graphs represent $G_{lysimeter}$ /G_{field} ratios for wheat 1978-79.

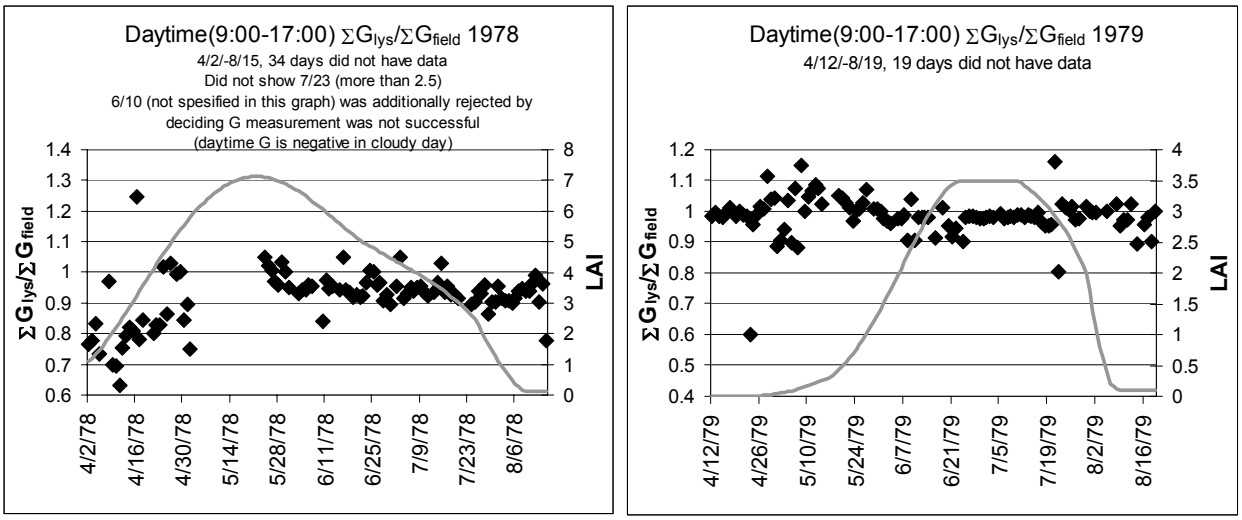

Figure7-2-1. Comparison of G at Lysimeter and G at field. The original G values used for calculating the ratios are accumulation of daytime in MJ/m^2 (9:00-17:00 which means 10:00-17:00 in the data; 10:00 data includes observation from 9:00 to 10:00).

7-3. Results: Effect of soil/sky condition

The following graphs show G/Rn vs LAI.

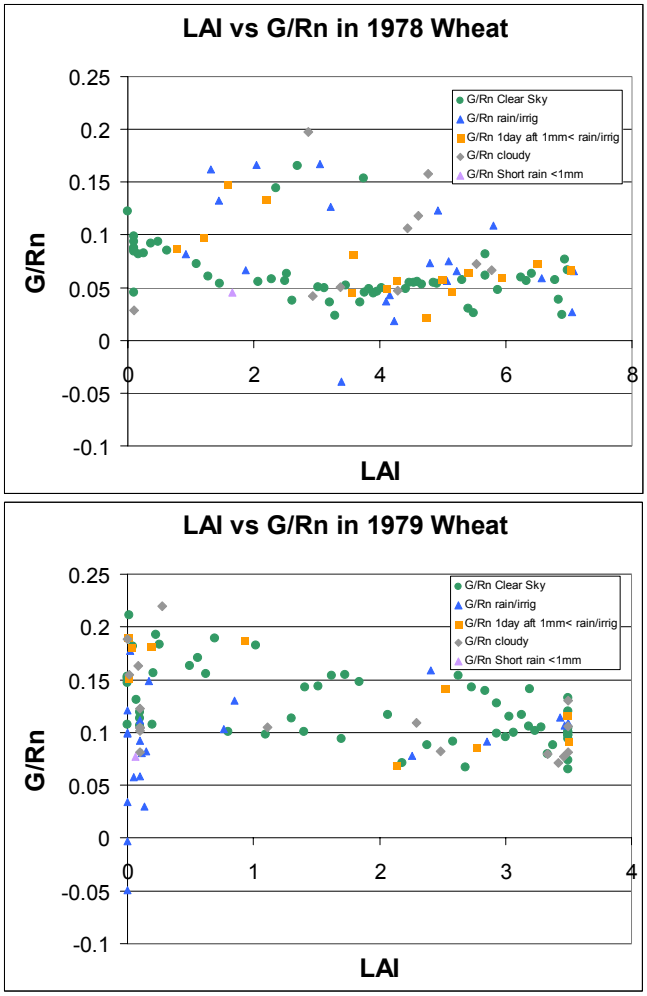

Figure7-3-1. Daytime G/Rn ratio for wheat including all soil/sky conditions

The wheat 1978-79 had the data both growing periods and senescent (wilting) periods. The following graphs show the differences between each phase.

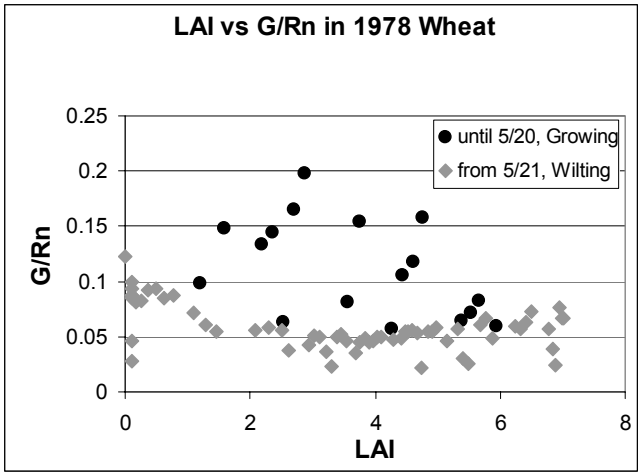
LAI vs G/Rn in 1978 Wheat
0.25
0.2
0.15
0.1
0.05
0
G/Rn
0
2
4
6
8
LAI
until 5/20, Growing
from 5/21, Wilting

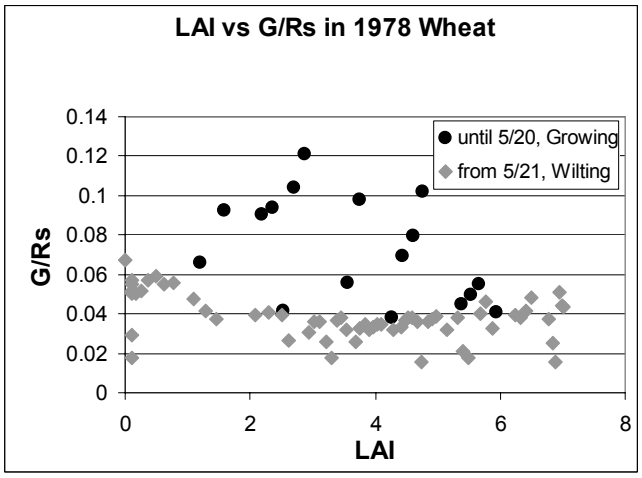
LAI vs G/Rs in 1978 Wheat
0.14
0.12
0.1
0.08
0.06
0.04
0.02
0
G/Rs
0
2
4
6
8
LAI
until 5/20, Growing
from 5/21, Wilting

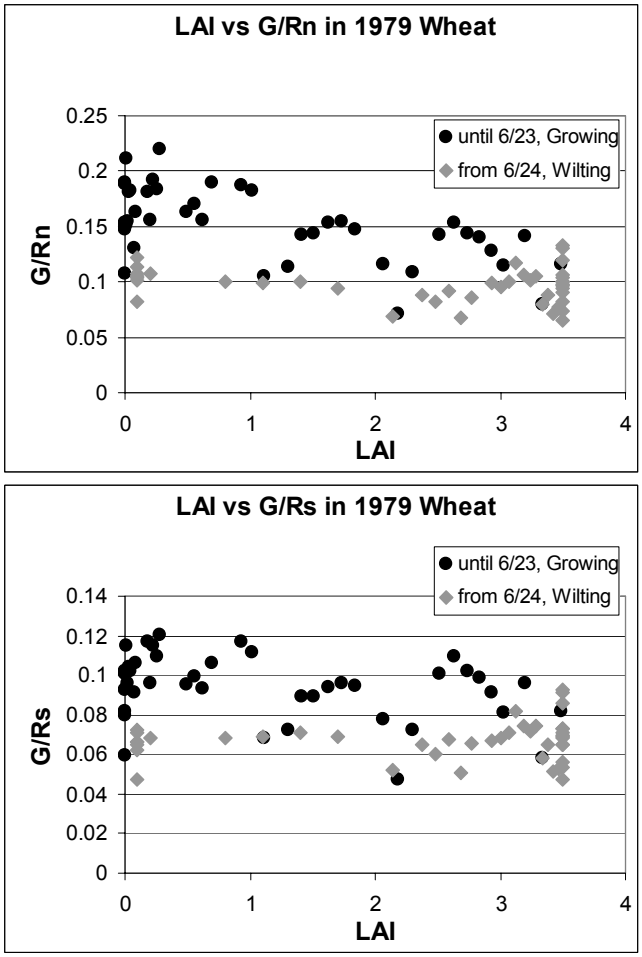

Figure 7-3-2. G/Rn and G/Rs vs LAI in two phases

Using the Figure 7-3-2 with the Figure 5-3-2 (1972 potato), the differences between growing periods and senescent periods are discussed:

In Figure 7-3-2, G/Rs in the growing period tends to be higher than the G/Rs value in the senescent period. Another trend is that the G/Rs value tends to be constant in senescent period, regardless the LAI values. These results are understandable since we defined the LAI as green-leaf LAI. In a senescent period, green-leaf LAI (which is our LAI) decreases day by day, but the total LAI (includes yellowish and dead leaves) does not change much. A wheat field in the end of cropping season has nearly zero green-leaf LAI although the field is still relatively fully covered by dead vegetation and the land surface must be cooler than under bare soil conditions.

In Figure 5-3-2 (1972 potato), there was no difference in G/Rs observed between the growing period and the senescent period. This may be for the following two reasons; (1) the LAI measurement in wilting period may not have been successful, and (2) a potato's senescing process is not like that for wheat.

Unlike for G/Rs, G/Rn is more complicated. Figure 5-3-2 shows that G/Rn in the senescent period of potatoes is higher than for the growing period, but Figure 7-3-2

shows the opposite trend in a wheat field. In senescing periods, both G and Rn for a specific green-leaf LAI decrease. Rn decreases because albedo increases (outgoing longwave radiation might increase also), and G decreases because the dead leaves prevent the solar radiation from directly reaching the soil surface.

7-4. Developed G equation for Wheat

The following graphs are the plots of G/Rn and G/Rs vs LAI with the regression line.

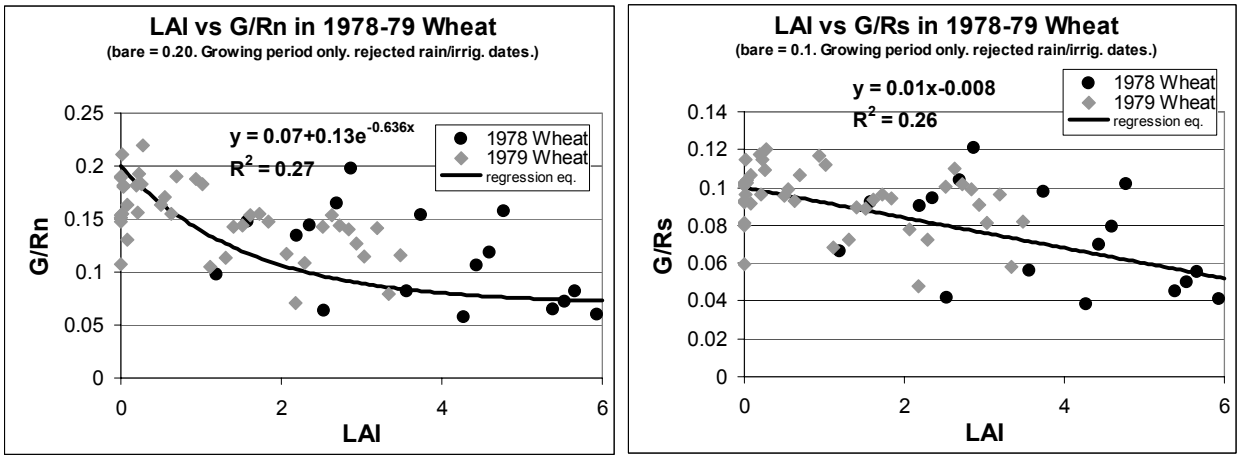

Figure.7-4-1 LAI vs daytime G/Rn ratio (left) and G/Rs ratio (right) in 1978-79 wheat (Only growing period)

The Figure 7-4-1 is the final results for wheat. In the G/Rs relationship, a straight line was used since an exponential relation was not confirmed by regression.

G/Rn and G/Rs for the two years somewhat agree with each other. However, G/Rn (and Rs) vs LAI showed large scatter for both years. It was unclear whether this scatter occurrs for wheat type crops, or due to a problem of data quality.

8. General Equation for all crops

Table 8-1 shows the constants for each crop and for a suggested general equation. The format of the equations is;

$$G / Rn = C_1 + C_2 e^{C_3 LAI}$$

Table 8-1. Constants for G/Rn, G/Rs vs LAI equation for Kimberly, Idaho crops.

For G/Rn	C1	C2	C3
Alfalfa	0	0.2	-0.294
Potato	0.05	0.2	-0.432
Beans	0.07	0.18	-0.96
General	0.050	0.180	-0.521
For G/Rs	C1	C2	C3
Alfalfa	-	-	-
Potato	0.03	0.09	-0.292
Beans	0.04	0.08	-0.85
General	0.041	0.078	-0.537

In table 8-1, for 1973-74 Beans, the original equation which was derived using an average of G_{lys} and G_{field}.

The following graph shows what the general equations look like.

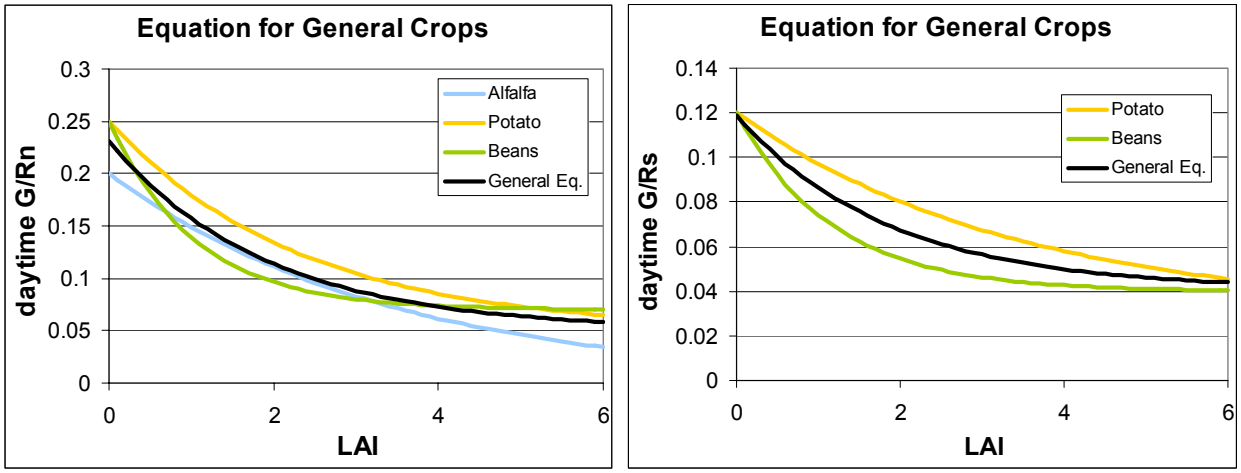

Figure 8.1. G/Rn and G/Rs vs LAI

The G/R_n equations for the three crops shown agreed well with each other and it appears that a general equation can be used for G/R_n for all crops.

Appendix XXX. Evaluation of evaporative fraction.

In the SEBAL-2001 application, ET for 24-hour periods was computed using the ratio to reference evapotranspiration (ET_r) rather than the EF function. This was due to the consistency in $K_c = ET/ET_r$ during daytime periods as compared to the evaporation fraction (EF) (EF = ET / (R_n – G)). The following is an analysis of EF for a bean crop grown at Kimberly on a precision lysimeter system during 1973 by Dr. J.L. Wright of the USDa-ARS.

Previous applications of SEBAL have used the Evaporative Fraction, EF to determine ET_{24}. EF is computed as:

$$EF = \frac{ET}{R_n - G}$$

where R_n is net radiation and G is soil heat flux. ET is evapotranspiration. In SEBAL, 24-hour ET is computed from ET determined at the instant of the satellite image as:

$$ET_{24} = EF\,(R_n - G)_{24} = ET_{inst}\,\frac{(R_n - G)_{24}}{(R_n - G)_{Inst}}$$

The assumption is that R_n – G explains most of the variation in ET during a day. However, as shown during this study, changes in wind speed and/or humidity during the course of a day can change the partitioning of R_n and G into ET and H. It has been determined that use of the ratio $K_c = ET / ET_r$ where ET_r is reference ET computed from ground-based measurements of solar radiation, wind speed, air temperature, and humidity is a more consistent ratio during daytime hours.

The following summarizes an analysis of EF for a season of snap beans during 1973.

2. Method and Limitation

By assuming that EF has a linear relation with time of day, the following items were calculated for each day of the season:

(1) Slope of the regression line of EF vs. time (9am-5pm)
(2) Intercept of the regression line (9am-5pm)
(3) R-square of the regression line (9am-5pm)

All calculations were made statistically, irregardless of weather conditions or irrigation. The following graph shows the EF trend for five days in July when R-squares were higher than 0.9.

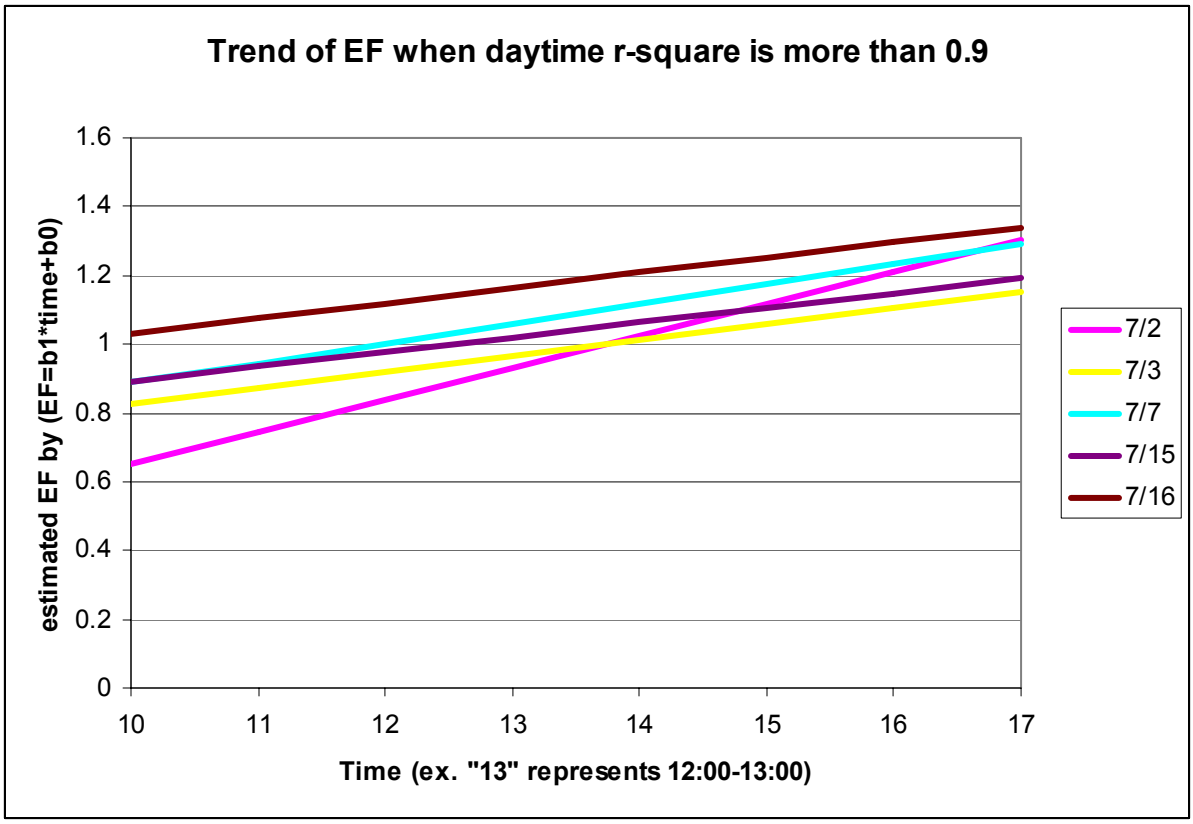

This graph indicates that EF changes during time of day, and that slopes of EF vs. time is similar for most days, but not for all days (7/2). It might be possible to calculate the daily EF using a correction factor, for example, as:

(Daily EF) = (EF at specific time of the day) * (Constant based on the slope)

The following graph shows EF trends when LAI values were small. The two dates had r-square values more than 0.6, slopes were opposite in sign. It appears that wind and humidity factors may impede the use of EF in an arid environment such as southern Idaho.

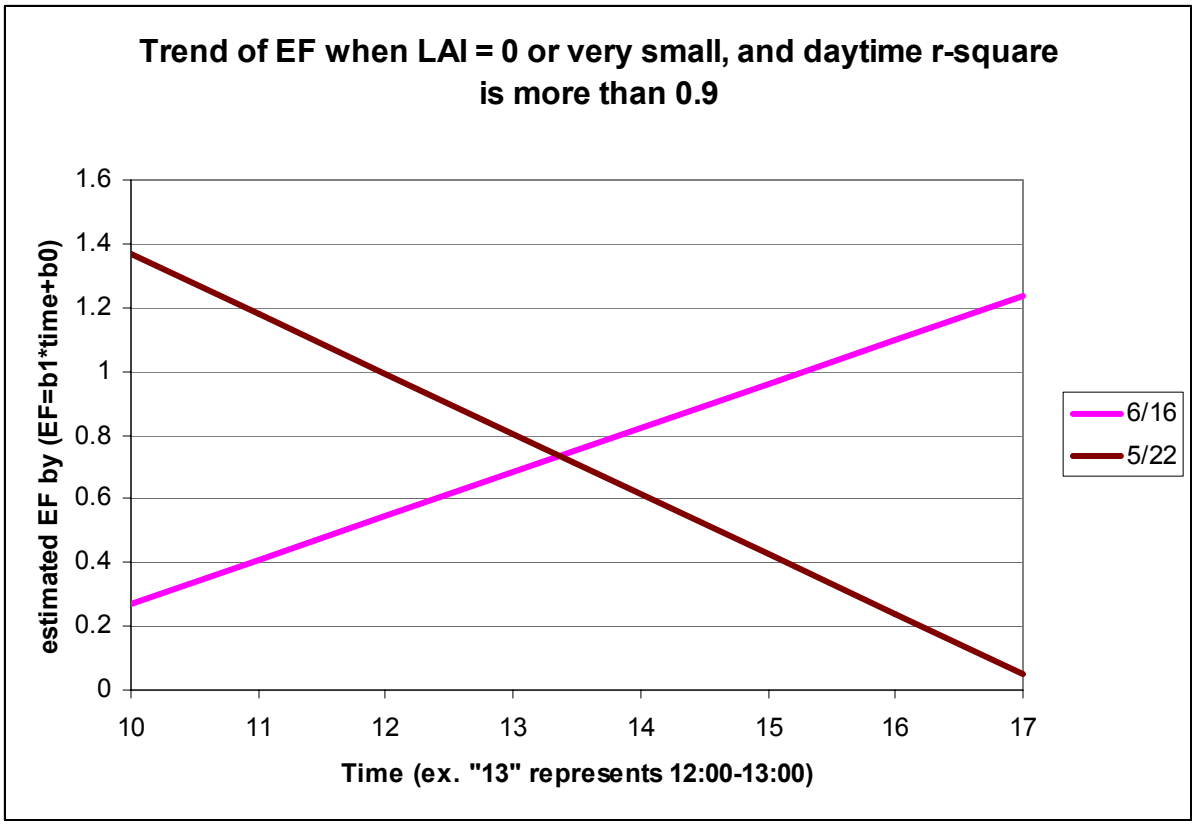
Trend of EF when LAI = 0 or very small, and daytime r-square is more than 0.9
estimated EF by (EF=b1*time+b0)
1.6
1.4
1.2
1
0.8
0.6
0.4
0.2
0
10
11
12
13
14
15
16
17
Time (ex. "13" represents 12:00-13:00)
6/16
5/22

Appendix 3. Determination of a Common Indicator Area Representing ET = 0 for 2000.

This appendix describes an effort to select an area common to both paths 39 and 40 that contains desert vegetaion. This common area was used in SEBAL during summer and fall periods to represent the "hot pixel" in SEBAL, ie. an area where ET can be presumed to be zero so that, from the energy balance, $H = R_n - G$. This allows the "dT" function to be established in SEBAL, where dT is the difference between surface temperature and air temperature.

Sage brush was selected due to its known roughness characteristics and its generally cooler surface temperature as compared to grassed areas of desert.

The following images of bands 2, 3 and 4 from Landsat 7 TM images are coordinated with photographs taken during a field visit (by Allen, Trezza, and Tasumi, in October, 2001). The area visited has latitude / longitude of approximately 42º 57' and 113º 44' and is located northwest of Rupert, Idaho.

A. The selected location (sage brush) for the "hot pixel" for late summer – fall:
(Lat / Long = 42 57 34/113 44 30 , x / y = 521062/206559)

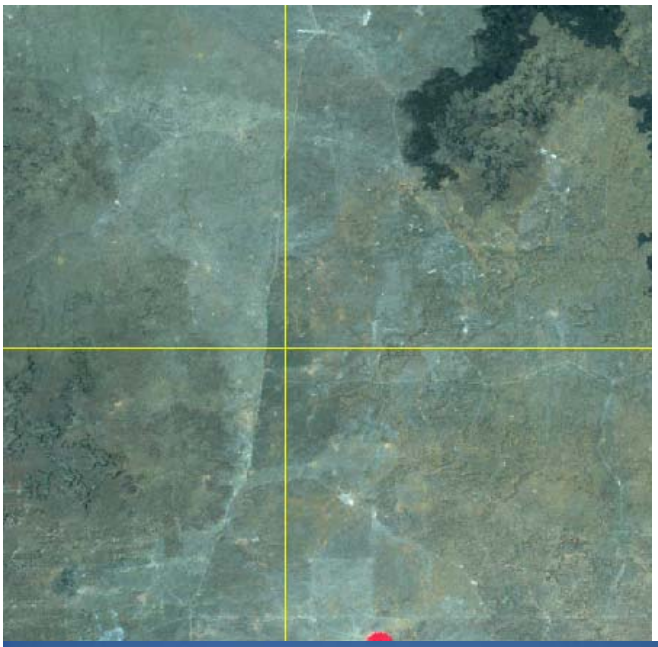

The lighter area to the left of the sagebrush is mostly grassland. The dark area to the northeast is a basalt flow having little or no vegetation.

B. Other information

Other locations having sage brush are shown in the following images/photographs, and were used to confirm accuracy of a land classification of both paths. The red colors represent well-watered, green vegetation (irrigated agriculture).

1. Sage Brush (42 46 35/113 50 44) Pic#0935
Original description: S&W of road 42 46 42.83/ 113 50 37.81

2. Dense Sage (42 46 45/ 113 51 39) Pic#0937
Original description: S&W of 42 46 43.08/ 113 51 35.98, very dense sage

3. Grass (42 48 43/ 113 49 43) Pic#0938
Original description: N of 42 48 40.06/ 113 49 42.16, for 1*1 mile

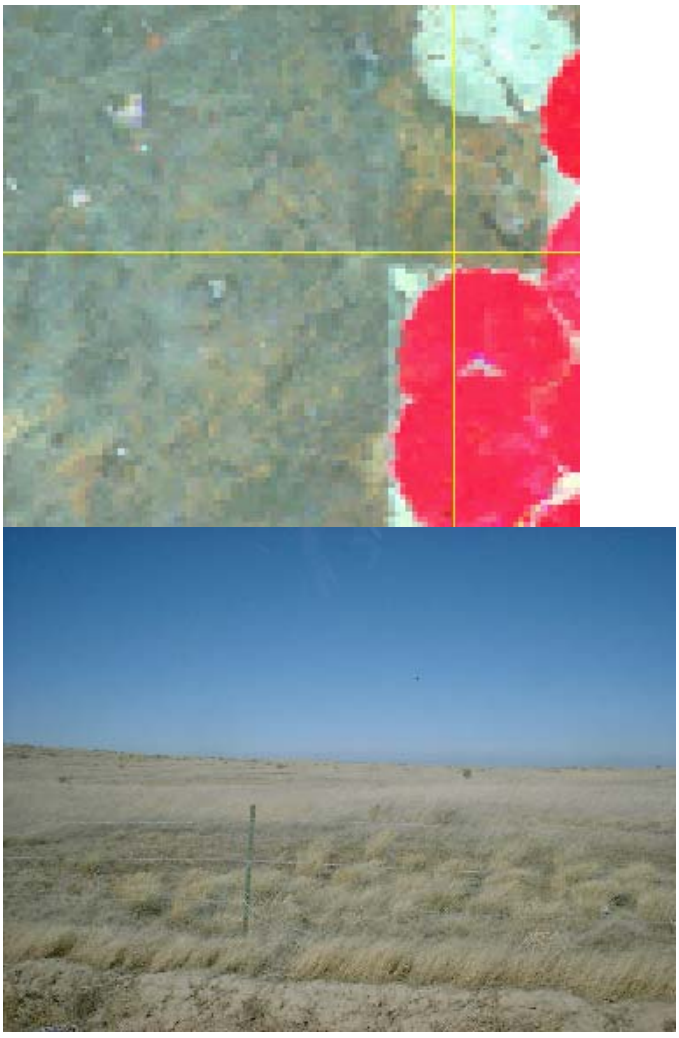

4. Grass (42 51 50/ 113 50 56) Pic#0939
Original description: No1 is tall, grass bush.

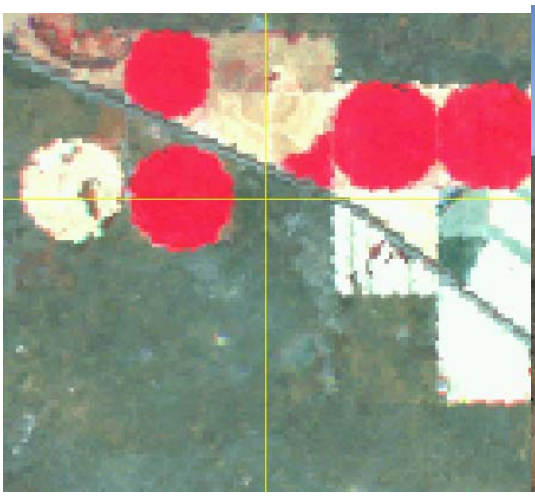

Appendix 4. Hourly Crop Coefficients and 24-hour Average Coefficients for Satellite Image Dates during 1989.

The following figures show hourly K_c ($K_c = ET_{lysimeter}/ET_r$) along with measured lsyimeter ET and reference ET determined for alfalfa (ET_r) and grass (ET_o) references. The K_c was based on ET_r. The first set of figures show K_c for grass during 1989. For nearly all dates and for both crop s (grass and sugar beets), $K_{c\ 24}$ is quite close to K_c 1100·

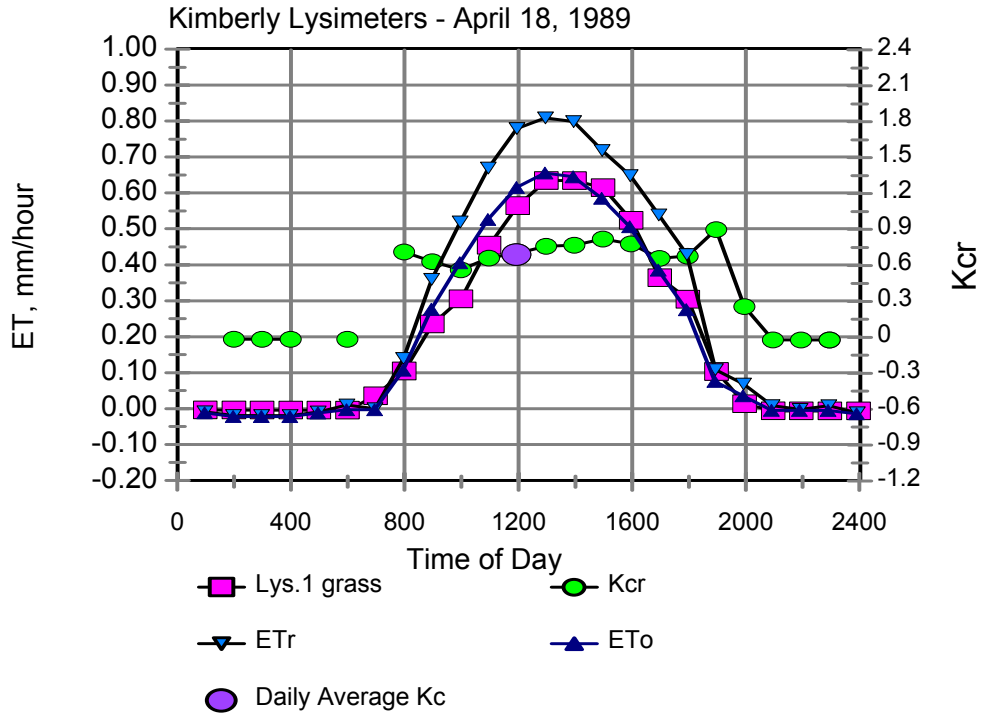
Kimberly Lysimeters - April 18, 1989
ET, mm/hour
Kcr
1.00
0.90
0.80
0.70
0.60
0.50
0.40
0.30
0.20
0.10
0.00
-0.10
-0.20
2.4
2.1
1.8
1.5
1.2
0.9
0.6
0.3
0
-0.3
-0.6
-0.9
-1.2
0
400
800
1200
1600
2000
2400
Time of Day
Lys.1 grass
Kcr
ETr
ETo
Daily Average Kc

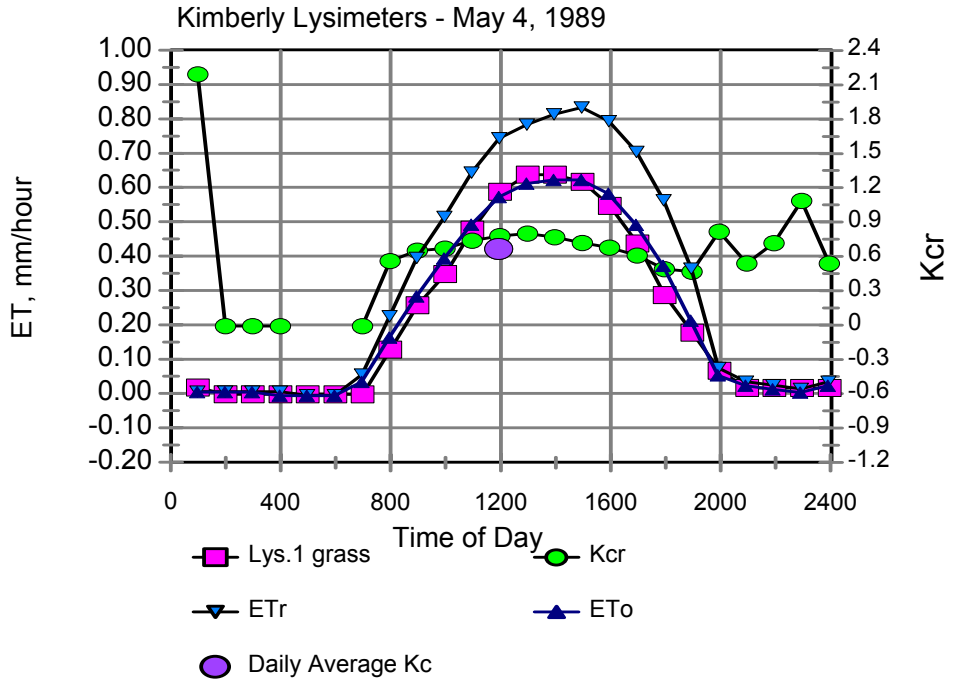
Kimberly Lysimeters - May 4, 1989
ET, mm/hour
Kcr
1.00
0.90
0.80
0.70
0.60
0.50
0.40
0.30
0.20
0.10
0.00
-0.10
-0.20
2.4
2.1
1.8
1.5
1.2
0.9
0.6
0.3
0
-0.3
-0.6
-0.9
-1.2
0
400
800
1200
1600
2000
2400
Time of Day
Lys.1 grass
Kcr
ETr
ETo
Daily Average Kc

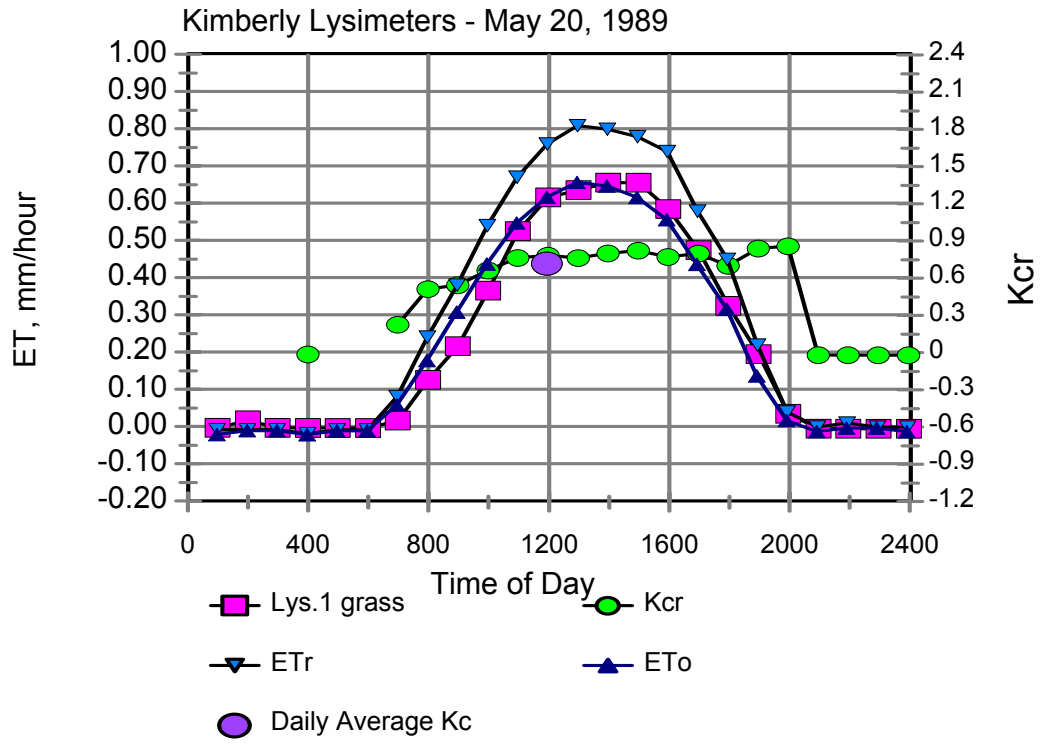
Kimberly Lysimeters - May 20, 1989
ET, mm/hour
Kcr
1.00
0.90
0.80
0.70
0.60
0.50
0.40
0.30
0.20
0.10
0.00
-0.10
-0.20
2.4
2.1
1.8
1.5
1.2
0.9
0.6
0.3
0
-0.3
-0.6
-0.9
-1.2
0
400
800
1200
1600
2000
2400
Time of Day
Lys.1 grass
Kcr
ETr
ETo
Daily Average Kc

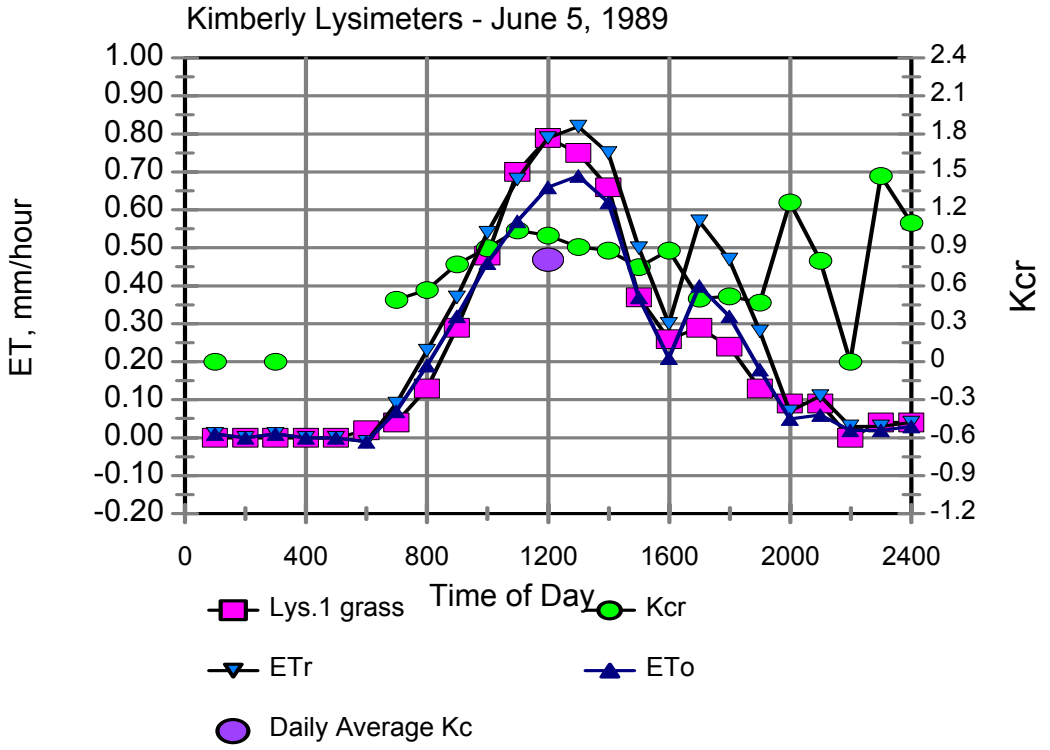
Kimberly Lysimeters - June 5, 1989
ET, mm/hour
Kcr
1.00
0.90
0.80
0.70
0.60
0.50
0.40
0.30
0.20
0.10
0.00
-0.10
-0.20
2.4
2.1
1.8
1.5
1.2
0.9
0.6
0.3
0
-0.3
-0.6
-0.9
-1.2
0
400
800
1200
1600
2000
2400
Time of Day
Lys.1 grass
Kcr
ETr
ETo
Daily Average Kc

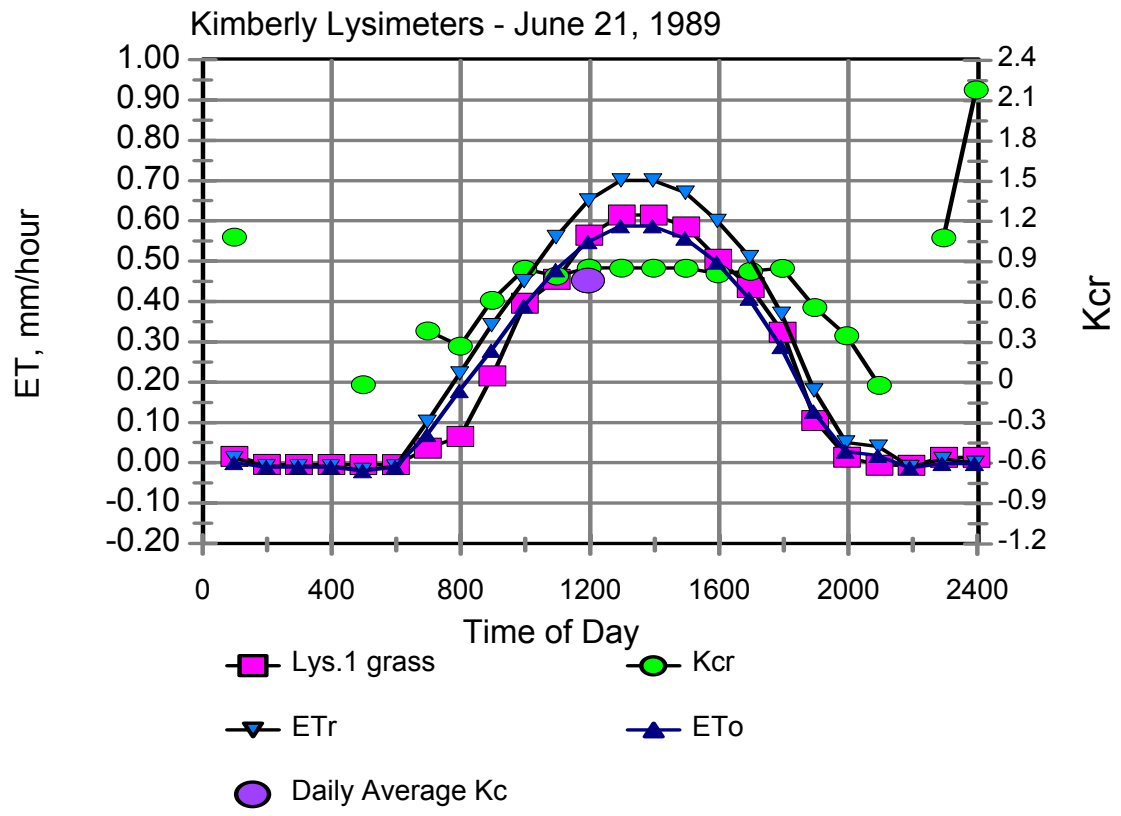
Kimberly Lysimeters - June 21, 1989
ET, mm/hour
Kcr
1.00
0.90
0.80
0.70
0.60
0.50
0.40
0.30
0.20
0.10
0.00
-0.10
-0.20
2.4
2.1
1.8
1.5
1.2
0.9
0.6
0.3
0
-0.3
-0.6
-0.9
-1.2
0
400
800
1200
1600
2000
2400
Time of Day
Lys.1 grass
Kcr
ETr
ETo
Daily Average Kc

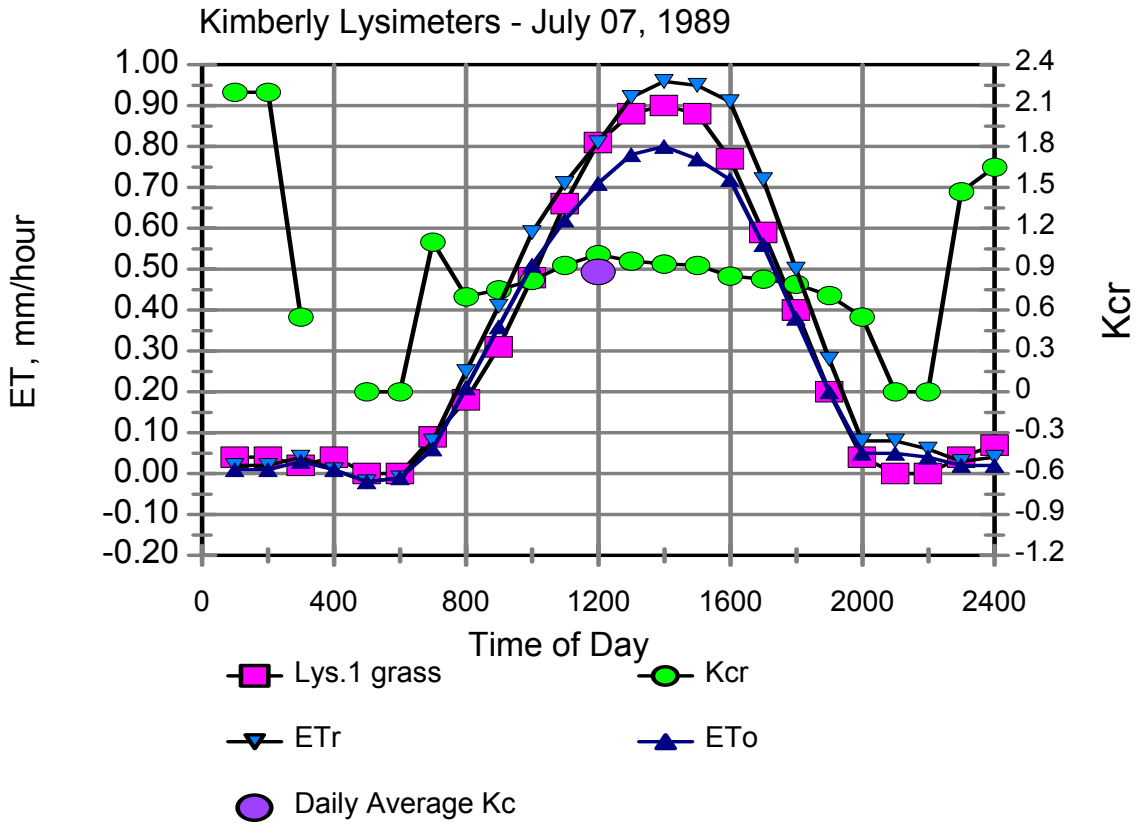
Kimberly Lysimeters - July 07, 1989
ET, mm/hour
Kcr
1.00
0.90
0.80
0.70
0.60
0.50
0.40
0.30
0.20
0.10
0.00
-0.10
-0.20
2.4
2.1
1.8
1.5
1.2
0.9
0.6
0.3
0
-0.3
-0.6
-0.9
-1.2
0
400
800
1200
1600
2000
2400
Time of Day
Lys.1 grass
Kcr
ETr
ETo
Daily Average Kc

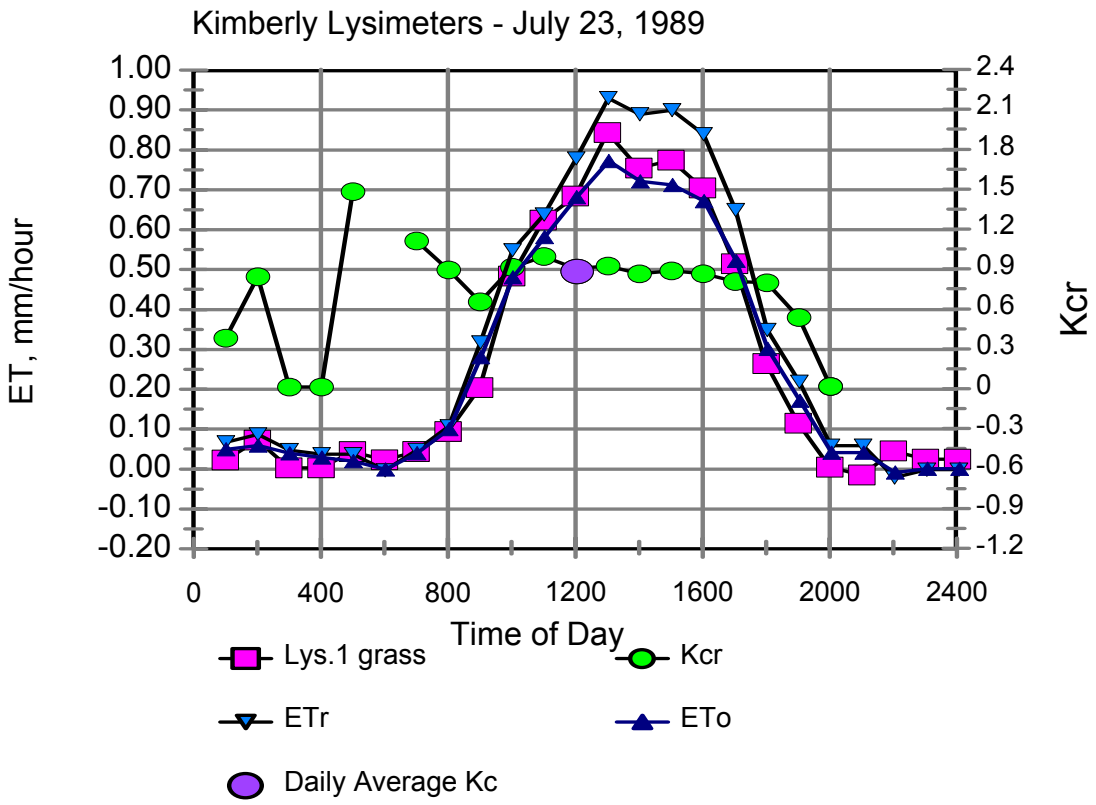
Kimberly Lysimeters - July 23, 1989
ET, mm/hour
Kcr
1.00
0.90
0.80
0.70
0.60
0.50
0.40
0.30
0.20
0.10
0.00
-0.10
-0.20
2.4
2.1
1.8
1.5
1.2
0.9
0.6
0.3
0
-0.3
-0.6
-0.9
-1.2
0
400
800
1200
1600
2000
2400
Time of Day
Lys.1 grass
Kcr
ETr
ETo
Daily Average Kc

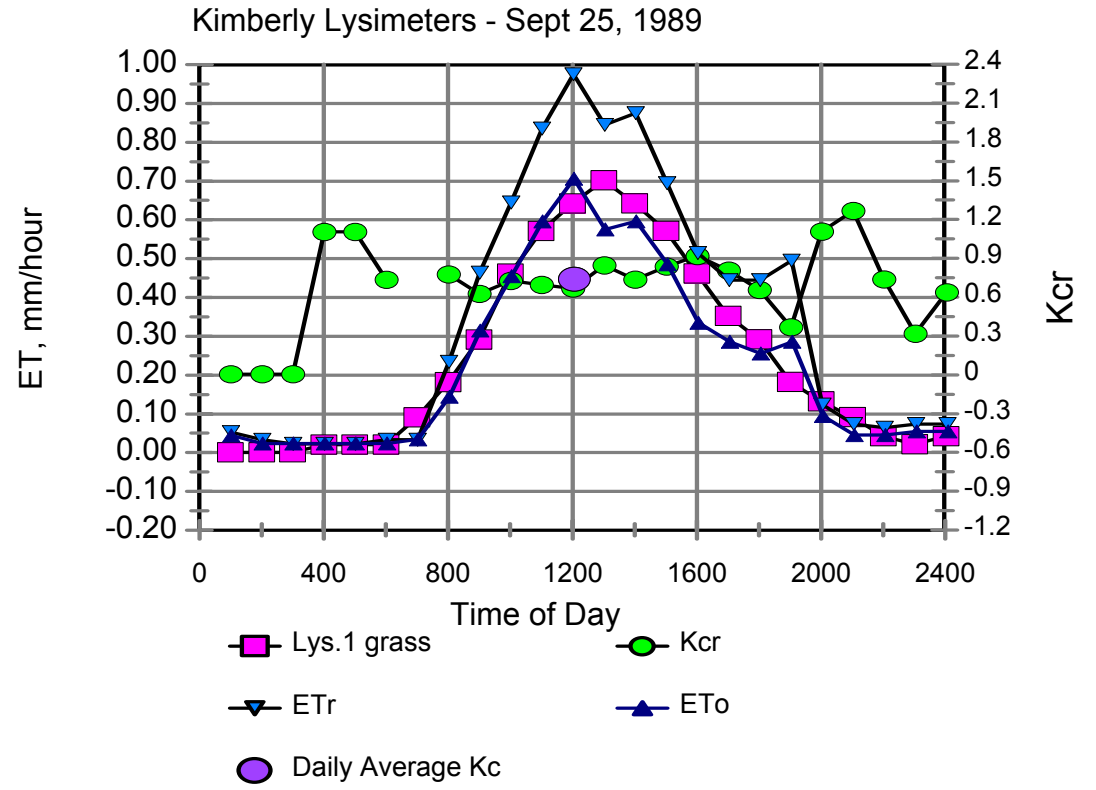
Kimberly Lysimeters - Sept 25, 1989
ET, mm/hour
Kcr
1.00
0.90
0.80
0.70
0.60
0.50
0.40
0.30
0.20
0.10
0.00
-0.10
-0.20
2.4
2.1
1.8
1.5
1.2
0.9
0.6
0.3
0
-0.3
-0.6
-0.9
-1.2
0
400
800
1200
1600
2000
2400
Time of Day
Lys.1 grass
Kcr
ETr
ETo
Daily Average Kc

The next set of graphs are for the same dates, but for a crop of sugar beets.

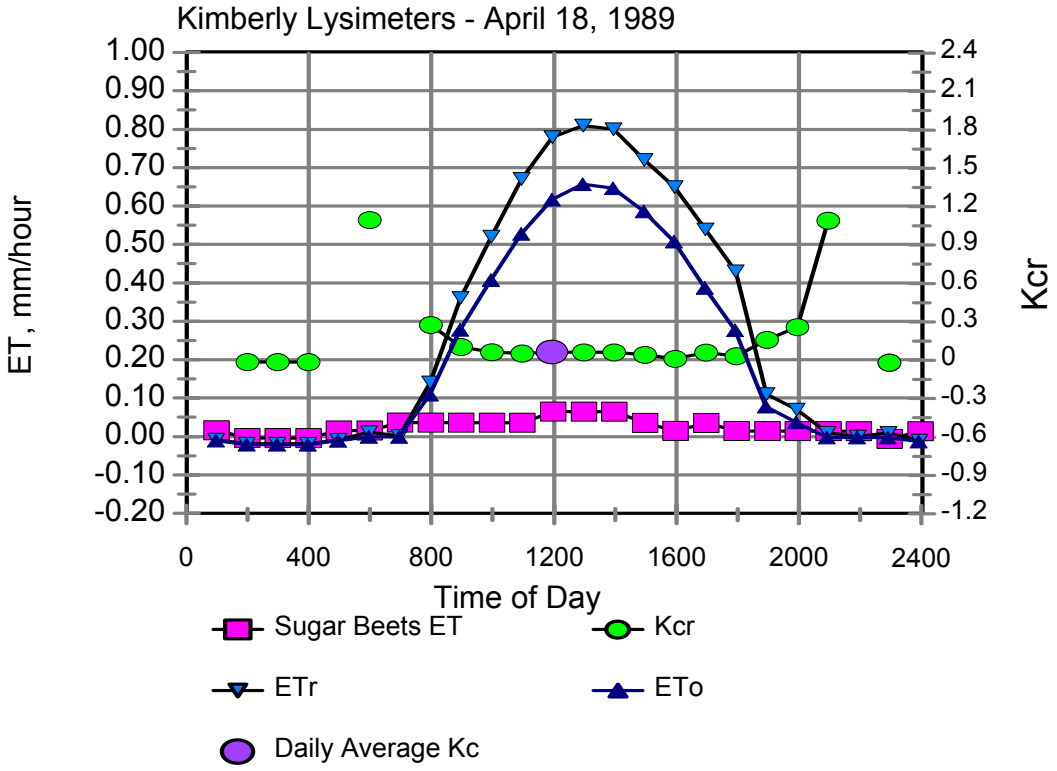

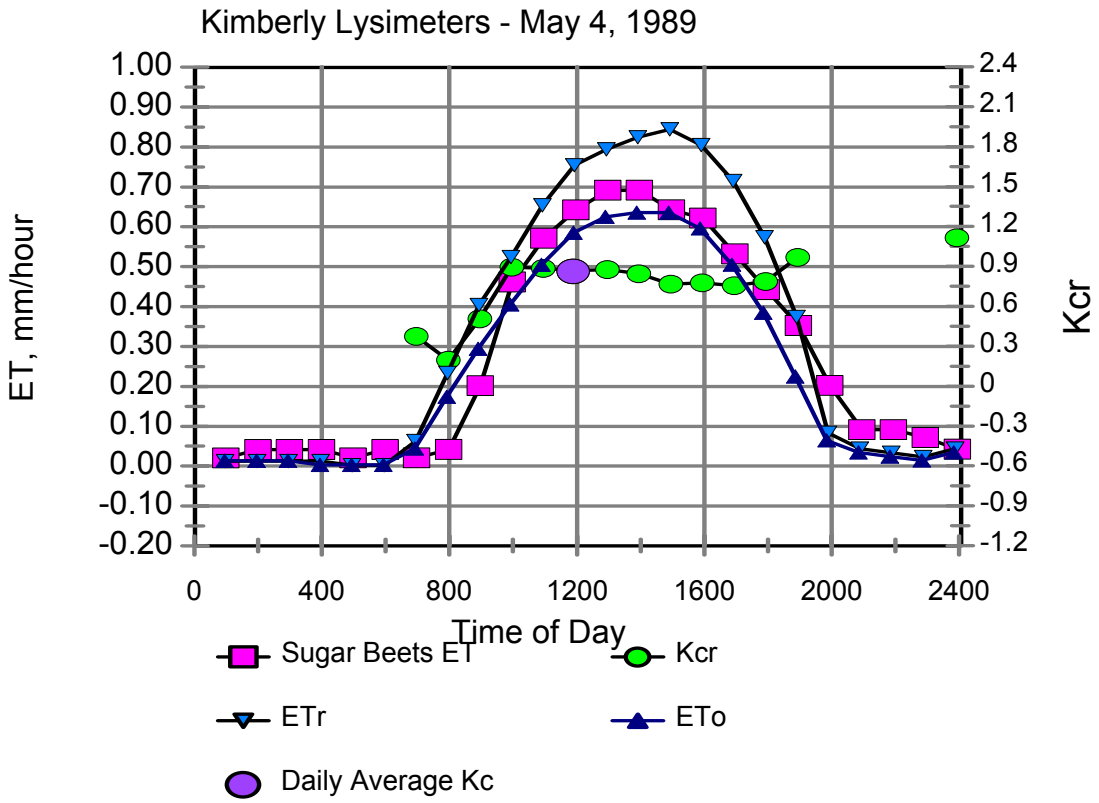

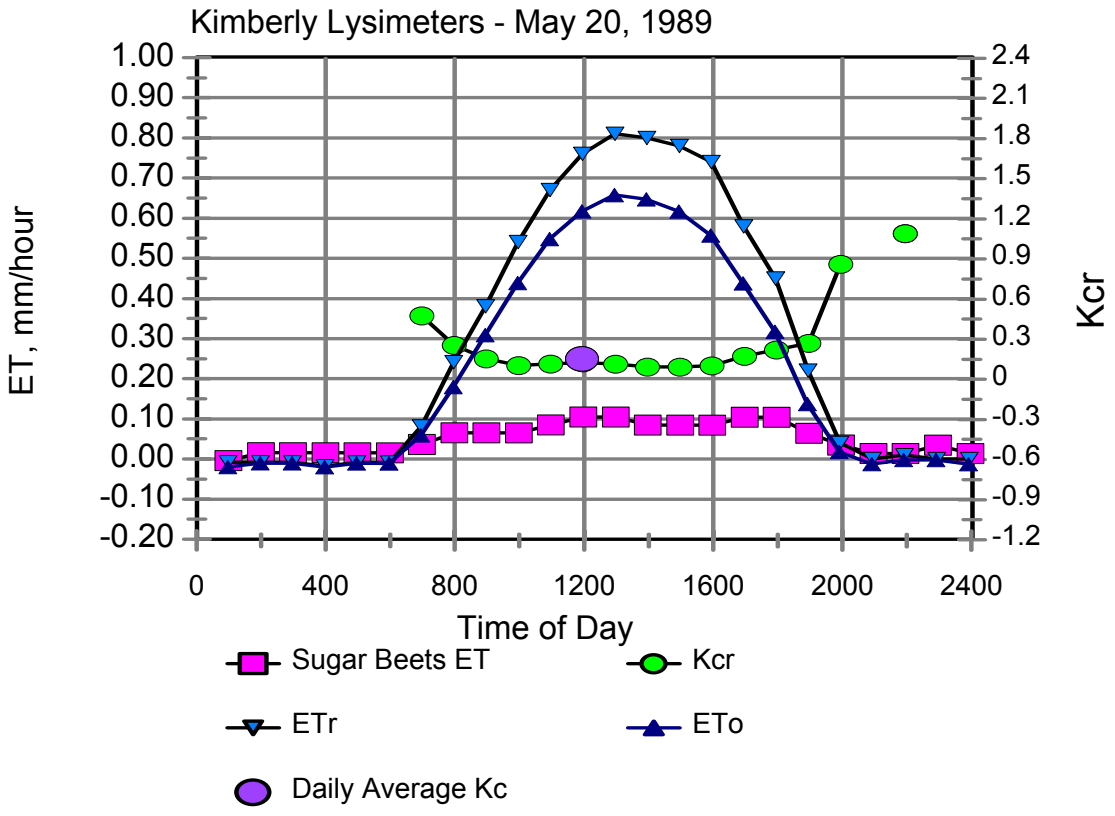
Kimberly Lysimeters - May 20, 1989
ET, mm/hour
Kcr
1.00
0.90
0.80
0.70
0.60
0.50
0.40
0.30
0.20
0.10
0.00
-0.10
-0.20
2.4
2.1
1.8
1.5
1.2
0.9
0.6
0.3
0
-0.3
-0.6
-0.9
-1.2
0
400
800
1200
1600
2000
2400
Time of Day
Sugar Beets ET
Kcr
ETr
ETo
Daily Average Kc

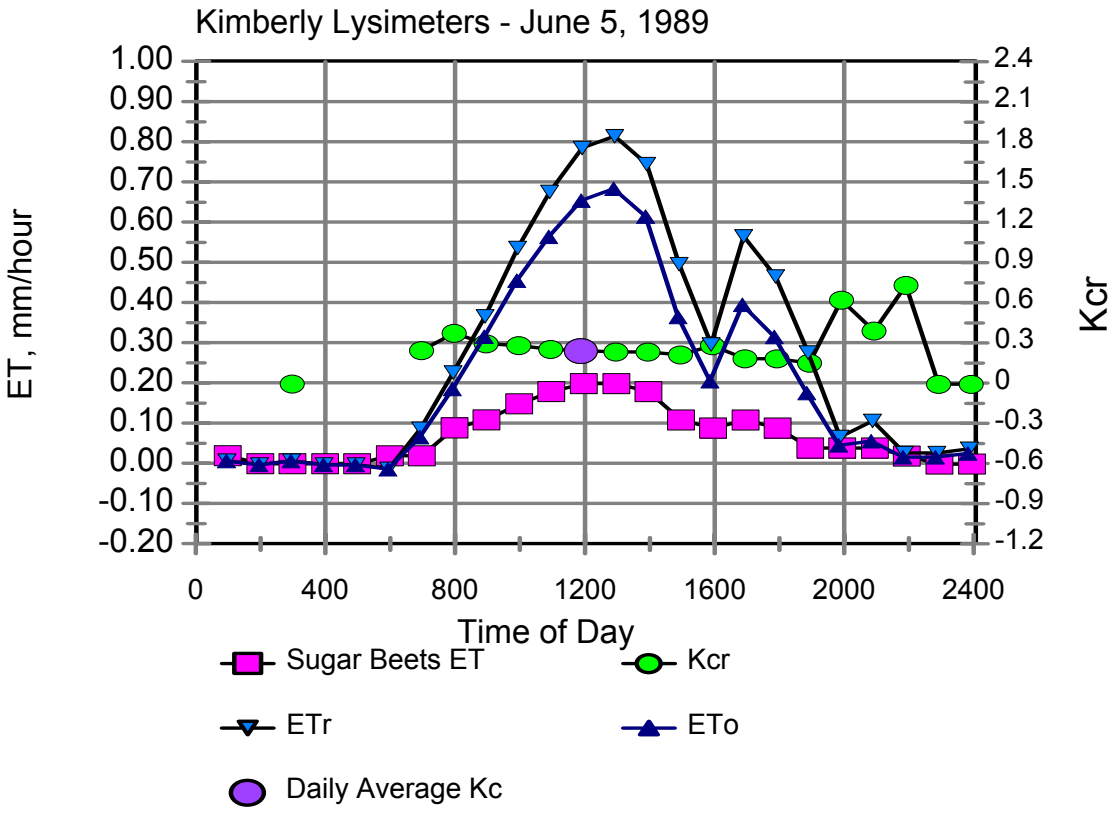
Kimberly Lysimeters - June 5, 1989
ET, mm/hour
Kcr
1.00
0.90
0.80
0.70
0.60
0.50
0.40
0.30
0.20
0.10
0.00
-0.10
-0.20
2.4
2.1
1.8
1.5
1.2
0.9
0.6
0.3
0
-0.3
-0.6
-0.9
-1.2
0
400
800
1200
1600
2000
2400
Time of Day
Sugar Beets ET
Kcr
ETr
ETo
Daily Average Kc

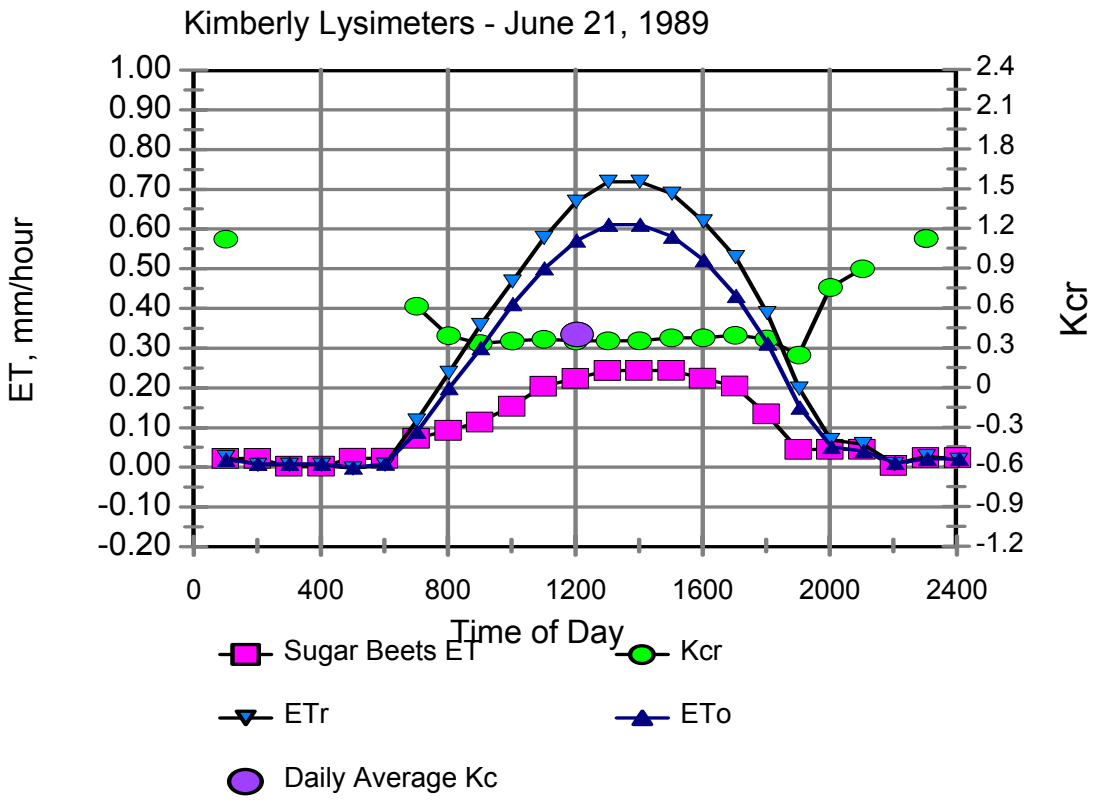
Kimberly Lysimeters - June 21, 1989
ET, mm/hour
Kcr
1.00
0.90
0.80
0.70
0.60
0.50
0.40
0.30
0.20
0.10
0.00
-0.10
-0.20
2.4
2.1
1.8
1.5
1.2
0.9
0.6
0.3
0
-0.3
-0.6
-0.9
-1.2
0
400
800
1200
1600
2000
2400
Time of Day
Sugar Beets ET
Kcr
ETr
ETo
Daily Average Kc

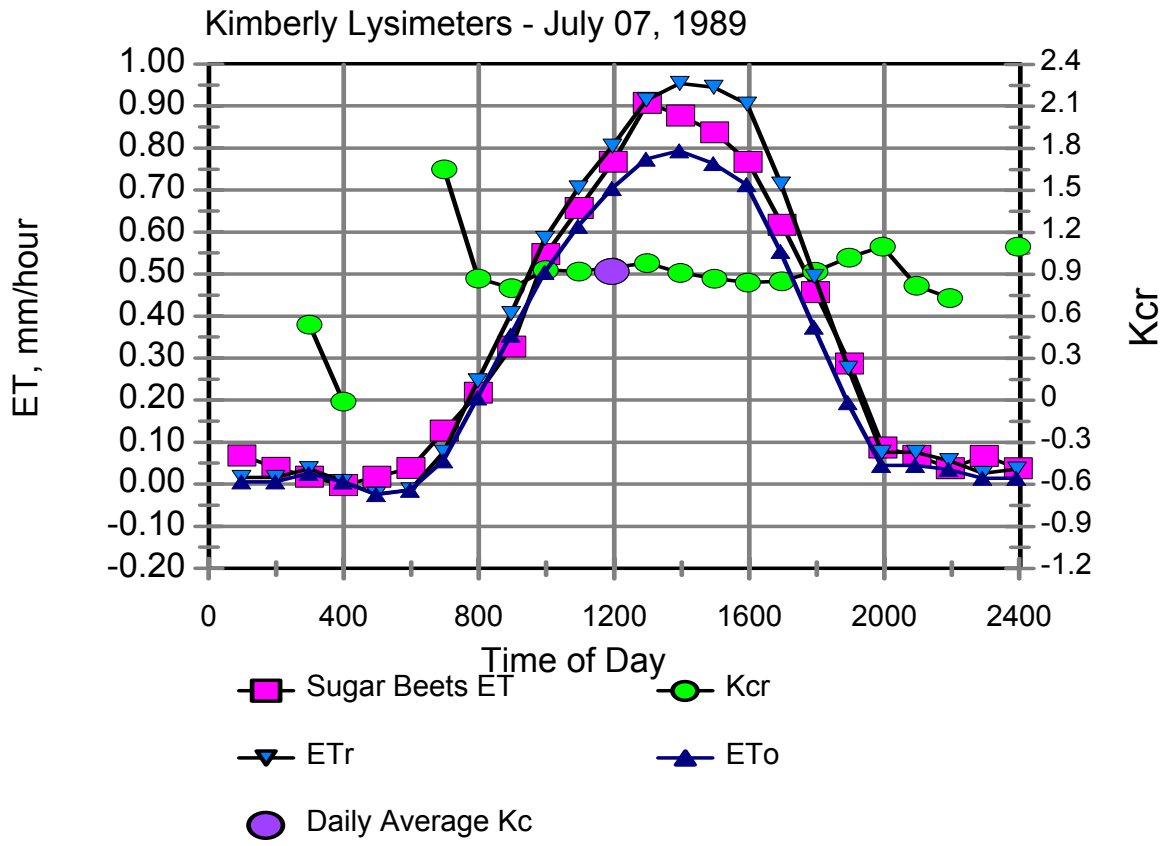
Kimberly Lysimeters - July 07, 1989
ET, mm/hour
Kcr
1.00
0.90
0.80
0.70
0.60
0.50
0.40
0.30
0.20
0.10
0.00
-0.10
-0.20
2.4
2.1
1.8
1.5
1.2
0.9
0.6
0.3
0
-0.3
-0.6
-0.9
-1.2
0
400
800
1200
1600
2000
2400
Time of Day
Sugar Beets ET
Kcr
ETr
ETo
Daily Average Kc

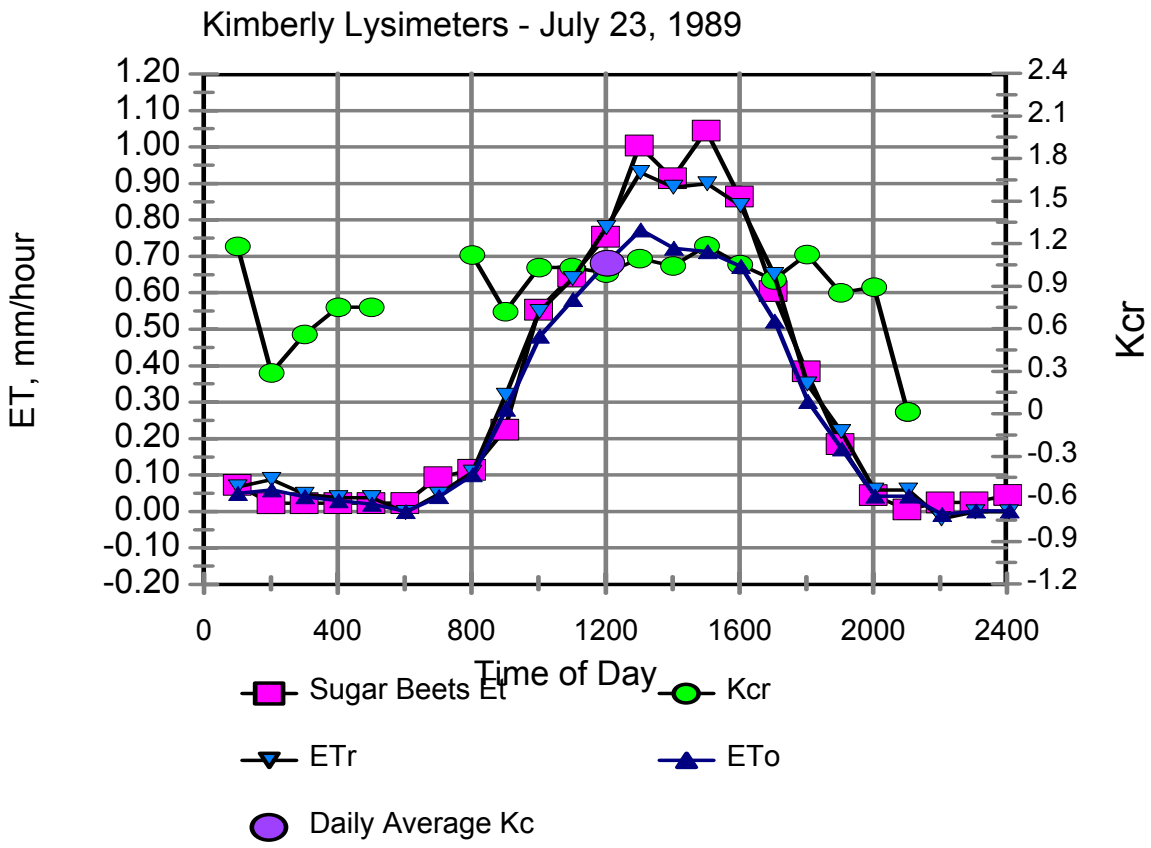
Kimberly Lysimeters - July 23, 1989
ET, mm/hour
Kcr
1.20
1.10
1.00
0.90
0.80
0.70
0.60
0.50
0.40
0.30
0.20
0.10
0.00
-0.10
-0.20
2.4
2.1
1.8
1.5
1.2
0.9
0.6
0.3
0
-0.3
-0.6
-0.9
-1.2
0
400
800
1200
1600
2000
2400
Time of Day
Sugar Beets Et
Kcr
ETr
ETo
Daily Average Kc

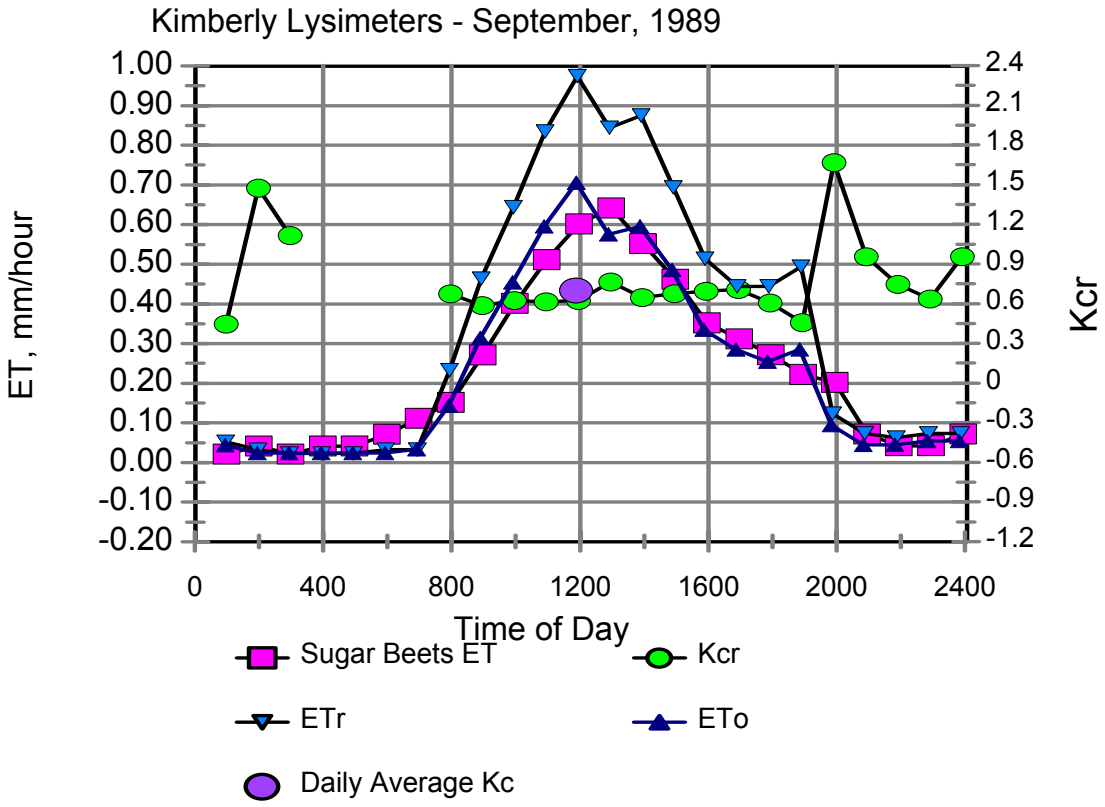
Kimberly Lysimeters - September, 1989
ET, mm/hour
Kcr
1.00
0.90
0.80
0.70
0.60
0.50
0.40
0.30
0.20
0.10
0.00
-0.10
-0.20
2.4
2.1
1.8
1.5
1.2
0.9
0.6
0.3
0
-0.3
-0.6
-0.9
-1.2
0
400
800
1200
1600
2000
2400
Time of Day
Sugar Beets ET
Kcr
ETr
ETo
Daily Average Kc

The following figure shows hourly and 24-hour K_c for a crop of potatoes during 1988, for a satellite image date.

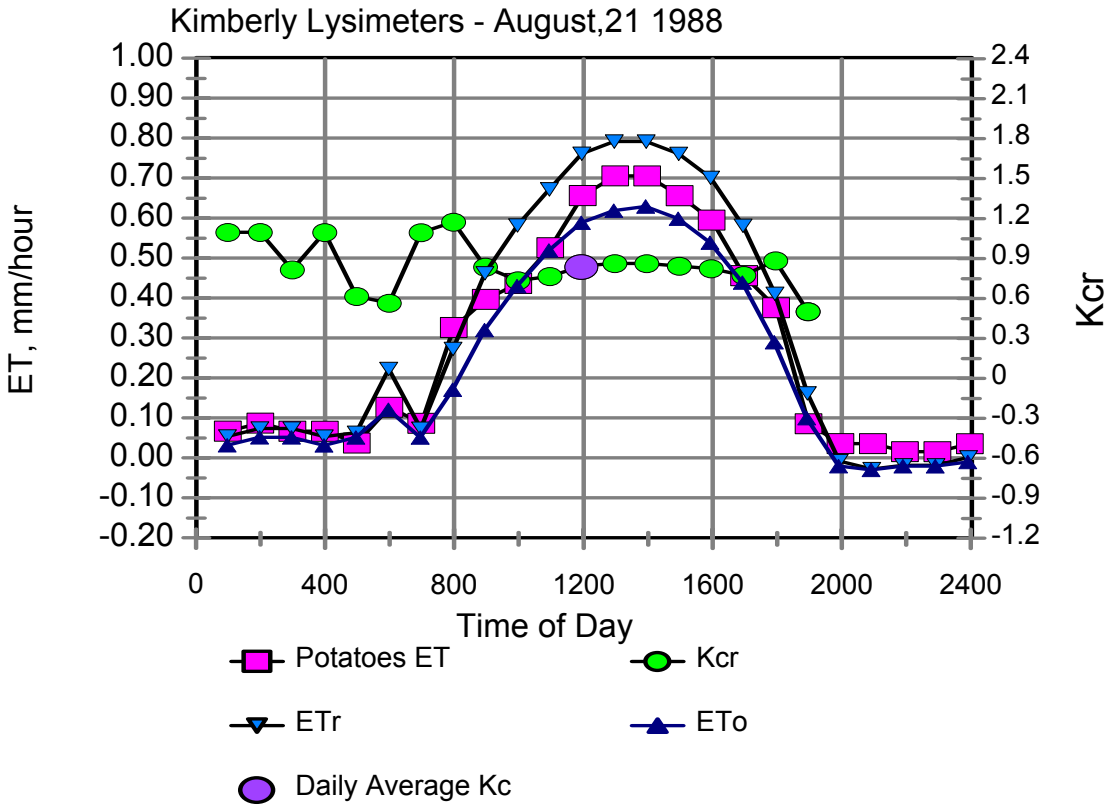

Appendix 5. Evaluation of evaporative fraction.

In the SEBAL-2001 application, ET for 24-hour periods was computed using the ratio to reference evapotranspiration (ET_r) rather than the EF function. This was due to the consistency in $K_c = ET/ET_r$ during daytime periods as compared to the evaporation fraction (EF) ($EF = ET / (R_n - G)$). The following is an analysis of EF for a bean crop grown at Kimberly on a precision lysimeter system during 1973 by Dr. J.L. Wright of the USDa-ARS.

Previous applications of SEBAL have used the Evaporative Fraction, EF to determine ET_{24}. EF is computed as:

$$EF = \frac{ET}{R_n - G}$$

where R_n is net radiation and G is soil heat flux. ET is evapotranspiration. In SEBAL, 24-hour ET is computed from ET determined at the instant of the satellite image as:

$$ET_{24} = EF\,(R_n - G)_{24} = ET_{inst}\,\frac{(R_n - G)_{24}}{(R_n - G)_{Inst}}$$

The assumption is that $R_n - G$ explains most of the variation in ET during a day. However, as shown during this study, changes in wind speed and/or humidity during the course of a day can change the partitioning of R_n and G into ET and H. It has been determined that use of the ratio $K_c = ET / ET_r$ where ET_r is reference ET computed from ground-based measurements of solar radiation, wind speed, air temperature, and humidity is a more consistent ratio during daytime hours.

The following summarizes an analysis of EF for a season of snap beans during 1973.

2. Method and Limitation

By assuming that EF has a linear relation with time of day, the following items were calculated for each day of the season:

(1) Slope of the regression line of EF vs. time (9am-5pm)
(2) Intercept of the regression line (9am-5pm)
(3) R-square of the regression line (9am-5pm)

All calculations were made statistically, irregardless of weather conditions or irrigation. The following graph shows the EF trend for five days in July when R-squares were higher than 0.9.

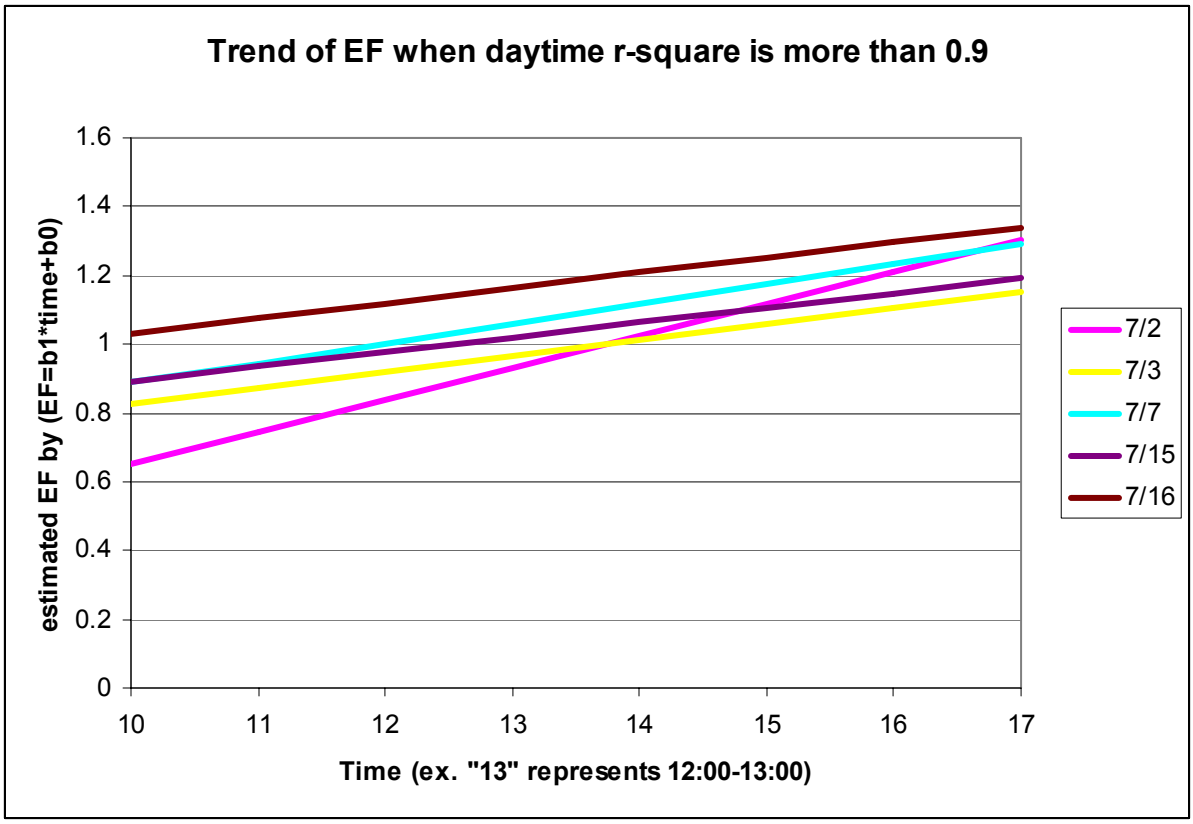

This graph indicates that EF changes during time of day, and that slopes of EF vs. time is similar for most days, but not for all days (7/2). It might be possible to calculate the daily EF using a correction factor, for example, as:

(Daily EF) = (EF at specific time of the day) * (Constant based on the slope)

The following graph shows EF trends when LAI values were small. The two dates had r-square values more than 0.6, slopes were opposite in sign. It appears that wind and humidity factors may impede the use of EF in an arid environment such as southern Idaho.

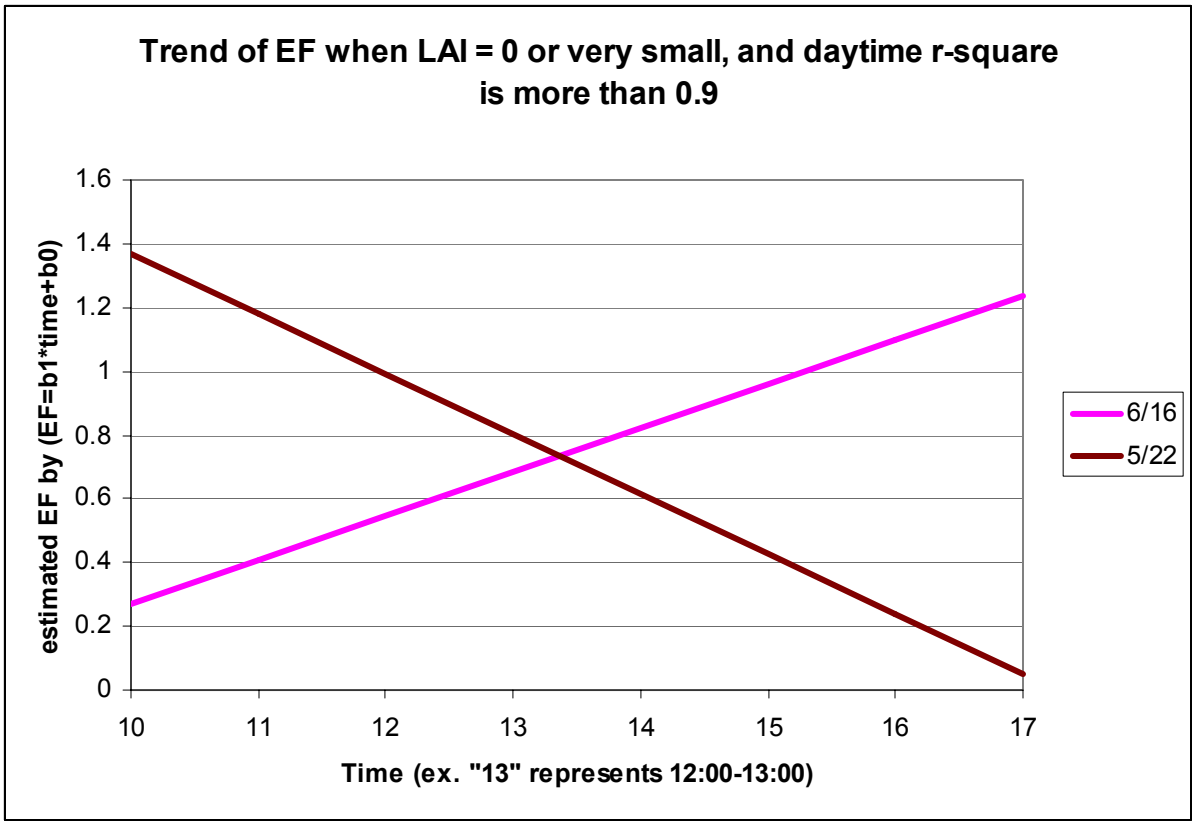
Trend of EF when LAI = 0 or very small, and daytime r-square is more than 0.9
estimated EF by (EF=b1*time+b0)
1.6
1.4
1.2
1
0.8
0.6
0.4
0.2
0
10
11
12
13
14
15
16
17
Time (ex. "13" represents 12:00-13:00)
6/16
5/22

Appendix 6. Development of the SAVI index for predicting LAI for Soil Heat Flux and Aerodynamic Roughness

1. Equations

The equation of the soil adjusted vegetation index (SAVI) is;

$$SAVI = \frac{(1+L)(R4-R3)}{(R4+R3+L)}$$

where, R3 is reflectance of band3, R4 is reflectance of band4, and L is a constant. Analysis for Kimberly images during 1986-1991 indicated that using L = 0.1 eliminated the effect of soil background in the Kimberly area.

The normalized difference vegetation index, NDVI, is calculated as;

$$NDVI = \frac{R4-R3}{R4+R3}$$

Generally, SAVI is applied using L = 0.5, so that SAVI is calculated as;

$$SAVI = \frac{1.5(R4-R3)}{R4+R3+0.5}$$

2. Evaluation for the Lysimeter fields

The Lysimeter 1 and 2 fields are located inside of the white rectangle in the false-colored picture to the right for 07/07/89. We selected 6 pixels for each field as being "representative" pixels for the field.

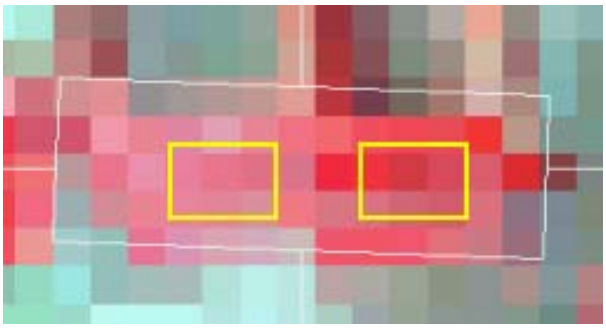

The following graphs show the average values for calculated NDVI, SAVI and LAI values for each field. In 1989, the Lys1 field was grass, and the Lys2 field was sugar beets. The grass field was narrow during this year due to planting of alfalfa in the north edge and sugar beets along the south edge.

A preliminary LAI was computed using a general SAVI-LAI relationship (average for many crops):

$$LAI = -\frac{\ln\left(\frac{0.69-SAVI}{0.59}\right)}{0.91}$$

from Bastiaanssen (1996).

Of course, SAVI-LAI equation depends on the crop type. Therefore, we can estimate more accurate LAI from TM image only by combination of a landuse map and a SAVI-LAI relationship for each crop type. The SAVI in the following figures was applied using L = 0.5.

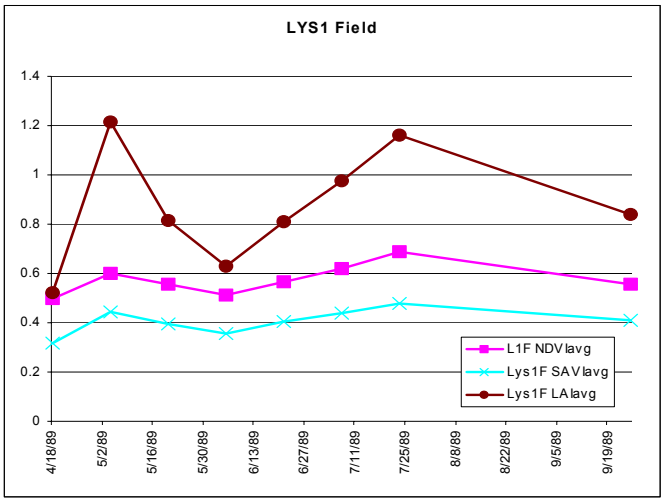

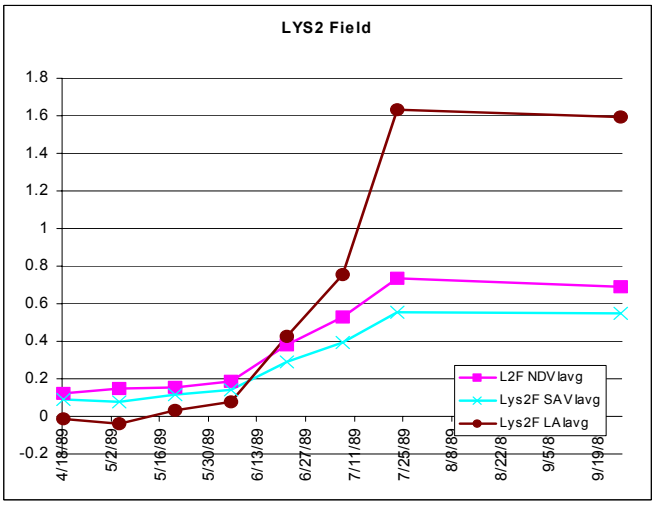

The following graphs show the variation of NDVI and SAVI for each pixel from the Lys1 and Lys2 fields.

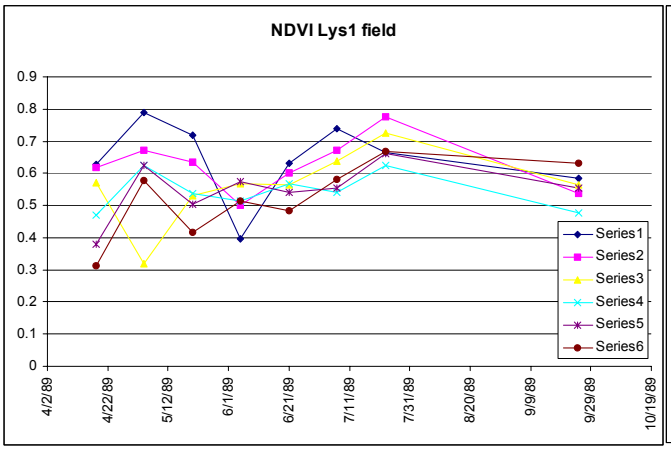

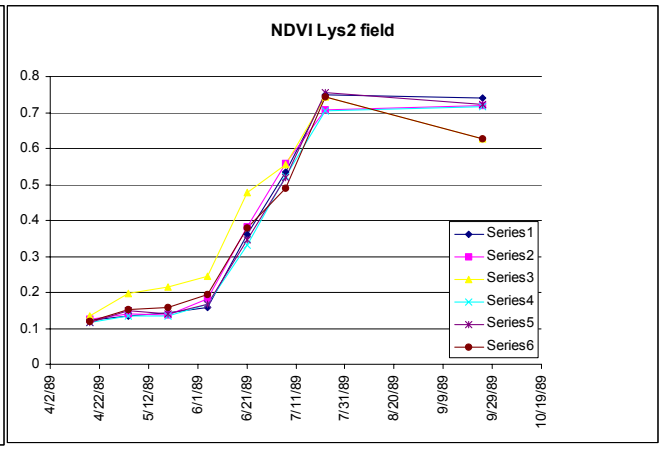

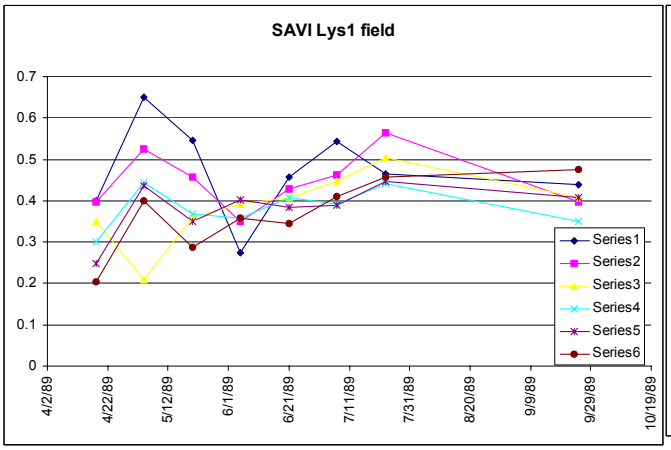

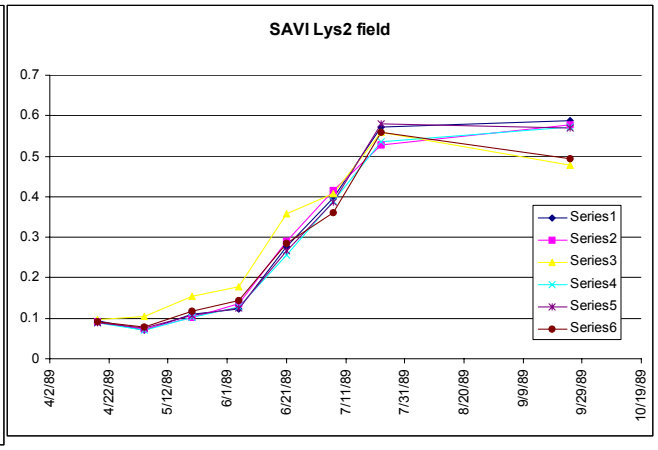

It is obvious that Lys1 field did not have “stable” NDVI and SAVI values with time (possibly due to cutting effects) while Lys2 field showed “stable” increasing values with time for 1989.

3. Center Pivot fields

The following are examples of indices derived for a center pivot irrigated area. Every example shows the values from one pixel. SAVI was applied using L = 0.5.

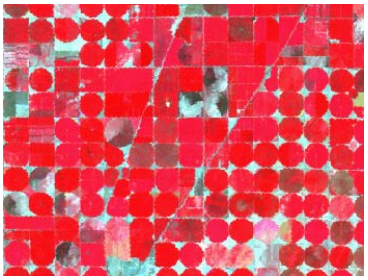

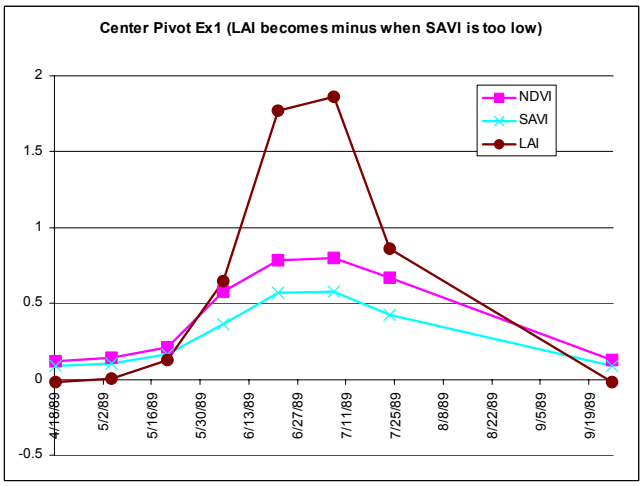

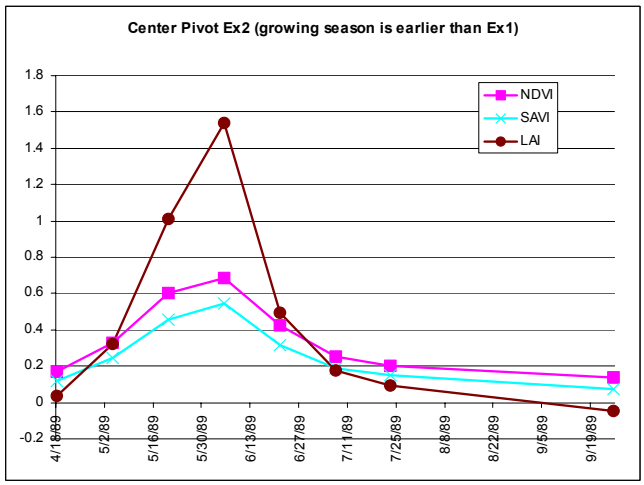

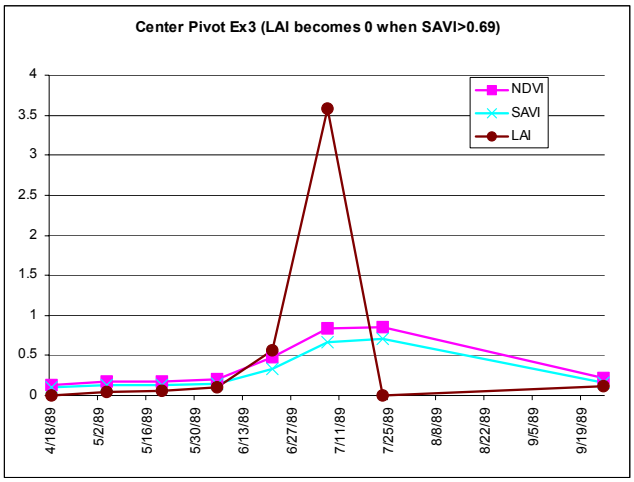

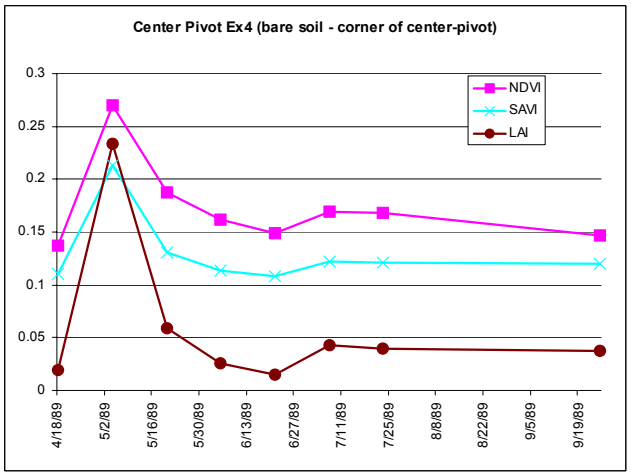

As shown in the example 3 above, the computed LAI value exhibited strange behavior when the SAVI was extremely high. The equation used for calculating LAI would not be appropriate for the specific crop.

4. Desert

The following example shows NDVI-SAVI-LAI in a desert area. The value is an average value for 40 pixels.

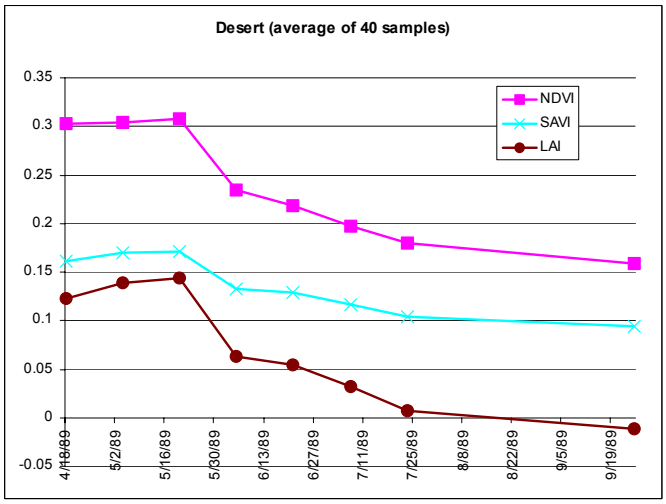

5. NDVI vs SAVI

The following two graphs show the NDVI and SAVI values calculated by same equations shown above using data from the literature based on reflectances of Visible and NIR for two types of vegetation.

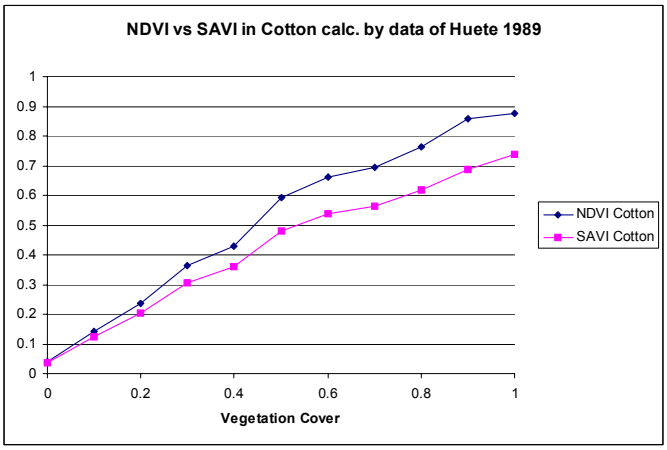
NDVI vs SAVI in Cotton calc. by data of Huete 1989
1
0.9
0.8
0.7
0.6
0.5
0.4
0.3
0.2
0.1
0
0
0.2
0.4
0.6
0.8
1
Vegetation Cover
NDVI Cotton
SAVI Cotton

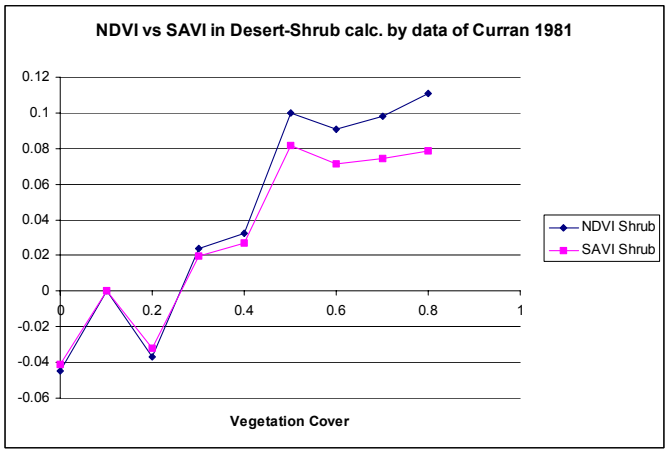
NDVI vs SAVI in Desert-Shrub calc. by data of Curran 1981
0.12
0.1
0.08
0.06
0.04
0.02
0
-0.02
-0.04
-0.06
0
0.2
0.4
0.6
0.8
1
Vegetation Cover
NDVI Shrub
SAVI Shrub

Evaluation of Values for L

Many remote sensing studies have applied L=0.5. When L=0, SAVI becomes NDVI.

The following graph shows calculated SAVI for Lys2 field in 1989 for various values for L.

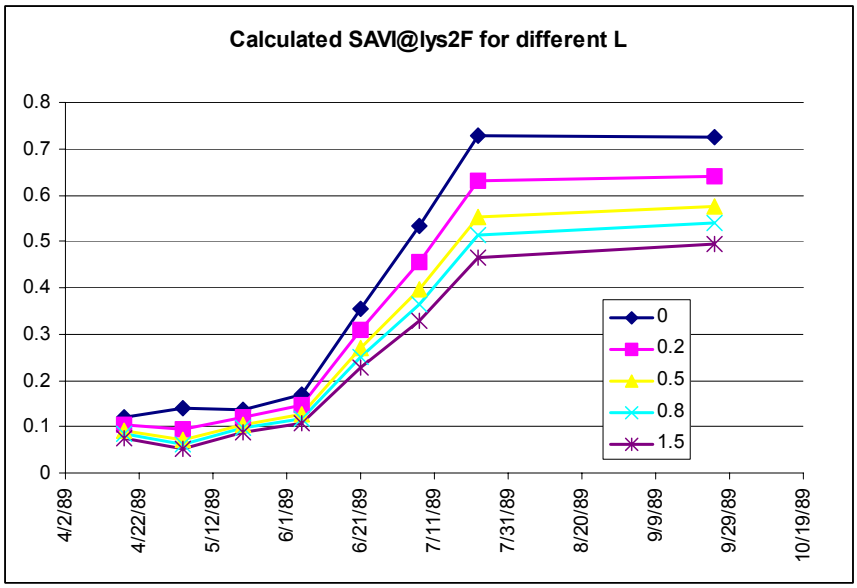

Fig. Calculated SAVI for different L values by the data of TM images (in 1989, Lys2 Fields)

The SAVI on 5/4(the second date) became less than SAVI of 4/18 when L was 0.2 or greater. This may be because SAVI (and NDVI) is affected not only by the amount of chlorophyll but also by albedo (includes the effect of soil moisture, shade and soil type), especially where vegetation cover is low.

The following pictures are TM false color images of first three image dates in 1989.

Fig. Lysimeter fields on 4/18, 5/4 and 5/20, 1989 (Left half is Lys2 field)

The Lys2 field is dark on May 4th, because of a recent irrigation. In 1989, sugar beets were planted on 4/27 (which was one week prior to the second date), and irrigation was practiced on 5/2, which is two days before the second date.

If we assume that both of 4/18 and 5/4 represent totally bare soil, then L = 0.1 in the SAVI equation represents a “good” value to eliminate the effect of background (See. the following graph).

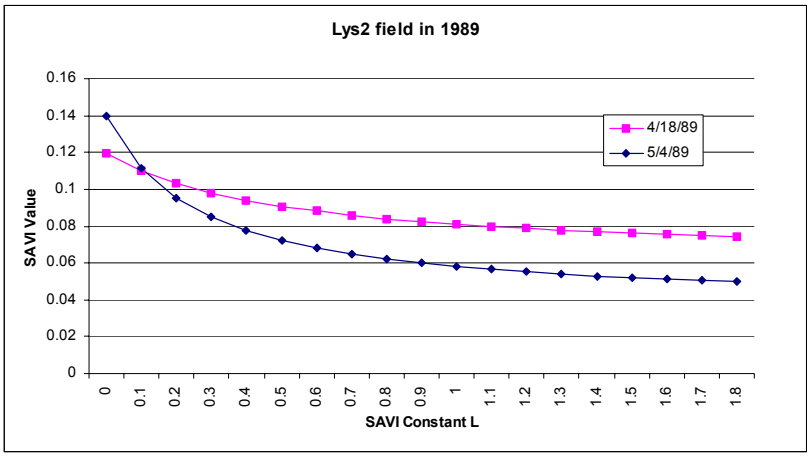

Fig. Changes of SAVI value by applying different L. Lys2 Field April and May, 1989

However, the above graph shows only for one location for two dates. To increase the sample data of bare soil, we evaluated three locations from desert on 9/25/89. In late September, there is almost no vegetation in desert areas (See. the following graph).

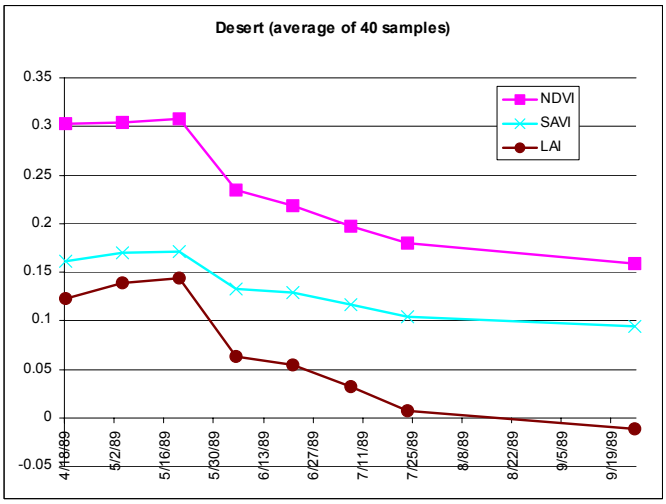

Fig. NDVI, SAVI and LAI for desert in 1989 (SAVI was calculated by L=0.5, LAI was calculated by using an averaged constants of many crops, See. the NDVI and SAVI comparison report No.1 for detail.)

The 40 sample pixels used for the above graph were randomly selected from a desert area. This time, out of the 40 sample pixels, the three pixels that had the lowest NDVI values in 9/25 were selected. These 3 pixels were regarded as “totally non-vegetation pixels”. The locations of the three pixels were in a same desert area, but not close to one another.

The following graph shows the change in SAVI values using different SAVI constants. The first two data are from Lys2 field pixels (average of 4 pixels), and the next three data are from a desert area on 9/25.

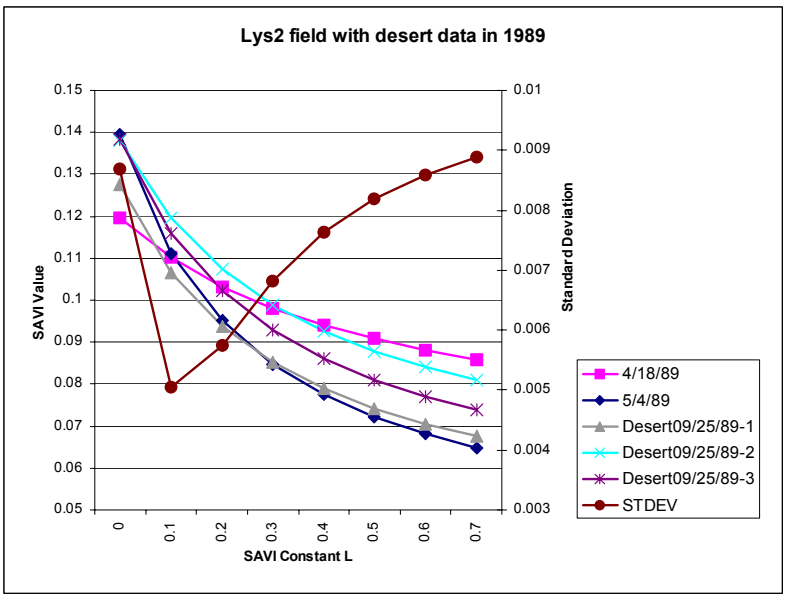

Conclusion

We suggest using L for SAVI = 0.1 for Idaho data to minimize impact of soil and soil wetness on vegetation prediction.

The standard deviation of the five sample data was minimized at L = 0.1. Although the number of samples is small, the data from the dry lysimeter field in April and wet condition in May corresponded well to a desert area in September.

Bastiaanssen has suggested the following equation for the SAVI vs LAI relationship (Bastiaanssen, 1998),

$$SAVI = c_1 - c_2 \exp(-c_3 LAI)$$

The c_1, c_2 and c_3 are coefficients that depend on the crop type.

Using this equation, LAI is computed from SAVI as;

$$LAI = -\frac{\ln\left(\frac{c_1 - SAVI}{c_2}\right)}{c_3}$$

The constants for the equation are as follows, based on literature:

Table xx. Regression coefficients of the SAVI vs LAI equation (Bastiaanssen, 1998). The MAX-SAVI was calculated during this study using the MAX-LAI information. The values 1 of c_3 were added by us.

	c1	c2	c3	MAX-LAI	MAX-SAV
Cotton-USA	0.82	0.78	0.6	3.5	0.72448
Maize-Itary	1.27	1.1	1.2	3.3	1.24903
Maize-USA	0.68	0.5	0.55	6	0.66156
Soybean-USA	0.72	0.61	0.65	6	0.70765
Wheat-USA	0.73	0.67	0.97	5	0.72475
Fruit tree-Itary	1.34	2.7	2.4	2.6	1.33474
Winter veges-Itary	1.31	2.75	2.2	4.2	1.30973
Bush&Grassland-Niger	0.14	0.3	1	1.2	0.04964
Grassland-Niger	0.13	0.35	1	1.3	0.03461
Millet-Niger	0.13	0.47	1	0.8	-0.0812
Degraded bush-Niger	0.11	0.28	1	1	0.00699
All crops	0.69	0.59	0.91	6	0.68749

2. SAVI and LAI in the Lys2 field in 1989

2-1. Analysis of equations in Bastiaanssen's textbook

SAVI computed with L=0.1 is higher in value than SAVI computed with L=0.5. This difference can make a large difference in LAI computed from Bastiaanssen's equation as shown in the following graph:

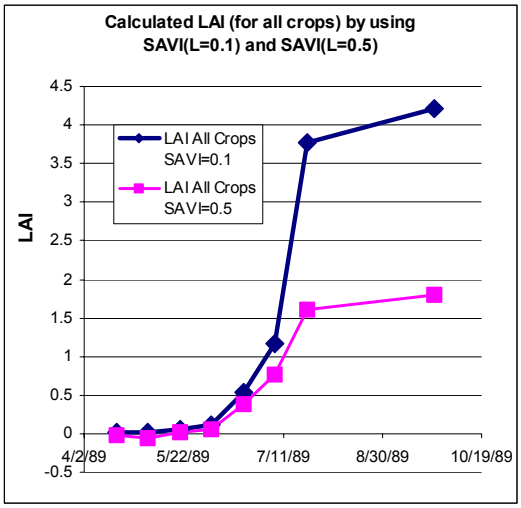

Figure. The difference of calculated LAI values by the different L values in SAVI calculation.

Since Bastiaanssen's equation (and also some other papers regarding SAVI) are based on SAVI(L=0.5), one must take care in applying empirical equations. The LAI values vary with crop type. The impact of the crop type on LAI estimation is shown in the following graph:

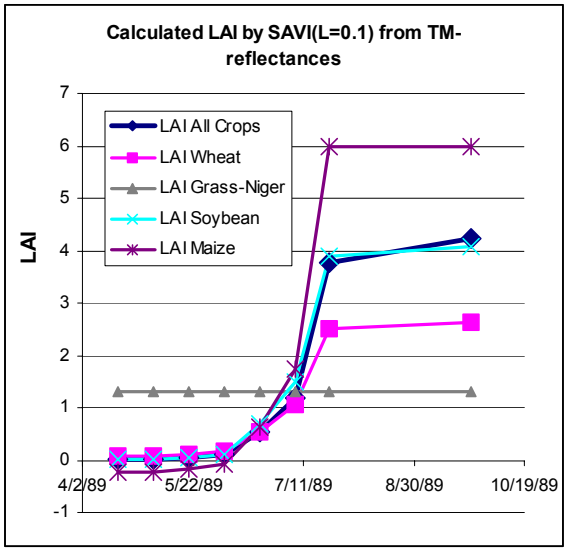

Figure. The impact of crop type on LAI estimation using SAVI(L=0.1).

Sometimes predicted LAI values become negative. Two equations for Maize are listed in the Table (one is from the USA and another is from Italy), The comparison is as follows:

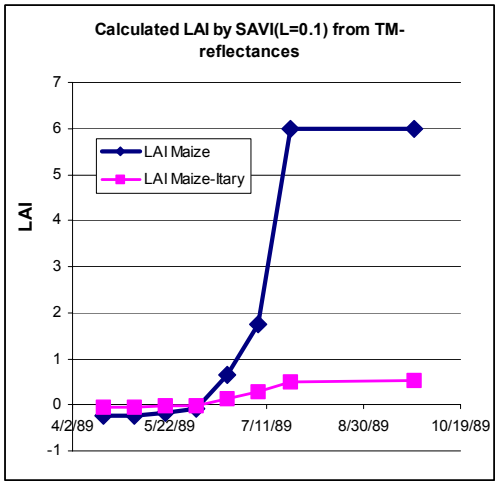

Figure. Estimated LAI using equation of Maize-USA and Maize-Itary with SAVI(L=0.1).

This evaluation is somewhat speculative because the SAVI used was from a sugar beet field. However, the result is still meaningful. There is a large difference in LAI values predicted for corn. These might stem from differences in crop density, difference of climate, and difference of the crop variety used to develop the relationships

2-2. Comparison with Measured LAI data

The Measured LAI data were plotted into the LAI graph and they corresponded well to equations for “all crops” and “soybean-USA”;

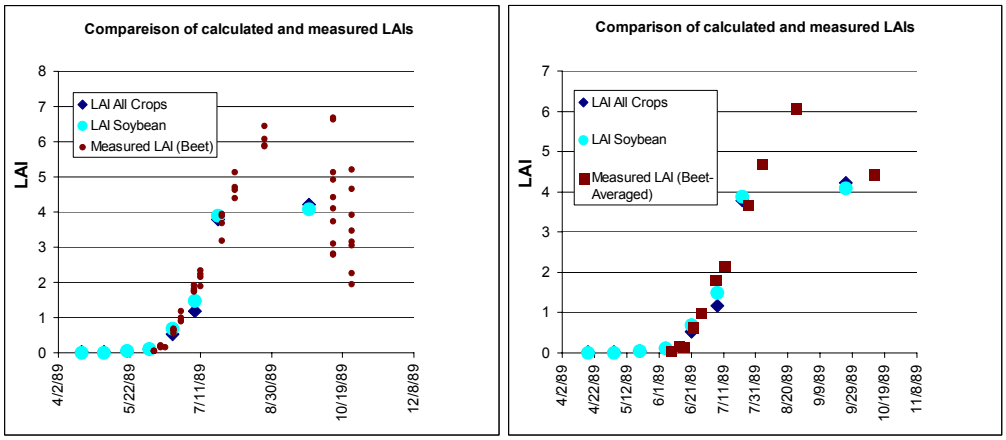

Figure. Measured LAI of Lys2 field(sugar beet, left: plot of all measured values, right: plot of averaged value), estimated LAI using “all crops” and “soybeans” equations with SAVI(L=0.1).

The results corresponded well except the last estimation (on 9/25/89). Also, the measured LAI values did not vary much for sampling days in Spring and Summer. This implies that the sugar beet field was quite homogeneous in 1989.

The reason that the last estimation was lower than the observation may be due to senescing leaves in late September.

2-3. LAI in Lys1 Field (grass)

Evaluation of reflectance data for Lys1 field speculative due to the small width of the grass. For the reflectance data for the grass field, we used the average value from 6 pixels.

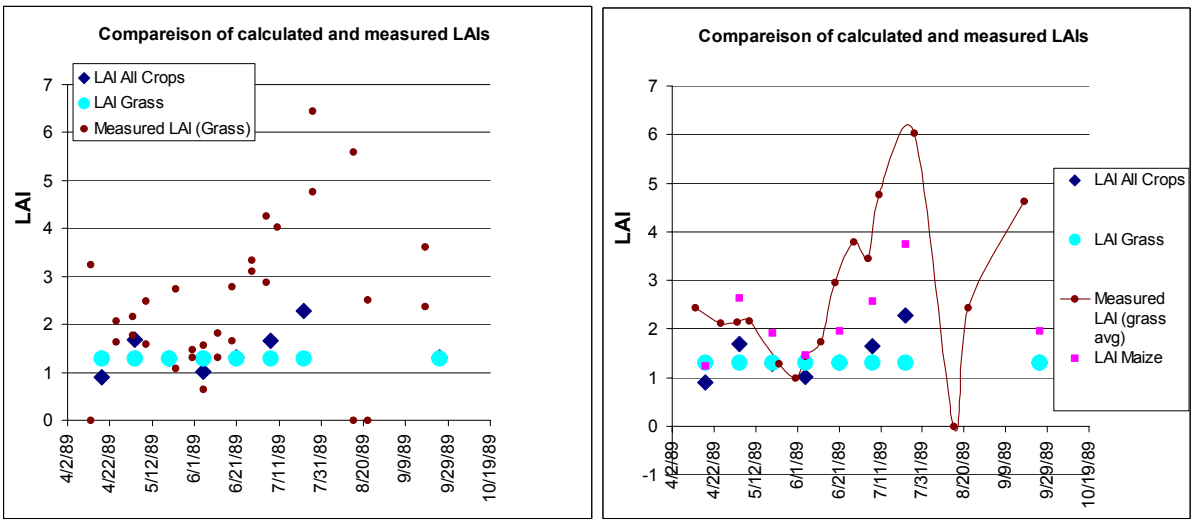

Figure. Measured LAI of Lys1 field(grass, left: plot of all measured values, right: plot of averaged value), estimated LAI using "all crops", "Grassland-Niger" and "Maize-USA"(only left) equations with SAVI(L=0.1).

The measured LAI for Lys1 field was unstable over time. It indicates that the canopy varied during the year due to clipping and perhaps stress. It is interesting that the average value for measured LAI was greater than an estimated value using "Maize-USA" coefficients.

3. Conclusion

It is difficult to conduct a detailed development of LAI prediction coefficients for Kimberly, since the measured LAI data are limited during satellite image dates. However at least we can confirm that the measured LAI for sugar beets corresponded very well with some equations.

4. Literature relationships for G from NDVI and SAVI

SEBAL-2000 used the following equation for G;

$$G/Rn = 0.30(1 - 0.98NDVI^4)$$

Bastiaanssen derived this regression equation using sets of data of G/Rn vs NDVI measured in many places.

The equation that Bastiaanssen has been using for SEBAL is;

$$G/Rn = \frac{Ts}{\alpha}(0.0032\alpha_{avg} + 0.0062\alpha_{avg}{}^2)(1 - 0.978NDVI^4)$$

The following is Choudhury's equation from the ASCE Hydrology Handbook:

$$G/Rn = 0.4e^{-0.5LAI}$$

Moran et. al.(1989) developed the following equation:

$$G/Rn = 0.58e^{-2.13NDVI}$$

Choudhury(1994) modified the previous equation by applying the relationship between SAVI and LAI developed by Baret and Guyot (1991) as:

$$G/Rn = 0.4\left(\frac{SAVI_{\max} - SAVI}{SAVI_{\max} - SAVI_{\min}}\right)^{\delta}$$

where δ is κ/κ', κ is extinction coefficient of Rn (which is 0.5??) and κ' is an extinction parameter to SAVI. Choudhury suggested that the relation between G and SAVI becomes nearly linear.

Appendix 7. Land Classification for paths 39 and 40 in southern Idaho

The application of SEBAL 2001 required the development of a land classification map. The classification was used in predicting aerodynamic roughness for nonagricultural land uses, for example, sagebrush, desert grass, water, basalt, mountain forests, and mountain grass/sage regions.

This appendix describes the process followed to develop a classification map for paths 39 and 40, rows 29, 30, and 31. Both Supervised classification (for path 39) and Unsupervised classification (for path 40) were applied during classification (by two different operators). Both methods worked well. The process used for path 40 is described here.

1. Landuse Type

The landuse map was designed to contain the following landuse types, which were of interest to the application of SEBAL:

Pixel value	Landuse Type
0	Background
1	Water
2	City and manmade structure
3	Vegetated field (at 8/22/00)
4	Forest at flat area
5	grassland
6	sage brush
7	bare soil includes both in field area and desert area
8	burned area
9	salty soil
10	basalt (dark gray)
11	basalt (black)
12	basalt (gray)
13	basalt (light gray)
21	mountain forest
22	mountain bare soil, dead grass, sage brush and other small vegetations

2. Unsupervised classification for path 40

An image which contained the following 8 layers was constructed for the June 4, 2000 image:

a. TM band1, 2000/06/04
b. TM band2, 2000/06/04
c. TM band3, 2000/06/04

d. TM band4, 2000/06/04
e. TM band5, 2000/06/04
f. TM Band6, 2000/06/04
g. TM band7, 2000/06/04

Unsupervised classification using 120 classes, and maximum 6 iterations was applied. The result of unsupervised classification was used as an information basis of the landuse map.

The Band 6 derived surface temperature was lapse corrected using a DEM. The T_{s_dem} and slope information was found to not work well in separating out land classes. This may have been because of two reasons:

(1) Each TM band has a wide range of pixel values, 0-255 in maximum. However, our T_{s_dem} values have only a limited range of approximately 0-50 K. The slope value range was also small, approximately, 0-35. To better reflect the variation of Ts and Slope relative to the –0255 range, we had to modify the value ranges of these two images. We applied the following DN adjustments:

*Modified Slope Information = Slope * 255/ Max Slope*

This caused the range of my Slope layer to become 0 to 255, and the slope information was better reflected in the classification.

(2) The classification used six layers of information for Visible and NIR radiation. Therefore, the weight of the Slope information was only 1/8. Also, the weight of Temperature information was only 1/8.

3. Water areas

In SEBAL 2000 water surface area was identified for each image using NDVI and B6 values.
For the derived landuse map for SEBAL-2001, the same method was used (with SAVI rather than NDVI) to identify water (which means that the result of unsupervised classification was not used). Locations of water were classified manually.

4. City areas

City areas were determined from unsupervised classification. However, it was difficult to identify some specific city areas. This may be due to city areas that are not homogeneous but are a mixture of many kinds of landuse types.

5. Vegetated fields

Vegetated fields were determined primarily from unsupervised classification. A careful review and modification was done manually to insure that all agricultural areas were classified as agricultural.

6. Forests

Forested areas were determined from unsupervised classification. After classifification, we applied two filters – (1) Assigned forests as City if the temperature was more than a certain value, and (2) Assign forests as bare soil if the LAI was less than 0.4.

7. Grassland, Sage brush and Bare soil

Basically, these landuse types were assigned by unsupervised classification. A bare soil area was determined using the information from known field areas (some pixels in desert areas which had similar pixel values automatically became bare soil). Next, in desert areas, grassland, sage brush and bare soil were assigned manually. For this determination, a true color image and NDVI changes between May and August were used. For desert areas, it was very difficult to predict the actual land use.

In SEBAL Phase2, we fixed the z_{om} values for grassland and sage brush. Therefore, it presents a problem if these landuses appear in agricultural field areas. To avoid such cases, areas that were categorized as grass or sage were evaluated for presence in agricultural areas. NDVI values for May, Jun and July were used to assign clusters as bare soil for places where NDVI had a high value in at least one month. After review, some landuses were modified manually.

8. Burned areas

Burned areas were assigned by using the result of unsupervised classification. Sometimes the separation between bare soil and burned areas was difficult. However, since some field areas were categorized as burned area, burned areas were treated in SEBAL as bare soil when predicting z_{om}. Therefore, low quality of burned area classification should not be a significant problem.

9. Salty soil (80%)

Salty soil was classified by albedo and temperature.

10. Basalt area (90%)

Basalt areas were classified by supervised classification.

11. Mountain forests and Mountain bare soils including grass, sage brush and other small vegetation (90%)

For mountain areas, a detailed classification was difficult since the various slope/aspect changes the “appearances” of similar surface types. Therefore, in this classification, mountain areas were separated into two landuse types only.

First, an area that had slopes of 5 degrees or more were defined as mountain areas. If there was a place that had >5 degree slope but was already assigned as agricultural area, it was kept as an agricultural area.

Next, places where LAI’s were 0.5 or more were categorized as mountain forest. Other areas were categorized as mountain bare soil. This class included grass or sage brush areas.

RESULTS

The color scheme and final classification for paths 40 and 39 is as follows:

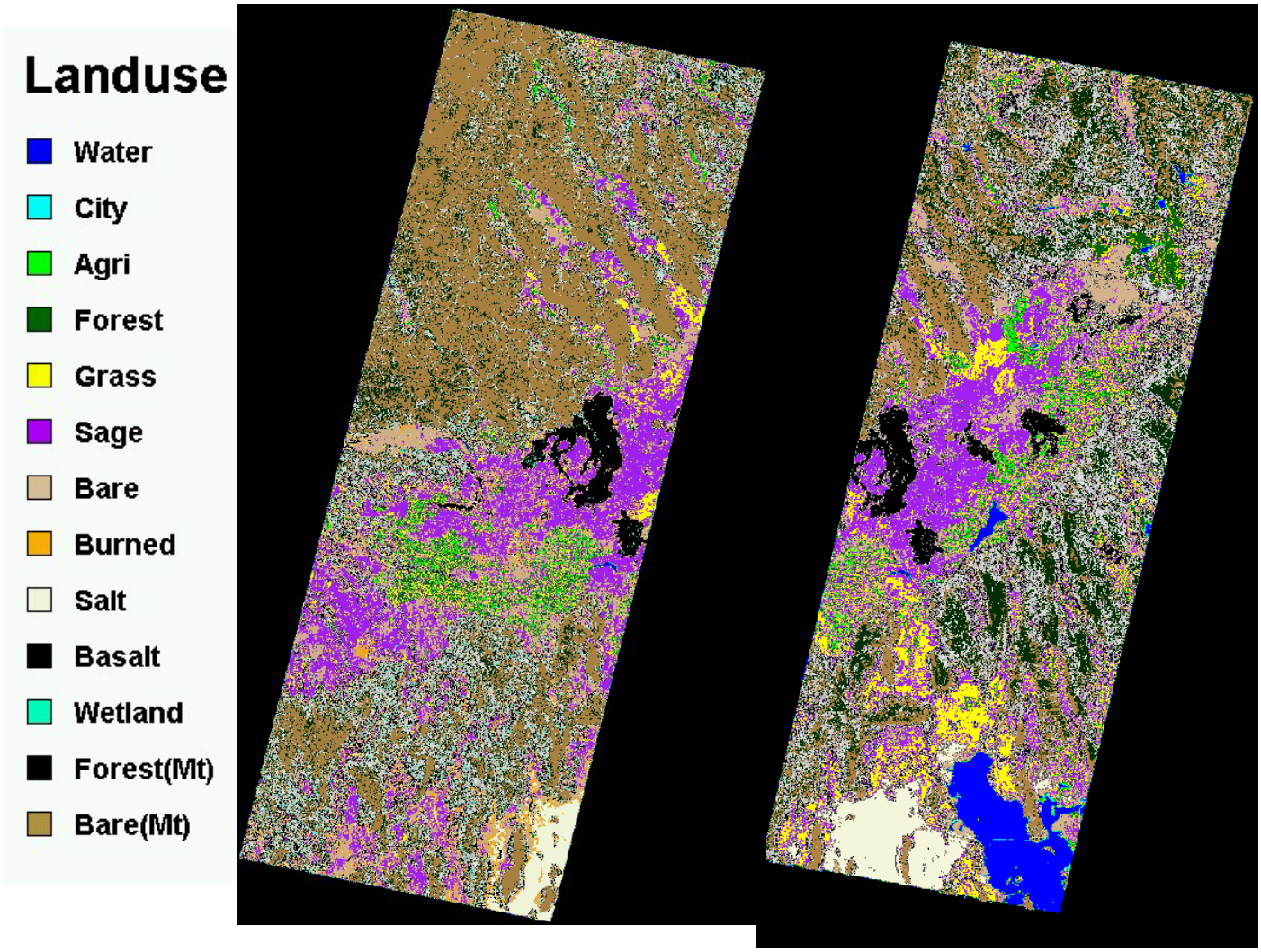
Landuse
Water
City
Agri
Forest
Grass
Sage
Bare
Burned
Salt
Basalt
Wetland
Forest(Mt)
Bare(Mt)

Results are considered to be good. There are some differences between classification of sage brush vs. desert grass between common areas of the two paths. However, this did not signficantly impact the prediction of ET by SEBAL. Classification of agricultural areas (either as agricultural or bare), considered to be of primary importance, was essentially the same between the two paths.